SAPIENZA
UNIVERSITÀ DI ROMA

DIPARTIMENTO DI INGEGNERIA MECCANICA E AEROSPAZIALE

DOTTORATO DI RICERCA IN
TECNOLOGIA AERONAUTICA E SPAZIALE
XXV CICLO

Indirect Optimization of Bang-Bang Control Problems and Applications to Formation Flying Missions

Advisor

Prof. Guido Colasurdo

Ph.D. Candidate

Alessandro Zavoli

MAY 2013

This thesis is dedicated to all the people who never stop believing in their dreams.

Acknowledgements

This thesis would not been possible without the direct or indirect support of many people, that I really would like to acknowledge with all my heart.

I would like to thank my ever-supportive family for offering whatever was needed all along the way, for the peaceful and serene environment where I grew up, and for all the efforts they made to sustain me during my studies.

I would like to thank my girlfriend Maria Vittoria, who supports me since the very beginning of my Ph.D. career. Her great patience and optimism helped me to overcome any challenge. She believed in me, even when I doubted.

I would like to thank my grandparents for the contagious enthusiasm they showed for even the smallest of my scholastic successes; my uncles, cousins, and relatives all for their warmth.

I would like to thank my uncle Sergio, for have being close to me since the beginning of this Roman adventure, when the nostalgia and the homesickness often came to visit me.

I would like to thank my friends, newer and older, that have been close to me despite the distance, and today celebrate this goal with me; my Ph.D. colleagues Marco and Michele, who supported me with their good company, and invaluable discussions about life, Ph.D.s, and politics; my GTOC6 team mates Alessandro and Stefano, whose enthusiasm, competence, and ambition push all the team up. I am also indebted with my Ph.D. colleague Francesco Simeoni, for the continuous exchange of ideas, suggestions, and reflections on orbital mechanics and optimal control strategies.

I would like to thank my internal reviewers Prof. Guido De Matteis and Prof. Francesco Nasuti, who provided me insightful comments, and hard questions. A special mention goes to my international reviewer Richard Epenoy whose competence, punctuality, and sound advice has been inspiring.

I am thankful to Prof. Lorenzo Casalino for his practical and effective suggestions on how to actually obtain the convergence with indirect methods, and for sharing with me some of his most valuable convergence tricks.

I would like also to express my deepest and sincere gratitude to my advisor Prof. Guido Colasurdo, for the continuous support of my Ph.D. study and research, for his patience, motivation, immense knowledge, and for his ability to cut straight to the root of a problem. I am indebted to him more than he knows.

Contents

List of Figures

LIST OF FIGURES

LIST OF FIGURES

List of Tables

Chapter 1

Introduction

Preface

Since the beginning of the Space Age, every effort in any discipline that concerns the space flight was devoted to develop innovative technical and theoretical solutions to increase, even by a small fraction, the payload mass. The reason is the very low percent of the total mass represented by the payload over the whole launcher mass (but the same holds for the scientific payload with respect to the total spacecraft mass). The optimization of the spacecraft trajectory contributes to achieve this goal, as it is primary aimed at reducing the propellant consumed during the orbital transfers. Obviously, other optimality criteria are possible beside propellant expenditure, such as the minimization of the flight duration or a combination of both, but the economy of propellant expenditure is usually the most pressing requirement.

Assuming that the configuration of flight vehicle is "frozen" (e.g., due to pressing, non modifiable, constraints of constructive, productive, or commercial nature) the responsible scientists and engineers look for the flight profile that permits to reduce the propellant consumed during the orbital transfers (thus freeing "space", and mass, for the payload), or to increment the mission duration or the number of revisits (thus increasing the "value" of the payload). On the other hand, the selection of flight profile plays a substantial role during the preliminary design of space missions, and it may affect the design of flight vehicle (i.e., its sub-systems). Indeed, it can make the difference between a feasible and an unfeasible mission (standing the present technology level). As an example, interplanetary missions for exploration of the Solar System (like

1. INTRODUCTION

Voyagers 1 and 2 missions and before them, Pioneers 10 and 11) using only the engine thrust, without exploiting some "tricks", such as gravity assist or ΔV-leveraging, would be almost unfeasible. Staying closer to our Planet, many missions, still feasible, would be economically too expensive, if wrong flight profiles were chosen; thus they would not be flown.

The way for researches in space trajectory optimization was opened by the pioneering work of Derek Lawden (Optimal Trajectories for Space Navigation of 1963) [1] and [Analytical method for Optimization] [2]. He studied simplified space flight missions (i.e., rocket ascent trajectory in vacuum, coplanar impulsive transfers) aiming to attain optimal analytical solutions. To deal with these optimization problems he made extensively use of results coming from optimal control theory, and in particular his most famous contribute is the physical interpretation he gave of the adjoint vector to velocity, or "Primer Vector". Optimal control theory dates back to the 17th century when Johann Bernoulli's posed his famous brachystochrone problem to his contemporaries. Several esteemed mathematicians including Wilhelm Gottfried Leibniz, the Marquis de l'Hopital, Isaac Newton and both Johann and Jakob Bernoulli submitted solutions to the brachystochrone problem, marking the beginnings of optimal control theory. With over 300 years of research in this area, many significant advancements have been made. Highlights of these advancements include the creation of calculus of variations, first elaborated by Euler in 1733 in the Elementa Calculi Variationum [3] from which the topic got its name. Also, in the 1950's, Richard Bellman pioneered work in dynamic programming [4] which led to sufficient conditions for optimality using the Hamilton-Jacobi-Bellman equation. Lev Pontryagin's development of the maximum (minimum) principle [5] in 1962 provided a method to determine the optimal control for constrained problems, often resulting in "bang-bang" solutions.

In the intervening several decades, interest in the subject has only grown, with space missions of sophistication, complexity, and scientific return hardly possible to imagine having been designed and flown in the 1960s. While the basics of optimization theory [the calculus of variations, Pontryagin's principle, Hamilton-Jacobi theory, or Bellman's principle] have not changed in this time, there has been a revolution in the manner in which they are applied and in the development of numerical optimization [6–8]. At the present day, the interest in space trajectory optimization is not extinguished. As an example, the European Space Agency encourage researches on this field

by providing grants and internships. Since some years ESA has been sponsoring a competition (GTOC) among universities and research institutes, in which a very complex optimization problem must be solved in a limited amount of time (usually a month): the aim is to promote and reward advances in trajectory design process [9, 10].

1.1 Research Topics

In the last three years, my research activity has been focused on the space trajectories optimization. The aim of this research was to investigate the mechanisms which cause some numerical methods to fail when dealing with real, difficult, optimization problems.

Improving the knowledge of the numerical methods used to deal with problems of this kind, trying to evaluate (by a direct comparison where possible) their strength points and limitations, is important not only to understand which one to use and in which situation, but it is also the first step in the path towards the development of new methods or towards improving the existing ones.

As far as possible, the proposed optimization problems, and their solutions, are also analyzed in depth from a physical point of view. The reason of such digressions is that a good knowledge of the physics that stands behind the problem is often necessary to produce a reliable initial guess which is required by any numerical method to succeed. Hence, understanding the problem is not less important than choosing the proper optimization algorithm. Usually, a same final orbit can be reached by exploiting several different flight profiles (that is, several thrust laws), which generate trajectories sometimes very close to each other; however, even small deviations from the optimal trajectory can badly deteriorate the mission performance. Theoretical tools (i.e., necessary and sufficient optimality conditions) allow one to distinguish between locally optimal and non-optimal trajectories, whereas conditions for the global optimality either do not exist or their use is limited by very restrictive hypotheses. Therefore, only the knowledge of the problem nature can help the mission designer to address the search for the optimal solution in the right direction.

Problems considered in this thesis belong to a specific class of optimal control problems whose solution exhibits a discontinuous control law: the so called bang-bang optimal control problems. The peculiar nature of these problems leads to several troubles in the optimization process, mainly of numerical origin, which dreadfully reduce the

user possibilities of attaining the optimal solution. Specific formulations of the problem, that lead to specific numerical algorithms, are essential to increase the convergence basin, hence the success probabilities of the optimization process. Some of the issues related to bang-bang optimal control problems are noticeable even in simple problems, but many others manifest themselves only when numerically challenging problems are considered.

Most of the space optimization problems belong to the class of bang-bang optimal control problems. Among them, formation-flying missions (i.e., missions that involve simultaneously more than one spacecraft) represent a proper topic for this research [11], due to the present interest expressed by the international scientific community in this kind of missions, which has continuously grown over the last decade. Such "distributed" space-systems (the same reasoning holds for both spacecraft formations and constellations) allow the creation of more powerful, flexible, and robust architectures than those offered by the traditional monolithic spacecraft of bigger size. They permit to obtain the same performance at a lower cost, but also to conceive space projects that would be otherwise impossible. However, formation flying missions do not come only with benefits: several new troubles arise and, with them, new research topics to investigate. Among them, the formation deployment (i.e., the problem of reaching the operative condition), the formation keeping, and the reconfiguration of the formation are especially interesting from a flight dynamics point of view. Being these problems also numerically challenging, they are a good benchmark to highlight all the issues that characterize bang-bang optimal control problems as well as for comparing the real performance of numerical optimization algorithms.

Specifically, the deployment problem of the Simbol-X project mission [12] is investigated in this thesis. This mission concerns a two-spacecraft formation that flies in a High Eccentricity Orbit (HEO), whose scientific goal is the creation of a powerful next-generation X-ray telescope. Being the "optical" elements split between the two spacecraft, an instrument of superior focal length (of the order of few tens of meters) is created. This allows for resolutions and magnifications just unthinkable for a traditional telescope carried by a single spacecraft. The mission project here considered completed successfully the Phase A of its development (i.e., the preliminary study); however, due to current budget restrictions, its development has been suspended. Nevertheless, the great scientific potential of the mission and the warm interest shown by the scientific

community for its payload, let one imagine that the project may be resumed in the future, or, perhaps, it will be the background for developing similar missions.

The interest in formation flight missions provides also new lymph to one of the better-known problems in astrodynamics: the rendezvous problem. In fact, the problem of creating the formation starting from a condition where two (or more) spacecraft fly on different orbits, is similar to a cooperative rendezvous problem. In this problem, each spacecraft has its own propulsive system which is used (or not used) in agreement with the others spacecraft to reach an assigned final condition which involves (in an explicit or implicit way) all the spacecraft. Differently from the "simple" rendezvous, which has been dealt with by many researchers in the past (hence a wide literature is available), the cooperative rendezvous did not receive as much attention and only few papers can be found on this topic.

From a strictly mathematical point of view, the constraints on the final state for a rendezvous problem are different from those of a formation deployment: at the rendezvous, all the spacecraft share the same state, whereas the formation deployment aims to place each spacecraft on a distinct orbit. In most cases, a unified formulation can be attained by rewriting the constraints; thus, in a certain way, the formation deployment can be seen as a generalization of the rendezvous problem, where the final state of all the spacecraft is not the same, but differs by some (constant or time-dependent) value. Apart from mathematical concerns, the actual difference between a cooperative rendezvous and a formation deployment cannot be too wide, as the formation flying mission requires, by definition, that the spacecraft are close to each other. Thus, the optimal trajectory of a rendezvous mission will not be too different from a deployment maneuver (assuming the same initial conditions, of course) or, in the worst case, it provides a reasonable starting point to investigate the deployment more in depth. Moreover, the rendezvous problem permits a more orderly and clear formulation that allows for a more generic investigation; hence theoretical interest in this problem is greater. Thus, in this thesis, the analysis of the Simbol-X mission is preceded by the study of a cooperative rendezvous mission, to highlight some theoretical aspects common to both problems.

1.2 Optimization Method

The formation deployment, as well as the cooperative rendezvous, can be posed as optimal control problems. Numerical methods for finding the solution of this kind of problem fall into two general categories: indirect methods and direct methods. In this thesis, an indirect method is adopted. This choice goes in the opposite direction with respect to the present trend, that shows a growth in the use of direct methods, motivated primarily by the difficulties that indirect methods present in the formulation of the mathematical problem and in its numerical solution. Direct methods rely on the discretization of state and/or control variables in order to reduce the infinite-dimension problem to a finite-dimension one. Accurate solutions may require a large number of discretization points and, consequently, high performance computers may be necessary even when quite simple problems are analyzed. Nowadays, the growing computational power of computers and the parallel use of many processors permits a thinner discretization, but the associated numerical complications remain; moreover the user cannot state if a solution is optimal, in the absence of a theoretical support. Indirect methods, instead, have a high theoretical value, and are extremely powerful as they permit to obtain the optimal solution with high precision while keeping the computational time relatively short. The choice of an indirect method is therefore "non-conformist", but well motivated by the previous sentences. This is also a choice of continuity with the work done in the Master thesis where DV-EGA missions were investigated in the three-body problem by using an indirect method.

The formation deployment of the Simbol-X mission presented in this thesis is a problem more complex than those usually addressed by indirect methods in literature. A mix of peculiar traits, combined with each other, makes the optimization of this mission really challenging. The spacecraft orbits are very high, and the trajectories are significantly affected by the gravitational perturbations of Moon and Sun. Moreover, the two spacecraft fly through a wide range of altitudes, hence the perturbative acceleration, as well as its dominant source, changes restless, weighing down the numerical computation.

Issues due to perturbative acceleration couple with those typical of bang-bang optimal control problems. The optimal thrust law still exhibits a discontinuous profile: intervals where the spacecraft exploits the maximum available engine thrust, alternate

with intervals where the engine is cut off and the spacecraft flies on a mere ballistic trajectory. However, lengths and sequence of these intervals change with the departure date, because they are sensitive to variation of the perturbative accelerations that, in turn, are time-dependent functions (i.e., they change as the departure date changes). The impact on the optimization process is severe: the " burn structure" (that is, number and location of the engine firings) of the optimal mission becomes hardly predictable and many sub-optimal solutions, close each other, are possible. The picture becomes more tangled as the time available for the deployment increases. Further, the relatively low intersatellite distance at the end of the transfer, coupled with the perturbations and the wish to minimize the propellant consumption, may bring the spacecraft too close each other, thus enhancing collision risks.

The use of the right numerical method (or just the most suitable version of it) is mandatory, when problems as difficult as the one previously described are faced. A proper numerical method permits to improve the accuracy of the obtained solution, to speed up the numerical calculation, to simplify the convergence process. Last but not least, sometimes choosing the right numerical method makes the difference between being or not being able to solve the problem. This thesis proposes to compare two techniques, conceptually well different, that aim to handle (or just reduce) issues related to discontinuous profile of the optimal control. The first, here called Multi-Bound Approach, was first proposed by Colasurdo [13]. This approach is founded on a preliminary subdivision of the trajectory into several arcs, which distinguishes clearly thrust and coast arcs, hence greatly improving the numerical behavior of the problem. In turn, it leaves open the question on how to guess at the correct trajectory subdivision.

The second one, here called Continuation-Smoothing Technique, dates back in the seventies, and has been lately improved by Epenoy et al. [14]. It tries to reduce the numerical issues by regularizing the control law. Suitable perturbative terms are initially added to the problem formulation to facilitate the convergence process and subsequently are made fade away. This approach was entirely "new" to our research group.

At the beginning of my research, I had at my disposal the original implementation of the Multi-Bound approach, which allowed for the solution of generic optimal control problems, once properly formulated as multipoint boundary value problems. An implementation of the Continuation-Smoothing was, instead, not available.

As the "historical" code (which implemented the Multi-Bound approach) would require a major revision to support the implementation of the Continuation-Smoothing technique, I developed from scratch a new code, which permits the solution of BVPs by means of a simple shooting method, and implements the two techniques chosen for handling the bang-bang control laws. This new code features many small technical improvements over the previous one, such as the use (as far as possible) of calls to high performance libraries. The introduction of the Object-oriented paradigm makes the code more modular (hence more flexible) and reusable with respect to the previous one. Despite the code was thought to deal with the formation deployment problem under investigation, it is quite versatile and easily adaptable to solve other optimal control problems.

The comparison between the two techniques proposed for handling the bang-bang control is not reduced to a mere comparison about the execution times, or the radius of convergence (which are however important); it is a comparison between two different viewpoints, sometimes antithetic, but also complementary, on the way of facing this problem. As far as possible, I will try to make clear the philosophy that stands behind both approaches, and to motivate why and when either method overperforms the other (hence in which cases either method should be used).

1.3 Thesis Summary

This section briefly describes the contents of the chapters in this thesis.

Chapter 2 presents in a concise manner the mathematical concepts and the numerical tools necessary to solve the optimization problems related to space transfers. A mathematical formulation of a generic multi-phase optimal control problem is provided. An overview of both direct and indirect methods follows. Theoretical aspects and numerical implementation of indirect methods are described in depth.

Chapter 3 deals with problems where the magnitude of the optimal control is bounded and assumes alternatively the maximum and the minimum permissible value: the bang-bang optimal control problems. The main difficulties related to this peculiar class of problems are investigated. Two different numerical techniques that can be adopted to overcome these numerical issues are proposed and compared each other. The effectiveness of each approach is demonstrated by applying them to a simple problem.

In Chapter 4, the techniques outlined in the previous chapter are used to solve a finite-thrust time-constrained cooperative rendezvous problem. A comparison between a truly cooperative strategy and a less coordinated (leader/follower) strategy is performed, in order to highlight the benefits of the cooperation, but also its limits. The cooperative rendezvous mission is useful to test the two algorithms previously introduced on a truly representative problem of space flight.

In Chapter 5, the optimal deployment of the Symbol-X formation is investigated. The mission is briefly outlined. Optimality conditions for the single spacecraft deployment and the formation deployments are derived. Emphasis is posed on the role that the perturbative forces, as well as the departure date, play on the deployment. Results are presented to show the difficulties faced and the effectiveness of the proposed solution method.

Finally, Chapter 6 summarizes significant contributions of this thesis and suggests future research directions.

Chapter 2

Methods for Optimal Control

2.1 Introduction

The aim of this chapter is to illustrate mathematical concepts and numerical tools necessary to solve the optimization problems related to space transfers. The most suitable mathematical formulation for an optimization problem which concerns a finite-thrust mission (e.g. a spacecraft deployment, or a rendezvous) is for sure a time-continuous optimal control problem. Even though the specific features of the mathematical problem depend on the peculiar mission under investigation, it is possible to pose any optimal control problem in a concise and quite general fashion. The mathematical formulation of such a generic multi-phase optimal control problem is presented in section [2.2.1]. Numerical methods that are employed for the numerical solution of optimal control problems (OCPs) are usually classified in direct methods or indirect methods, c.f. Betts [15]. An overview of both classes is proposed in section [2.2.2]. A more exhaustive description of the adopted optimization method (i.e., the indirect one) is then provided in section [2.3]. Both theoretical aspects and numerical implementation are faced. In particular, section [2.3.1] deals with the optimal control theory, which is used to derive the first order necessary conditions for optimality. These conditions are presented here in a general form that can be used to handle both time-fixed and time-free problems, and also problems with interior (point) constraints. First order optimality conditions lead to the formulation of a Hamiltonian Boundary Value Problem, that can be a two point boundary value problem (TPBVP) or even a multipoint boundary value problem (MPBVP). The analytical solution of these algebraic-differential problems is

usually impossible to find out, especially when the system dynamics is nonlinear; thus proper numerical methods need to be used [16, 17]. An overview of several suitable methods is provided in section [2.3.2]. Special care is given to the description of the shooting method, because it has been employed to solve numerically the optimization problems proposed in Chapters 4 and 5.

2.2 The Optimal Control Problem

2.2.1 General Statement

An optimal control problem consists in establishing which control law, among all the admissible ones, allows the system under investigation, characterized by a certain dynamics, to evolve from an initial to a final state, so that every constraint is fulfilled and the optimization criteria or merit index is maximized (or minimized). Each of these aspects of an OCP are discussed hereafter.

Through the thesis the following notation will be used in order to provide a concise and clear, as much as possible, formulation of the equations: vector variables and vector functions are considered column vector and will be marked with the superscript bar (“ $\bar{}$ ”); matrixes have a double bar (“ $\bar{\bar{}}$ ”). In some circumstances, Euclidean vectors, such as position, velocity, or acceleration, will be marked with the superscript “ $\vec{}$ ” to highlight their peculiar nature.

The state of the system at the time t is defined by a vector $\bar{x}(t) \in \mathbb{R}^n$, which allows to describe, in a complete and unequivocal way, at any instant, all the features of interest concerning the system under examination (e.g., position, velocity, and mass of a spacecraft). The function $\bar{x}(\cdot)$ defines the trajectory during all the integration interval $[t_0, t_1]$. The evolution in the time domain of the system state is defined by a set of first order ordinary differential equations, which are obtained typically by applying the fundamental principles of mechanics to the spacecraft system. The ODE system can be generically written as:

$$\frac{d\bar{x}}{dt}(t) = \bar{f}(\bar{x}(t), \bar{u}(t), t) \tag{2.1}$$

where $\bar{u}(t) \in \mathbb{R}^m$ is the control vector (i.e., the vector which collects all the control variables) at time t. The thrust vector created by a rocket engine, the incidence of the ailerons of an aircraft, the torque applied on a reaction wheel are examples of control

variables. The optimal trajectory is usually subjected to constraints of various kind. In case of constraints involving only state and time at the extremes of the trajectory (i.e., at its beginning or end), these constraints can be written as a set of homogeneous (usually non-linear) algebraic equations:

$$\bar{\chi}\left(\bar{x}_0, \bar{x}_f, t_0, t_f\right) = 0 \tag{2.2}$$

where the function $\bar{\chi} : [\mathbb{R}^n, \mathbb{R}^n, \mathbb{R}, \mathbb{R}] \rightarrow \mathbb{R}^q$ collects all the imposed constraint; symbols $\bar{x}_0$ and $\bar{x}_f$ stand for $\bar{x}\left(t_0\right)$ and $\bar{x}\left(t_f\right)$, respectively.

Sometimes, even the control vector $\bar{u}\left(t\right)$ is constrained; therefore it has to belong to the set of admissible controls U (e.g., as far as solar electric propulsion is concerned, the engine is often not allowed to work whenever the spacecraft is inside a shadow cone). In case of finite-thrust missions, as those considered in the next Chapter, the thrust magnitude at any time is limited (i.e., it must be less or equal to a given value). The optimization criterion which completes the optimal problem specifics, is expressed by an objective function or Merit Index J that has to be extremized. In general, the merit index is a functional, sum of two terms:

- The first one (φ) depends exclusively on the values that the state and time variables assume at the boundaries. It measures the weight of reaching a certain final state;

- The second one (Φ) depends on the values which control, independent, and state variables assume at any point along the trajectory. It measures the cost of the evolution of the system from the initial to the final point.

Thus, the merit index can be written in its complete form as follows:

$$J = \varphi\left(\bar{x}_0, \bar{x}_f, t_0, t_f\right) + \int_{t_0}^{t_f} \Phi\left(\bar{x}\left(t\right), \bar{u}\left(t\right), t\right) dt \tag{2.3}$$

This is the so called Bolza form of the merit index. A concise mathematical formulation

of the Bolza optimal control problem can now be presented:

$$(P_{Bolza}) = \begin{cases} \min\limits_{u \in U} J = \varphi\left(\bar{x}_0, \bar{x}_f, t_0, t_f\right) + \int\limits_{t_0}^{t_f} \Phi\left(\bar{x}\left(t\right), \bar{u}\left(t\right), t\right) dt \\ \dfrac{d\bar{x}}{dt}\left(t\right) = \bar{f}\left(\bar{x}\left(t\right), \bar{u}\left(t\right), t\right), \quad \forall t \in [t_0, t_f] \\ \text{s.t.} \\ \quad \bar{\chi}\left(\bar{x}_0, \bar{x}_f, t_0, t_f\right) = 0 \end{cases} \tag{2.4}$$

Introducing suitable auxiliary variables, the functional can always be rewritten in the "Lagrange Form" (i.e., the one with $\varphi = 0$), or in the "Mayer Form" (i.e., the one with $\Phi = 0$). The latter is often preferred because it allows a simpler problem formulation and also simpler analytical expression of the first order necessary conditions (see section [2.3.1]). Often, optimization problems are constrained at some interior points, or the evolution of the system changes abruptly there. It might be useful to split the trajectory into a certain number n_f of subintervals, called indistinctly arcs or phases. Initial and final points of each phase are referred to as boundaries: those relative to the initial and final points of the whole trajectory are called "external boundaries", whereas those which are inside the trajectory are named "internal boundaries". What arises is a multi-phase optimal control problem. Signs "+" and "-" are employed to indicate whenever a variable (either state or time) is referred to the point immediately before or after a boundary. Therefore, the state variables at the beginning of the j-th arc are indicated with the symbol $\bar{x}_{(j-1)+}$ and the corresponding time is $t_{(j-1)+}$, while $\bar{x}_{j-}$ and t_{j-} refer to the values assumed by state and time at the end of the same arc. Notice that whenever an arc duration is unknown, a new parameter must be introduced; its optimal value will be given by the optimization process. The state and time variables at the boundaries can be collected respectively in the vectors:

$$\bar{X}_+ = \left\{\bar{x}_{(j-1)+},\ \forall j = 1, \ldots, n_f\right\} \quad \text{and} \quad \bar{X}_- = \left\{\bar{x}_{j-},\ \forall j = 1, \ldots, n_f\right\} \tag{2.5}$$

$$\bar{T}_+ = \left\{t_{(j-1)+},\ \forall j = 1, \ldots, n_f\right\} \quad \text{and} \quad \bar{T}_- = \left\{t_{j-},\ \forall j = 1, \ldots, n_f\right\} \tag{2.6}$$

Constant unknown parameters, if any, can be thought to be included in the vector $\bar{x}$. The constraint equation in its most general form becomes:

$$\bar{\chi}\left(\bar{X}_+, \bar{X}_-, \bar{T}_+, \bar{T}_-\right) = 0 \tag{2.7}$$

Remembering that the whole integration domain is split into n_f sub-intervals, the merit index can be written as follows:

$$J = \varphi\left(\bar{X}_+, \bar{X}_-, \bar{T}_+, \bar{T}_-\right) + \sum_{j=1}^{n_f} \int_{t_{(j-1)+}}^{t_{j-}} \Phi\left(\bar{x}\left(t\right), \bar{u}\left(t\right), t\right) dt \tag{2.8}$$

A concise mathematical formulation of the Bolza multi-phase optimal control problem can now be presented:

$$(P_{Bolza-multi}) = \begin{cases} \min\limits_{u \in U} J = \varphi\left(\bar{X}_+, \bar{X}_-, \bar{T}_+, \bar{T}_-\right) + \sum\limits_{j=1}^{n_f} \int\limits_{t_{(j-1)+}}^{t_{j-}} \Phi\left(\bar{x}\left(t\right), \bar{u}\left(t\right), t\right) dt \\ \dfrac{d\bar{x}}{dt}\left(t\right) = \bar{f}\left(\bar{x}\left(t\right), \bar{u}\left(t\right), t\right), \quad \forall t \in [t_0, t_f] \\ \text{s.t.} \\ \quad \bar{\chi}\left(\bar{X}_+, \bar{X}_-, \bar{T}_+, \bar{T}_-\right) = 0 \end{cases} \tag{2.9}$$

2.2.2 Numerical Methods: an Overview

Many methods for solving optimal control problems has been devised during the past years. Most of them are listed in the state of art of trajectory optimization as depicted by J. T. Betts [15]. These methods can be grouped into two categories: direct methods and indirect methods. The difference is made by the introduction (or not) of adjoint variables (c.f. section [2.3]) associated to the state ones. Nevertheless, both approaches try to transform the original optimization problem which has an infinite dimension into a new one with a finite dimension. In extreme synthesis, indirect methods first derive the optimality conditions and then discretize the problem, while in direct methods the optimization problem is first discretized and then optimized.

Indirect Methods

Indirect methods are founded on the principles of variational calculus for deriving the necessary optimality conditions. Adjoint (or costate) variables are time-continuous functions associated to the state variables, which are exploited to include the respect of the differential constraint (i.e., the state dynamics) into the optimization criteria. Similarly to what happens in finite-dimension optimization, Lagrange multipliers are also introduced in the merit index to ensure the respect of the algebraic constraints. Variational calculus suggests both necessary and sufficient conditions for the optimality

of the solution. Necessary (or first order) conditions for the optimality are obtained by posing the first variation of the merit index equal to zero. The fundamental results are:

- Euler-Lagrange equations (which define the evolution of the adjoint variables),
- optimality conditions for the controls, (which are algebraic equations that link the control variables at any time to state and adjoint variables),
- transversality conditions (which are algebraic conditions that define, explicitly or implicitly, the value of state and adjoint variable at the boundaries of the trajectory).

Necessary conditions form a Hamiltonian boundary-value problem (HBVP), which is solved numerically for extremal trajectories. These trajectories may correspond indistinctly to maximum, minimum or saddle points of the merit index. The Legrendre-Clebsch equations provide the second order (or sufficient) conditions for the optimality. However, in practice the derivation of these conditions is often too difficult (or even impossible). Therefore, the user must rely on his physical knowledge of the solution; of course, if many solutions are attained, the optimal solution is found by choosing the extremal trajectory with the best merit index. Notice that necessary conditions must be derived analytically. In simple cases this is an easy task to perform, whereas it becomes more and more difficult as the problem becomes more realistic (hence complex). In the latter cases, a manual derivation require a lot of time and it is an error-prone process. Some commercial products, such as Matlab's Symbolic Math Toolbox [18] or Mathematica [19], offer the capability of performing symbolic operations (both algebraic and differentiation). Unfortunately, these programs are unable to rearrange the result into a simple form as a human user would do. Otherwise, Automatic Differentiation (AD) can be used to numerically evaluate the required derivatives. This is quite convenient in case of the derivation required by Euler-Lagrange differential equations, whereas it is of less help for the derivation of the transversality conditions. The derivatives are evaluated with high accuracy (more than using finite difference approximations), but the computational burden for each evaluation is bigger than using the corresponding analytical expression. In the aggregate, automatic differentiation is quite convenient in the case of complex derivations, unless the algorithm performance is not the principal requirement.

Direct Methods

Direct methods rely on a conversion or transcription of the original continuous optimal control problem into a discrete optimization problem subject to algebraic constraints, which is also known as nonlinear programming (NLP) problem. To attain this result, the continuous functions involved in the problem are discretized over a mesh. The collection of all these discrete values form the set of unknown variables which will be optimized. The category of direct methods is quite broad and encompasses very different techniques [20]. In particular, the choice of which quantities are discretized and how the continuous-time dynamics is approximated, varies widely amongst the different direct methods. Two of the more common types of direct methods are the semi-discrete (or control) parameterization and the fully-discrete (or state and control) parameterization. In a control parameterization method [21, 22], the control alone is approximated and the differential equations are solved via numerical integration. In state and control parameterization methods [23–25], even the state is discretized (not necessarily on the same mesh of the control) and the differential equations are converted into algebraic constraints, more or less complex depending on the numerical integration scheme (e.g., trapezoidal rule, Simpson's rule, Gauss quadrature). The NLP problem related to the fully-discrete parameterization can be written in its most general form as:

$$\begin{cases} \min\limits_{\bar{\xi},\bar{\pi},\bar{v}\in U} \; h\left(\bar{\xi},\bar{\tau},\bar{v},\bar{\pi}\right) \\ s.t. \\ \quad \bar{\eta}\left(\bar{\xi},\bar{\tau},\bar{v},\bar{\pi}\right) = 0 \\ \quad \bar{\gamma}\left(\bar{\xi},\bar{\tau},\bar{v},\bar{\pi}\right) \geq 0 \end{cases} \tag{2.10}$$

where $\bar{\xi}$, $\bar{v}$ collect the state and control values at the discrete times $\bar{\tau}$, and $\bar{\pi}$ is a vector of additional unknown parameters. Vector Function $\bar{\eta}$ expresses equality constraints, such as those related to the integration scheme and to the boundary conditions; vector function $\bar{\gamma}$ refers to inequality constraints (usually coming from the discretization of path constraints). The set U is the set of the admissible controls. The resulting NLP can be solved numerically by well developed algorithms [26, 27] which attempt to satisfy a set of conditions (called Karush-Kuhn-Tucker (KKT) conditions) associated with the NLP. In case of semi-discrete parameterization, the system dynamics is still governed

by the set of time-continuous differential equations. Therefore, once a control law is assigned (i.e., $\bar{v}$ is assigned), it is possible to obtain the corresponding trajectory by integrating the ODE system starting from the initial point $\bar{x}(t_0) = \bar{x}_0$ over the assigned time horizon. The problem can be again written in the NLP form, hiding the ODE integration inside the objective function:

$$\begin{cases} \min\limits_{\bar{x}_0, t_0, \bar{\pi}, \bar{v} \in U} h(\bar{x}_0, t_0, \bar{\pi}, \bar{v}) \\ s.t. \\ \quad \bar{\chi}(\bar{x}_0, t_0, \bar{\pi}, \bar{v}) = 0 \\ \quad \bar{\gamma}(\bar{x}_0, t_0, \bar{\pi}, \bar{v}) \geq 0 \end{cases} \tag{2.11}$$

This parameterization allows the reduction of the problem dimension (i.e., the number of unknowns) with respect to the fully-discrete. Actually, the problem dimension is usually low/medium in case of a semi-discrete parameterization, but the sensitivity to the initialization is lower using the fully-discrete parametrization. Besides to traditional deterministic numerical methods (e.g., SQP), which are applied in fully-discrete parametrization, meta-heuristic or stochastic algorithms (e.g., simulated annealing [28], genetic [29, 30] and evolutionary [31] algorithms) can also be employed. These algorithms are receiving a great attention recently, as they are intrinsically apt to multi-disciplinary and multi-objective optimization and in principle are capable of achieving the global optimum in a very large search space. Moreover they can be applied also to non-smooth objective function. However, to keep the problem dimension under a reasonable value, the control usually must be approximated by simple parametric representations. Therefore the accuracy of these optimization methods is modest. Also, they are often much slower than the deterministic algorithms, which indeed have a higher risk of getting stuck in local optima.

Comparison

An accurate comparison of direct and indirect methods can be found in Betts [15]. A wide number of similarities between the methods is highlighted as well as important differences. The primary advantages of indirect methods are the high accuracy of the solution and the assurance that the solution satisfies the first-order optimality conditions. Indirect methods are fast due to the reduced number of unknowns variables, and they may offer an interesting theoretical insight into the problem characteristics.

However, three main drawbacks of indirect techniques need to be underlined: analytic expressions for the optimum necessary conditions must be derived; the region of convergence for the root-finding algorithm may be small; finally, for problems with path constraints, it is necessary to have an a priori knowledge of the sequence of constrained and unconstrained arcs. On the other side, direct methods typically require a large number of variables to accurately describe the problem, therefore each optimization usually takes long computational times, that can be somehow reduced by taking the matrix sparsity into account. Indeed, high performance computers may be necessary even when quite simple problems are analyzed. The discretization is responsible of the increase of the convergence radii over the indirect methods. As results their initialization require less care (and they do not require an initial guess for the adjoint variables at all). They still rely on a tentative guess and may not converge to the optimal solution, but whereas convergence difficulties prevent indirect methods from finding a solution, direct methods find at least a suboptimal one. Another point of success of direct methods is that even complex control or state constraints can be handled easily and that, in case of path inequality constraints, the sequence of free and constrained arcs does not need to be known a priori. Lastly, they have the advantage that the first-order necessary conditions do not need to be derived. This is fine, because the analytical derivation may be a difficult (sometimes even impossible) task. As drawback, direct methods either provide an inaccurate costate evaluation or they do not provide costate information at all. This implies that it is always uncertain whether the solution found by NLP is truly an optimal solution to the original optimal control problem. Well-known software packages employing direct methods include Optimal Trajectories by Implicit Simulation (OTIS) [32], Sparse Optimal Control Software (SOCS) [33], Graphical Environment for Simulation and Optimization (GESOP) [34], Direct Collocation (DIRCOL) [35], Nonlinear Trajectory Generation (NTG) [36], and Direct and Indirect Dynamic Optimization (DIDO) [37]. Very few commercial products offer the possibility for solving optimal control problems by using an indirect method; among them, it is worth to name just the most interesting and known: BNDSCO [38].

2.3 Indirect Methods

The aim of this section is to provide a deeper insight of the adopted optimization method. Both theoretic foundations and the numerical implementation will be faced. First, a simple but general formulation of the first order necessary condition for the optimality is derived, which leads to the formulation of a Hamiltonian Boundary Value Problem. Subsequently, some numerical methods for the solution of these problems are presented, with particular emphasis on the shooting method, which has been employed throughout this thesis.

2.3.1 Optimal Control Theory

Indirect methods are based on the application of the optimal control theory to the specific mission under investigation. The optimal control theory, which is based on the principles of variational calculus, aims at searching for the extremal value (maximum or minimum) of a merit index, the corresponding trajectory $\bar{x}^*(\cdot)$, and the optimal control $\bar{u}^*(\cdot)$. The derivation of the optimality condition starts by defining a modified or augmented merit index J^*, which is needed to include a measure of the respect of the system evolution law (i.e., the state dynamics) and of the boundary constraints into the original merit index. This is made possible by the introduction of Lagrange multipliers, collected into the vector $\bar{\mu}$, associated to the constraint equations, and by the introduction of adjoint variables $\bar{\lambda}(t)$ which are functions associated to the state variables. The modified merit index can be written as:

$$J^* = \varphi + \bar{\mu}^T \bar{\chi} + \sum_{j=1}^{n_f} \int_{t_{(j-1)+}}^{t_{j-}} \left(\Phi + \bar{\lambda}^T \left(\bar{f} - \dot{\bar{x}}\right)\right) dt \tag{2.12}$$

The merit index and its augmented counterpart coincide if the state evolves according the differential equations and if all the constraints are fulfilled. The same holds for their extreme values. Manipulating eq. (2.12) by integrating by part, the state derivatives

can be eliminated and a simpler expression is obtained:

$$J^* = \varphi + \bar{\mu}^T \bar{\chi} + \sum_{j=1}^{n_f} \left(\bar{\lambda}^T_{(j-1)+} \bar{x}_{(j-1)+} - \bar{\lambda}^T_{j-} \bar{x}_{j-} \right) + \tag{2.13}$$
$$+ \sum_{j=1}^{n_f} \int_{t_{(j-1)+}}^{t_{j-}} \left(\Phi + \bar{\lambda}^T \bar{f} - \dot{\bar{\lambda}}^T \bar{x} \right) dt$$

It is useful to regroup some of these terms to define an important function, that will often appear in the following section: the Hamiltonian function H:

$$H = \Phi + \bar{\lambda}^T \bar{f} \tag{2.14}$$

The augmented merit index is hence differentiated (square brackets indicate matrixes):

$$\begin{aligned} \delta J^* = & \left(-H_{(j-1)+} + \frac{\partial \varphi}{\partial t_{(j-1)+}} + \bar{\mu}^T \frac{\partial \bar{\chi}}{\partial t_{(j-1)+}} \right) \delta t_{(j-1)+} + \\ & + \left(H_{j-} + \frac{\partial \varphi}{\partial t_{j-}} + \bar{\mu}^T \frac{\partial \bar{\chi}}{\partial t_{j-}} \right) \delta t_{j-} + \\ & + \left(-\bar{\lambda}^T_{(j-1)+} + \frac{\partial \varphi}{\partial \bar{x}_{(j-1)+}} + \bar{\mu}^T \left[\frac{\partial \bar{\chi}}{\partial \bar{x}_{(j-1)+}} \right] \right) \delta \bar{x}_{(j-1)+} + \\ & + \left(\bar{\lambda}^T_{j-} + \frac{\partial \varphi}{\partial \bar{x}_{j-}} + \bar{\mu}^T \left[\frac{\partial \bar{\chi}}{\partial \bar{x}_{j-}} \right] \right) \delta \bar{x}_{j-} + \\ & + \sum_j \int_{t_{(j-1)+}}^{t_{j-}} \left(\left(\frac{\partial H}{\partial \bar{x}} + \dot{\bar{\lambda}}^T \right) \delta \bar{x} + \frac{\partial H}{\partial \bar{u}} \delta \bar{u} \right) dt \qquad j = 1, ..., n_f \end{aligned} \tag{2.15}$$

The necessary condition for the optimality imposes that the functional J^* is stationary; hence its first variation must be null for any choice of the variations $\delta \bar{x}$, $\delta \bar{u}$, $\delta \bar{x}_{(j-1)+}$, $\delta \bar{x}_{j-}$, $\delta t_{(j-1)+}$, δt_{j-} compatible with the differential equations and the boundary conditions. The necessary condition for the optimality becomes the simultaneous nullification of all the coefficient of the variations in eq. (2.15). Additional variables $\bar{\lambda}(\cdot)$ and constants $\bar{\mu}$, previously introduced, can be chosen in order to ensure the fulfillment of the stationarity of the merit index ($\delta J = 0$). Specifically, the Euler-Lagrange equations (i.e., the differential equations that govern the evolution of the adjoint variables) are obtained by nullifying the coefficient of $\delta \bar{x}$ under the integral sign:

$$\frac{d\bar{\lambda}}{dt} = -\left(\frac{\partial H}{\partial \bar{x}} \right)^T \tag{2.16}$$

whereas the algebraic equation for the controls are obtained by nullifying the coefficient of $\delta\bar{u}$ under the integral sign:

$$\left(\frac{\partial H}{\partial \bar{u}}\right)^T = 0 \tag{2.17}$$

Often, the control is subjected to external constraints. Usually it must belong to a given admissibility set (that is the case when the thrust magnitude must be between a minimum and a maximum value). In the most general case, this constraint depends on the independent variable or on the state ones; however, in this discussion, only explicit and constant bounds on the control (as the one previously stated) will be dealt with. If such a constraint is present, the optimal control value in any point of the trajectory is the one that belongs to the admissibility domain and maximize (if J has to be maximized) or minimize (if a minimum of J is sought) the Hamiltonian in that point. This result is known as Pontryagin Maximum Principle. In practice, two cases arise:

- the optimal control value is the one given by equation (2.17) if it is encompassed in the admissibility domain; hence the control constraint is not active in that point (the control is "locally un-constrained");

- The optimal control is set to the edge of the admissibility domain (i.e. it assumes the maximum of minimum value), if the one provided by equation (2.17) does not belong to the admissibility domain (the control is "locally constrained")

A peculiar case arises whenever the Hamiltonian is affine with respect to a bounded control variable. In that case, this variable does not appear explicitly in any of equations (2.17) and thus the corresponding control is undetermined. This case will be extensively discussed in Chapter 3, where special methods to deal with this kind of optimal control problem are presented. The reader can refer to [39] for details concerning the solution of problems with more complex control or control and state constraints. For what concerns the other coefficients of eq. (2.15), their nullification leads to the formulation of the so called transversality (or optimality) conditions. Nullifying the coefficient of

$\delta\bar{x}_{j-}$, $\delta\bar{x}_{(j-1)+}$, δt_{j-}, $\delta t_{(j-1)+}$, one obtains respectively:

$$-\bar{\lambda}_{j-}^T + \frac{\partial\varphi}{\partial\bar{x}_{j-}} + \bar{\mu}^T\left[\frac{\partial\bar{\chi}}{\partial\bar{x}_{j-}}\right] = 0 \tag{2.18}$$

$$\bar{\lambda}_{(j-1)+}^T + \frac{\partial\varphi}{\partial\bar{x}_{(j-1)+}} + \bar{\mu}^T\left[\frac{\partial\bar{\chi}}{\partial\bar{x}_{(j-1)+}}\right] = 0 \tag{2.19}$$

$$H_{j-} + \frac{\partial\varphi}{\partial t_{j-}} + \bar{\mu}^T\frac{\partial\bar{\chi}}{\partial t_{j-}} = 0 \tag{2.20}$$

$$-H_{(j-1)+} + \frac{\partial\varphi}{\partial t_{(j-1)+}} + \bar{\mu}^T\frac{\partial\bar{\chi}}{\partial t_{(j-1)+}} = 0 \tag{2.21}$$

for $j = 1, ..., n_f$

where the subscript "$j-$" and "$j+$" indicate values referred to instants immediately before or after the j-th boundary. In many circumstances, this distinction is fundamental because dependent and independent variables may be discontinuous at an internal boundary. Starting from the general transversality conditions just derived, it is possible to define a small set of practical specific rules, useful to understand quickly most of the problems:

- if a state variable x is assigned explicitly at the initial point (that is, the constraint vector $\bar{\chi}$ contains an equation of kind $x_0 - \tilde{a} = 0$ with $\tilde{a}$ an assigned value), the corresponding adjoint variable λ_{x_0} is "free", that is, unconstrained there. An analogous rule applies to the final point;

- if the initial value of a state variable x_0 appears neither in any constraint, nor in the objective function φ, then the corresponding adjoint variable is zero at the initial time ($\lambda_{x_0} = 0$); an analogous statement holds for the final boundary;

- If a state variable x is continuous at an internal boundary j and its value is not assigned explicitly or implicitly (that is $\bar{\chi}$ contains the equation $x_{j+} = x_{j-}$), then the corresponding adjoint variable is itself continuous ($\lambda_{x_{j+}} = \lambda_{x_{j-}}$);

- If a state variable x is continuous at an internal boundary j but its value is explicitly assigned, (i.e., the constraint vector $\bar{\chi}$ contains an equation of kind $x_{j+} = x_{j-} = \tilde{a}$ with $\tilde{a}$ an assigned value), than the corresponding adjoint variable λ_x has a free jump at that boundary (that is, the value of $\lambda_{x_{j+}}$ is independent from $\lambda_{x_{j-}}$) and must be determined by the optimization procedure.

Analogously, if the Hamiltonian does not depend explicitly on time, the eqs. (2.20), and (2.21) provide, in peculiar circumstances, very simple boundary conditions:

- if the initial time t_0 does not appear neither in the boundary conditions nor in the objective function explicitly, then the Hamiltonian is zero at the initial time ($H_0 = 0$); in an analogous way, if the final time t_f does not appear explicitly in $\bar{\chi}$ and φ, than the Hamiltonian at that time is zero ($H_f = 0$);

- if the time t_j of an internal bound does not appear explicitly in the function φ, and the only condition regarding it is the time continuity ($t_{j+} = t_{j-}$), than the Hamiltonian is continuous at the j-th boundary ($H_{j+} = H_{j-}$);

- if the time t_j is assigned explicitly (i.e., $\bar{\chi}$ contains the equation $t_{j+} = t_{j-} = a$), then the Hamiltonian has a free jump at that boundary (that is, the value of H_{j+} is independent from H_{j-}) and must be determined by the optimization procedure.

The Hamiltonian boundary value problem can now be stated in its general form:

$$\begin{cases} \dfrac{d\bar{x}}{dt}(t) = \bar{f}\left(\bar{x}(t), \bar{u}(t), t\right) \\ \dfrac{d\bar{\lambda}}{dt}(t) = -\left(\dfrac{\partial H}{\partial \bar{x}}\right)^T \qquad , \quad \forall t \in [t_0, t_f] \\ \text{s.t.} \\ \quad \dfrac{\partial H}{\partial \bar{u}} = 0, \quad \forall t \in [t_0, t_f] \\ \qquad -\bar{\lambda}_{j-}^T + \dfrac{\partial \varphi}{\partial \bar{x}_{j-}} + \bar{\mu}^T \left[\dfrac{\partial \bar{\chi}}{\partial \bar{x}_{j-}}\right] = 0 \\ \quad \bar{\lambda}_{(j-1)+}^T + \dfrac{\partial \varphi}{\partial \bar{x}_{(j-1)+}} + \bar{\mu}^T \left[\dfrac{\partial \bar{\chi}}{\partial \bar{x}_{(j-1)+}}\right] = 0 \\ \qquad H_{j-} + \dfrac{\partial \varphi}{\partial t_{j-}} + \bar{\mu}^T \dfrac{\partial \bar{\chi}}{\partial t_{j-}} = 0 \\ \quad -H_{(j-1)+} + \dfrac{\partial \varphi}{\partial t_{(j-1)+}} + \bar{\mu}^T \dfrac{\partial \bar{\chi}}{\partial t_{(j-1)+}} = 0 \end{cases} \tag{2.22}$$

A concise form is in general preferable. Let $\bar{y} \in \mathbb{R}^{2n+p}$ be a vector which collects state $\bar{x}(t)$, adjoint $\bar{\lambda}(t)$ and (constant) unknown parameters $\bar{c} \in \mathbb{R}^p$:

$$\bar{y}(t) = \left(\bar{x}(t), \bar{\lambda}(t), \bar{c}\right)^T \tag{2.23}$$

Recalling the notation of section [2.2.1] (eq 2.5), it is possible to define two vectors that collect the values that $\bar{y}$ assumes at either side of the boundaries (e.g., at the interfaces):

$$\bar{Y}_+ = \left\{\bar{y}_{(j-1)+},\ \forall\, j = 1, \ldots, n_f\right\} \qquad \bar{Y}_- = \left\{\bar{y}_{j-},\ \forall\, j = 1, \ldots, n_f\right\} \tag{2.24}$$

The Hamiltonian BVP can now be rewritten as:

$$\begin{cases} \dfrac{d\bar{y}}{dt}(t) = \bar{F}\left(\bar{y}(t), \bar{u}(t), t\right), \quad \forall t \in [t_0, t_f] \\ \text{s.t.} \\ \quad \dfrac{\partial H}{\partial \bar{u}} = 0, \qquad \forall t \in [t_0, t_f] \\ \quad \bar{\Psi}\left(\bar{Y}_+, \bar{T}_+, \bar{Y}_-, \bar{T}_-\right) = 0 \end{cases} \tag{2.25}$$

where $\bar{\Psi}$ is the vector of the boundary conditions.

2.3.2 Numerical Methods for Indirect Optimization

Indirect methods permit to obtain the solution of optimal control problems via the solution of Hamiltonian boundary problems. Numerical methods than can be employed to solve generic BVPs falls into two categories: shooting techniques and collocation methods. Beside these general-purpose methods, a sequential gradient restoration algorithm can be used to solve nonlinear BVPs that come from optimal control problems. Shooting methods transform a BVP into a sequence of IVPs leaded to convergence by a Newton-like method (or a gradient one). They are appealing because simple to understand, yet very efficient as they exploit performing and well-established algorithms for the solution of initial value problems. However, the success of their use is strongly linked to the behavior of the IVP: whether the system dynamics is unstable or chaotic, convergence issues arise and the solution might not be attained. Collocation methods are conceptually different, as no initial value problem is explicitly integrated; instead, an approximate solution is sought over the entire interval of interest. This permits a more global approach to the BVP solution, where convergence issues due to IVP instability are avoided. Unfortunately, these methods rely on low order quadrature schemes, therefore their computational efficiency is lower than a shooting method. Sequential Gradient Restoration [40, 41] is a very robust algorithm that has been extensively used in aerospace vehicle problems. It relies on the solution of many auxiliary linear two

point boundary value problems, whose solution is found via the method of particular solutions. The solution of the original HBVP is found iteratively, after performing a sequence of gradient and restoration steps.

The purpose of this section is to outline key features of these methods and their more suitable application fields, in order to justify the choice of the simple shooting technique as solution method used in the remaining part of this thesis. For a more comprehensive treatment of the numerical solution of boundary value problems the reader can refers to Ascher [17, 42] and Keller [16].

Shooting Methods

Shooting techniques are useful and easy-to-understand methods to solve boundary value problems. The solution procedure consists in finding the vector of initial values and unknown parameters $\bar{y}_0^*$ which permits the fulfillment of all the boundary conditions (within a prescribed tolerance). The value of the dependent variables at the boundaries (i.e., $\bar{Y}_+$, $\bar{Y}_-$) can be calculated via numerical integration of the ODE system once initial conditions $\bar{y}_0$ are fully assigned. Thus, it is possible to rewrite (implicitly) the boundary condition vector in terms of the initial values only. The result is a multi-application, named Shooting Function S, which associates to any initial "state" a residual on the boundary conditions:

$$\begin{aligned} S : \mathbb{R}^K &\to \mathbb{R}^K \\ \bar{y}_0 &\mapsto \bar{\Psi}\left(\bar{Y}_+\left(\bar{y}_0\right), \bar{T}_+\left(\bar{y}_0\right), \bar{Y}_-\left(\bar{y}_0\right), \bar{T}_-\left(\bar{y}_0\right)\right) \end{aligned} \tag{2.26}$$

where K is the problem dimension (without any further simplification K equals the dimension of $\bar{y}_0$, therefore $K = 2n + p$). The roots of the shooting function provide the BVP solutions.

The task to be performed consists formally in solving a (nonlinear) root-finding problem which can be handled by standard (and well-established) numerical algorithms [43]. Ideally, the boundary value problem is transformed into a sequence of initial value problems (since any iteration of the root-finding method involves, at least, the solution of an IVP) led to convergence by means of a gradient or (better) a Newton-like method. The intuitive appeal of this approach is strengthened by the advanced state of numerical analysis for IVPs: good numerical methods for such problems are well developed [44]; efficient, flexible, general-purpose software is readily available in any mathematical

software library NetLib [45, 46], Nag [47]. Thus, one is able, at least in principle, to solve BVPs numerically with minimal problem analysis and preparation.

Unfortunately, the convergence of this method cannot be guaranteed under general assumptions (otherwise the existence of other solution methods would be inexplicable). Simple shooting is usually successful if the ODE system is not seriously unstable or very stiff for step-by-step solution, and good initial estimates can be found for the unknowns. A sufficiently good initial guess is required because shooting with a wrong initial guess may lead to an IVP whose solution might not exist over the whole integration domain and this would prevent the iterative process from converging. On the other hand, the stability of the IVP is required to guarantee the stability of the shooting algorithm. In fact, even when the BVP is well-conditioned, the simple shooting method can be useless if the IVP is unstable (i.e., it has fast -growing/-decaying modes or it has a chaotic behavior) because it would lead to a disastrous accumulation of round-off errors. This situation arises, for example, when dealing with the restricted three body problem. Here the chaotic dynamics reduce greatly the convergence possibilities of this method [48, 49] which usually does not converge at all, unless the machine precision is incremented (i.e., using quadruple precision).

There are many variant of the single shooting method that aim to enlarge its applicability field and reduce the drawbacks just highlighted; among them the most important is surely the multiple shooting method. The idea is to split the integration domain into smaller sub-domains. Analogously to single shooting, the values of the dependent variables at the beginning of each sub-domain(i.e. shooting node) are assumed as problem unknowns, but here separate integrations (i.e. solution segment) over each sub-domain are performed. The continuity of the original solution is restored by adding proper conditions at the edges of each interval. A new shooting function, which encompasses both continuity and the boundary conditions, is defined. As results, this method is more robust than the previous one; in fact the round-off error accumulation is bounded because each integration domain is smaller. On the other side, the number of unknowns is greater because it includes state and adjoint variables at any mesh point; more unknowns need to be guessed and hence the computational time increases. Again, it can be reduced by exploiting the structure of the new problem (i.e. the sparsity of the new shooting function); however, the simplicity of the single shooting method, which

is also its charming feature, is lost. For these reason the simple shooting method was preferred in this thesis.

Collocation Methods

In collocation methods, the (continuous) solution components of the boundary value problem (that are both state, adjoint and control variables) are approximated by piecewise-continuous functions. First, the time horizon is split into several sub-intervals, thus creating a mesh. Each sub-interval contains a small number of collocation points (whose number and position depend on the order of the method). The values of the BVP dependent variables at the collocation points are the newly-defined problem unknowns. At each collocation point the approximated solution has to verify exactly the differential equations of the BVP; instead, the continuity of piecewise function is enforced at any mesh point, together with boundary conditions, if any. Depending on the form of the approximated solution, we can have polynomial collocation, if the approximate solution is piecewise-polynomial, or orthogonal collocation, if the solution is approximated by a finite orthogonal polynomial expansion (notice that collocation points are located in different spots in either case). The nonlinear system of equations, which arise, is solved by means of a Newton-like method. The attained precision strongly depends on the mesh selection (and on the order of the polynomial approximation). The bigger the sub-interval number, the better the precision. Therefore, whenever high accuracy is demanded, the number of unknowns grows and the computation time increases consequently. As for direct methods, by exploiting the sparsity of the equations' system and proper parallelization techniques, it is possible to reduce the computation time. Finite difference methods can be assimilated to collocation methods, albeit there are some differences. Indeed, they share qualitatively the same strength and weakness points.

Gradient Restoration algorithm

A peculiar method to solve nonlinear Hamiltonian boundary value problems is the sequential Gradient Restoration algorithm proposed by Miele [40]. Here the solution of the original BVP is found through a cycle of gradient and restoration phases, each one involving the solution of a linear boundary value problem. The gradient phase aims to reduce the error in the optimality conditions, while the restoration phase is designed to force constraints satisfaction. To attain these goals, both phases are written as optimal

control problems. In the gradient phase the first-order change of the functional becomes the merit index to be minimized, subjected to the linearized differential equations, the linearized boundary conditions, and a quadratic constraint on the variations of control and additional unknown parameters. In the restoration phase, a functional quadratic in the variations of control and parameters is the merit index to minimize, subjected to the linearized differential equations and the linearized boundary conditions. The Hamiltonian BVPs associated to these optimal control problems are linear; hence their solution can be attained by the method of particular solution. After each gradient iteration, many restoration iterations are repeated until the error in the constraints (both algebraic and differential ones) of the original, nonlinear, HBVP is (almost) completely reduced to zero. Then a new gradient iteration takes place. The cycle ends when at the end of a restoration phase both errors in the optimality conditions (of the nonlinear HBVP) and errors in the constraints are below a given tolerance. This method proved to be very robust and it has been extensively used in aeronautical and space optimization. An important property is that it produces a sequence of feasible suboptimal solutions. The main drawbacks of this technique is the slow convergence rate to the final solution.

In this thesis an indirect method is used to obtain the solution of optimal control problems. The Hamiltonian boundary problems that arose are solved by means of a Simple Shooting Method. This choice is motivated by the simplicity, then flexibility, and the superior speed of this method in comparison to the others.

Chapter 3

Techniques for Bang-Bang Optimal Control Problems

3.1 Introduction

In the context of optimal control problems (not restricted to space applications, but more frequently in that case), there are many problems where the magnitude of the optimal control is bounded and assumes alternatively the maximum and the minimum achievable value. Control laws which exhibit such behavior are referred as bang-bang controls and the associated optimal control problems are therefore named bang-bang optimal control problems (or problems with bang-bang solution). The principal subject of this Chapter is the analysis of the main difficulties related to this peculiar class of problems and of the numerical solution methods that can be adopted to overcome them.

A general formulation for this kind of problems and the application of Pontryagin Maximum Principle in these specific instances are proposed in section [3.2.1]. The boundary value problems generated by a "pure" application of the Optimal Control Theory to this class of OCP are shown to be difficult to solve as they are. The principal issue in the numerical solution process consists of the precise determination of the switching instants, especially whenever their number is high. Numerical issues are due to the fact that the shooting function associated to the problem may be discontinuous and/or non-differentiable. Moreover, the Jacobian matrix of the shooting function may be singular for a given set of values. The radius of the attraction basin for the root of the shooting function is therefore reduced. A greater difficulty in the initialization

of the shooting method is induced. Last but not least, the RHS of the ODE system contains discontinuous terms that may corrupt the computed values of the shooting function.

In this Chapter, two different ways to handle these issues are described. A Multi-Bound approach is proposed first in section [3.3]. A different approach which makes use a mix of smoothing and continuation techniques is presented in section [3.4].

The Multi-Bound approach arises from the following considerations: when the switch on/off sequence is known (or reasonably guessed), it is possible to solve the problem (and avoid the numerical issues due to the bang-bang control) by performing a transformation which exploits this knowledge in order to restrict the search domain (that is, the solution domain). A mission structure is set, defining a sequence of phases where the control magnitude is alternatively maximum (propelled arcs) or null (coast arcs). This result is achieved by implementing a different set of differential equations in each arc: the thrust term is present in the propelled ones, it is removed in the coasting ones. The arc durations, which are usually unknown, become additional unknown parameters, whose values state clearly the switch instants of the control law. An equal number of boundary conditions have to be added (one for each switch point). Discontinuities are no longer present inside any arc (they are present only at arc extremities). The integration is therefore simpler, straightforward, and the regularity of the shooting function (as well as the Jacobian Matrix) is enhanced. The solution of this augmented problem is checked "a posteriori" (i.e., after it is solved) in order to ensure that it is the correct solution of the original bang-bang optimal control problem; otherwise a different phase sequence is tried until Pontryagin Maximum Principle is satisfied.

Conversely, smoothing techniques aim to regularize the problem (i.e., the control) and hence to enlarge the convergence basin of the root-finding method. A continuation is performed in order to achieve the solution of original problem, starting from the solution of a more regular problem, and moving through a series of auxiliary problems. A way to produce a more regular control consists in modifying the objective function of the problem introducing a perturbation term which depends on a parameter. The problem nature changes, due to transformation of the merit index; the optimal solution (i.e., the optimal control) and the shooting function are made more regular. The perturbation parameter is updated by either a continuation or a homotopy procedure [50, 51]. A rigorous justification of the convergence of the auxiliary problem sequence

to the original one can be demonstrated (under some hypothesis) and a simple proof is also provided in section [3.4.1.2]. The "par excellence" perturbation term, is a quadratic penalty. The reader can refer to Dadebo [52], Edgar [53, 54], or Jacobson [55] for further details. Afterwards, great effort was spent to improve the choice of the perturbation function in order to obtain better results than those obtained with the quadratic one: a whole class of (almost always) continuously differentiable control law was obtained, employing different perturbative terms [14]. Special emphasis is given here to smoothing techniques based on the use of a barrier function, since it was adopted to solve the complex problem formulated in Chapter 4 and 5. In the following sections these rudimentary concepts will be deeply explained and the effectiveness of each approach will be proved on a simple problem (sections [3.2.3] and [3.4.2]).

3.2 Bang-Bang control problems

In this section, a general formulation and the necessary optimal conditions related to Bang-Bang control problems are provided. The difficulties encountered during the numerical solution process are stated in section [3.2.2]. A simple example is proposed in section [3.3.3] in order to show the related issues.

3.2.1 Problem Formulation

The formulation of an optimal control problem proposed in Chapter 2 is as general as possible and the differential equations may be nonlinear in both state and control variables. Henceforward only systems that can be modeled with differential equations which are affine in the control vector will be considered. Most of space trajectory optimization problems (including those faced in this thesis) can be arranged to match this formulation. It will be shown that for this kind of system, if the control is constrained in magnitude and the merit index is linear in the control magnitude, the control shows a bang-bang behavior.

The problem under analysis has a dynamic model that can be written in the following form:

$$\dot{\bar{x}}\left(t\right) = \bar{f}\left(\bar{x}\left(t\right), t\right) + \bar{\bar{g}}\left(\bar{x}\left(t\right), t\right)\bar{u}\left(t\right) \ , \qquad \forall t \in \left[t_0, t_1\right] \tag{3.1}$$

The control is constrained in modulus; without any loss of generality this can be stated by:

$$\|\bar{u}(t)\| \leq 1 \tag{3.2}$$

The dimension of the state and control vectors are the same as those provided previously in section [2.2]. The system dynamics depends on the state of the system, but in general it may also depend explicitly on the independent variable time (for non autonomous systems). However, it is always possible to write a non-autonomous problem in an autonomous form simply by adding a fictitious state variable. Therefore the more concise notations $\bar{f}(\bar{x}(t))$ and $\bar{\bar{g}}(\bar{x}(t))$ can be used without any lack of generality. The system dynamics is split into two parts: a free-motion part, which correspond to the vector $\bar{f}(\bar{x}(t))$ whose dimension is $n \times 1$, and a controlled-motion part, which correspond to the vector $\bar{\bar{g}}(\bar{x}(t))\,\bar{u}(t)$, where $\bar{\bar{g}}$ is a $n \times m$ matrix and $\bar{u}(t)$ a $m \times 1$ vector. The functions $\bar{f}(\cdot)$ and $\bar{\bar{g}}(\cdot)$ are assumed to be sufficiently smooth. Initial and final constraint are the same discussed in Chapter 2.

A really simple derivation of the optimal control law is provided. Use is made only of the Pontryagin Maximum Principle and of elementary geometric considerations. Let J be the merit index (here expressed in the Lagrange form) to be maximized:

$$J = -\int_{t_0}^{t_f} \|\bar{u}(t)\| dt \tag{3.3}$$

Let U be the set of all the permitted command $u(t)$, constrained to a magnitude less or equal to one:

$$U = \left\{ \bar{u} \in L^2([t_0, t_1]; \mathbb{R}^m),\ \|\bar{u}(t)\| \leq 1, \quad \forall t \in [t_0, t_1] \right\} \tag{3.4}$$

The Hamiltonian associated to this problem can be stated as:

$$H\left(\bar{x}(t), \bar{u}(t), \bar{\lambda}(t), t\right) = -\|\bar{u}(t)\| + \bar{\lambda}(t)^T \left[\bar{f}(\bar{x}(t)) + \bar{\bar{g}}(\bar{x}(t))\,\bar{u}(t)\right] \tag{3.5}$$

The optimal control law $\bar{u}^*(t)$ can be found by applying the Pontryagin Maximum Principle, thus by definition:

$$\bar{u}^*(t) = \arg \max_{\|\bar{w}\| \leq 1} \left[\bar{\lambda}(t)^T \bar{\bar{g}}(\bar{x}(t))\,\bar{w} - \|\bar{w}\|\right], \qquad \forall t \in [t_0, t_1] \tag{3.6}$$

Clearly, if $\bar{\lambda}(t)^T \bar{\bar{g}}\left(\bar{x}\left(t\right)\right) = 0$, then $u^*\left(t\right) = 0$. Otherwise, the analytical expression of $\bar{u}^*\left(t\right)$ must be obtained through some mathematical manipulations. Rewriting the vector $\bar{w}$ in order to make evident its magnitude β and its direction $\hat{v}$, one gets:

$$\bar{w} = \beta\hat{v}, \qquad \text{with}\, \beta \geq 0,\ \|\hat{v}\| = 1 \tag{3.7}$$

The Hamiltonian can now be stated as:

$$H\left(\bar{x}\left(t\right), \bar{u}\left(t\right), \bar{\lambda}\left(t\right), t\right) = \bar{\lambda}(t)^T \bar{f}\left(\bar{x}\left(t\right)\right) + \beta\left(t\right)\bar{\lambda}(t)^T \bar{\bar{g}}\left(\bar{x}\left(t\right)\right)\hat{v}\left(t\right) - \beta\left(t\right) \tag{3.8}$$

and the optimal control is defined by:

$$\bar{u}^*\left(t\right) = \arg \max_{\substack{\|\hat{v}\|=1 \\ 0\leq\beta\leq 1}} \left[\beta\left(\bar{\lambda}(t)^T \bar{\bar{g}}\left(\bar{x}\left(t\right)\right)\hat{v} - 1\right)\right], \qquad \forall t \in [t_0, t_1] \tag{3.9}$$

Independently of the control magnitude (which must be non negative in any case), the control direction $\hat{v}$ that maximize the Hamiltonian must be a unity vector parallel to $\bar{\bar{g}}(\bar{x}\left(t\right))^T \bar{\lambda}\left(t\right)$. Therefore:

$$\hat{v}\left(t\right) = \frac{\bar{\bar{g}}(\bar{x}\left(t\right))^T \bar{\lambda}\left(t\right)}{\left\|\bar{\bar{g}}(\bar{x}\left(t\right))^T \bar{\lambda}\left(t\right)\right\|} \tag{3.10}$$

and the Hamiltonian becomes:

$$H\left(\bar{x}\left(t\right), \bar{u}\left(t\right), \bar{\lambda}\left(t\right), t\right) = \bar{\lambda}(t)^T \bar{f}\left(\bar{x}\left(t\right)\right) + \beta\left(t\right)\left(\left\|\bar{\bar{g}}(\bar{x}\left(t\right))^T \bar{\lambda}\left(t\right)\right\| - 1\right) \tag{3.11}$$

The coefficient of the control magnitude $\beta\left(t\right)$ is collected in a function named Switch Function:

$$S_F\left(t\right) = \left\|\bar{\bar{g}}(\bar{x}\left(t\right))^T \bar{\lambda}\left(t\right)\right\| - 1 \tag{3.12}$$

Considering fixed any other variable, the control magnitude $\beta\left(t\right)$ that maximizes the Hamiltonian is the maximum (allowed) value if the Switch Function is positive, the minimum if negative. The optimal control function is therefore:

$$\bar{u}^*\left(t\right) = \begin{cases} 0 & \text{if } \left\|\bar{\bar{g}}(\bar{x}\left(t\right))^T \bar{\lambda}\left(t\right)\right\| = 0 \\ \beta^*\left(t\right) \frac{\bar{\bar{g}}(\bar{x}(t))^T \bar{\lambda}(t)}{\left\|\bar{\bar{g}}(\bar{x}(t))^T \bar{\lambda}(t)\right\|} & \text{if } \left\|\bar{\bar{g}}(\bar{x}\left(t\right))^T \bar{\lambda}\left(t\right)\right\| \neq 0 \end{cases} \tag{3.13}$$

with

$$\beta^*\left(t\right) = \begin{cases} 0 & \text{if } S_F\left(t\right) < 0 \\ 1 & \text{if } S_F\left(t\right) > 0 \end{cases} \tag{3.14}$$

This control law is named bang-bang, since its magnitude jumps alternatively from the maximum to the minimum allowable values (i.e., 0 and 1) and vice versa.

The case of a Switch Function identically null over a finite time interval is not considered in eq. (3.14). In that occurrence, a singular arc arises: along the portion of the optimal trajectory where $S_F = 0$, the Hamiltonian is not an explicit function of the control variables and higher-order necessary conditions are needed to determinate the optimal control. In particular, all the time derivatives of the Switch Function up to the least order at which the control appears explicitly have to be posed equal to zero [39]. However, singular arcs do not exist in the numerical problems considered in this thesis; thus equation (3.14) encompasses all the possible instances.

3.2.2 Numerical Issues

The most important numerical issues that the user may find in searching for the solution of an optimal bang-bang problem are summarized in this section. As described in section [2.3.2], the value of the shooting function (i.e., the errors on the boundary conditions) of a given BVP are obtained (at least partially) by numerical solution of the underlying ODE system. This set of differential equations contains some terms that are not continuous in time, due to the presence of a bang-bang control law. In these cases, the numerical integration algorithm with adaptive stepsize (such as Runge-Kutta-Fehlberg [47], but also Adam Moulton [56] which moreover is a multistep one, that is, it uses past solution history to advance the integration) cannot work properly; fixed stepsize methods would behave better in case of discontinuities, but their efficiency is too low to make them useful in practical applications. They might not ensure that the result is achieved with the prescribed accuracy, especially (but not only) when the number of discontinuity instances (i.e., switch points) is high (see [57, 58]). Moreover, for some values of the unknown parameters, the shooting function may not be evaluable (the integration cannot be terminated) or the attained results has poor precision. The Newton method or the Hybrid-Powell method [43], which descends from the Newton one, are used to search of the root of the shooting function. In theses cases, the shooting function must be sufficiently regular (i.e., the Jacobian matrix must be non singular) in a neighborhood of the root, so that the numerical method could converge. This neighborhood is often quite small in case of the shooting function associated to a bang-

bang control problem. For these reasons, some peculiar techniques must be used to enlarge the attracting basin of the shooting function roots.

3.2.3 An illustrative example

In this section, a simple example is faced in order to highlight the numerical issues previously announced. The problem under investigation is the well-known rocket sled problem: a one-dimensional mass point, with constant mass, has to cover a fixed distance in a fixed time, arriving and departing with zero velocity. The maximum value of acceleration or deceleration provided by the control is limited. The goal is to minimize the control consumption. Numerical data for this application, are nondimensional distance $x_f - x_0 = 1/2$; nondimensional time $t_f - t_0 = 2$; control constraint $|u| \leq 1$. The mathematical formulation of the OCP is:

$$OCP = \begin{cases} \max J = \displaystyle\int_0^2 -|u(t)|\, dt \\ \ddot{x} = u(t), \qquad t \in [0,2] \\ \text{s.t.} \\ \quad |u| \leq 1 \\ \quad x(0) = 0; \qquad \dot{x}(0) = 0 \\ \quad x(2) = 1/2; \quad \dot{x}(2) = 0 \end{cases} \tag{3.15}$$

The problem can be easily rewritten in order to obtain a system of first order differential equations as in eq. (3.1); it is sufficient to use position and velocity to describe the system state. Therefore, one has state vector $\bar{x} = \begin{bmatrix} x & v \end{bmatrix}^T \in \mathbb{R}^2$, control variable $\bar{u} = [u] \in \mathbb{R}$, free dynamics $\bar{f}(\bar{x}(t)) = \begin{bmatrix} v & 0 \end{bmatrix}^T$, and controlled dynamics $\bar{\bar{g}}(\bar{x}(t))^T \bar{u} = \begin{bmatrix} 0 & u \end{bmatrix}^T$. The adjoint vector $\bar{\lambda} = \begin{bmatrix} \lambda_x & \lambda_v \end{bmatrix}^T \in \mathbb{R}^2$ is introduced. Finally, the Hamiltonian can be stated:

$$H = \lambda_x v + \lambda_v u - |u| \tag{3.16}$$

Adjoint variables are subject to Euler-Lagrange equations (2.16):

$$\dot{\lambda}_x = 0 \qquad\qquad \dot{\lambda}_v = -\lambda_x \tag{3.17}$$

The switch function is stated by eq. (3.12):

$$S_F(t) = \left\| \bar{\bar{g}}(\bar{x}(t))^T \bar{\lambda}(t) \right\| - 1 = |\lambda_v(t)| - 1 \tag{3.18}$$

hence, the control law is:

$$u(t) = \begin{cases} \beta(t) \dfrac{\lambda_v}{|\lambda_v|} & \text{if } \lambda_v \neq 0 \\ 0 & \text{if } \lambda_v = 0 \end{cases} \qquad \text{with} \qquad \beta(t) = \begin{cases} 0 & \text{if } S_F \leq 0 \\ 1 & \text{if } S_F > 0 \end{cases} \tag{3.19}$$

that can also be written in a more concise form:

$$u(t) = \begin{cases} -1 & \text{if } \lambda_v < -1 \\ 0 & \text{if } -1 \leq \lambda_v \leq 1 \\ +1 & \text{if } \lambda_v > +1 \end{cases} \tag{3.20}$$

The BVP that arises is:

$$BVP = \begin{cases} \dot{y} = \bar{F}(y(t), u(t), t) = \begin{cases} \dot{x} = v \\ \dot{v} = u \\ \dot{\lambda}_x = 0 \\ \dot{\lambda}_v = \lambda_x \end{cases}, \qquad t \in [0, 2] \\ \\ \begin{matrix} x(0) = 0 & x(2) = 1/2 \\ v(0) = 0 & v(2) = 0 \end{matrix} \end{cases} \tag{3.21}$$

Due to its simplicity, this BVP can be solved analytically. The solution of the boundary value problem is unique and it is attained for $[\lambda_{x_0}, \lambda_{v_0}] = \left[\sqrt{2}, \sqrt{2}\right]$. The optimal trajectory $\bar{x}^*(\cdot)$ and the associated control law $u^*(\cdot)$ are shown in Figure 3.1 and 3.2.

From a numerical point of view, the BVP can be solved by a shooting method, that is, by looking for the roots of the associated shooting function S, which is defined as:

$$\begin{aligned} &S : \mathbb{R}^2 \to \mathbb{R}^2 \\ &\bar{z} = [\lambda_{x_0}, \lambda_{v_0}] \mapsto \bar{x}_f - [1/2,\ 0] \end{aligned} \tag{3.22}$$

Some of the issues concerning the solution of bang-bang control problems (anticipated in section [3.2.2]) can be found even in this simple example. The BVP is numerically well conditioned, and the loss of accuracy along the integration is not noteworthy. Instead, there are significant regions of the search space where the Jacobian matrix of the shooting function is not defined or where it singular.

Figure 3.3(a) and 3.3(b) show the behavior of the shooting function components $S_1(\bar{z}) = x_f - 1/2$ and $S_2(\bar{z}) = v_f$ over a portion of the search space. The uniqueness of the solution is visually confirmed by Figure 3.3(c), which presents the norm of

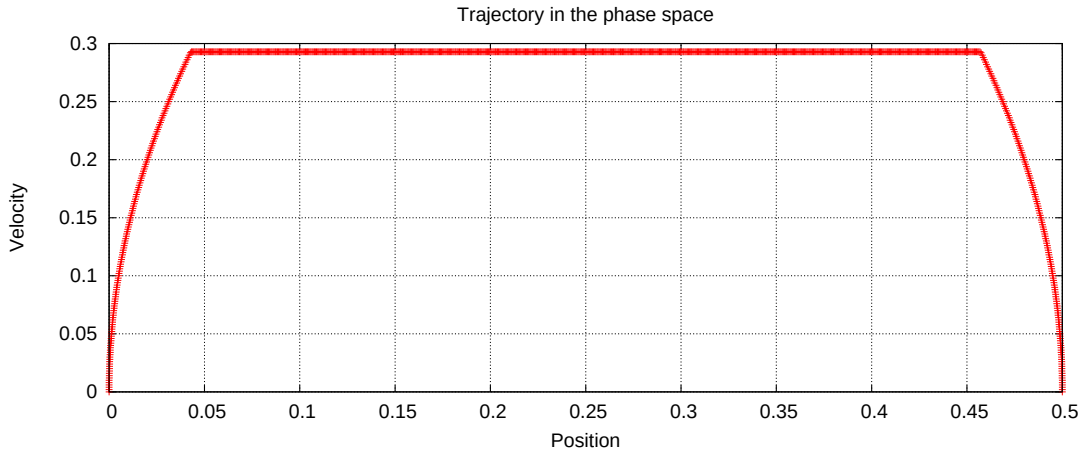

Figure 3.1: Optimal trajectory for the rocket sled problem in the phase space.

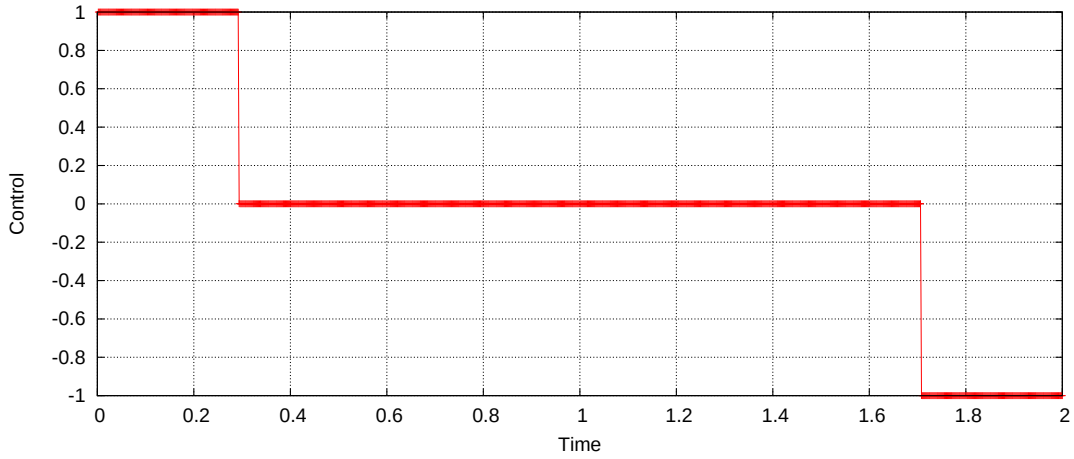

Figure 3.2: Optimal control law u^* for the rocket sled problem.

the shooting function over the same domain. In particular, the surface of both error components shows the existence of 3 plateaux, where the Jacobian matrix is singular.

The search space can be partitioned into zones with different control structures, meaning that each guess that belongs to that region corresponds to a solution with the same control structure. A graphical presentation of these zones is presented in Figure 3.4. Each region is named so that its subscript provides immediately all the information on the control structure (number of switches and the control value); in particular, the subscript contains the value assumed by the control variable all along

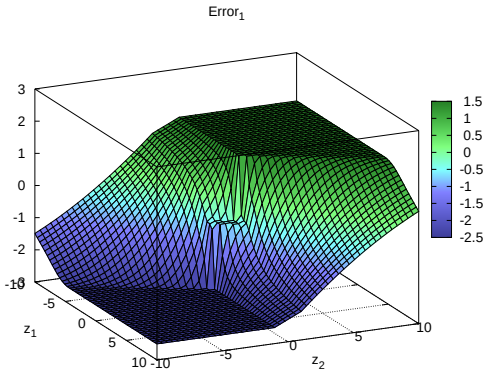

(a) First Error Component

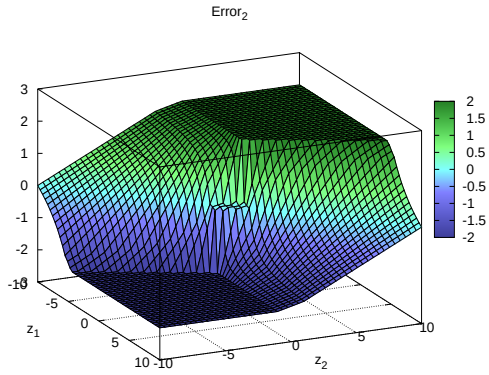

(b) Second Error Component

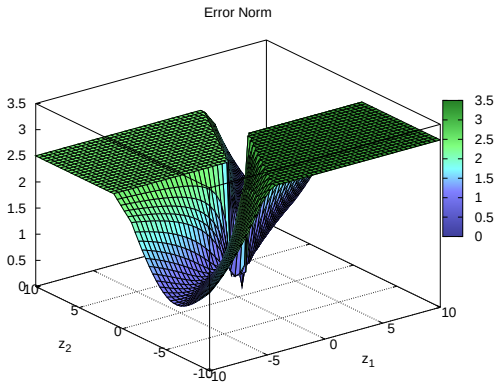

(c) Error Norm

Figure 3.3: Components and norm of the Shooting function for the rocket sled problem.

the trajectory (e.g. $U_{+1,0,-1}$ stands for a region with a acceleration, $u = 1$, a coasting, $u = 0$, and a deceleration, $u = -1$). Observe that this graphical analysis of the control structure as a function of the unknown vector $\bar{z}$ is here possible (and quite clear) only because the search space has dimension 2 (that is, $\bar{z} \in \mathbb{R}^2$), whereas in practical cases it cannot be used due to the higher problem dimensionality.

Nine different control law regions exist. Control structures can feature 0, 1, or 2 switching points. In three regions (U_{+1}, U_0, U_{-1}) there are no switching points. These regions extend over the sets:

$$U_1 = \{\bar{z} \mid z_2 > 2z_1 - 1 \ \wedge \ z_2 > 1\} \tag{3.23}$$

$$U_0 = \{\bar{z} \mid 2z_1 - 1 < z_2 < 2z_1 + 1 \ \wedge \ -1 < z_2 < +1\} \tag{3.24}$$

$$U_{-1} = \{\bar{z} \mid z_2 < 2z_1 - 1 \ \wedge \ z_2 < -1\} \tag{3.25}$$

Here there is a "lack of control", or, to be precise, a lack of possibility of modifying the control (hence the trajectory) by a small change of the unknowns. Therefore, the shooting function is constant in these regions, and the Jacobian matrix singular.

The Jacobian is not defined along the 4 semi-straight lines (highlighted in bold in Figure 3.4) that bound regions where the Jacobian is singular:

$$l_1 = \{z_2 = 1 \ \wedge \ z_1 < 1\} \tag{3.26}$$

$$l_2 = \{z_2 = 2z_1 + 1 \ \wedge \ z_1 \geq -1\} \tag{3.27}$$

$$l_3 = \{z_2 = 2z_1 - 1 \ \wedge \ z_1 < 1\} \tag{3.28}$$

$$l_4 = \{z_2 = -1 \ \wedge \ z_1 \geq -1\} \tag{3.29}$$

In the same figure, dotted lines separate zone with different control laws where the transition is instead smooth.

Ignoring the knowledge of the analytical solution, the numerical shooting method proposed in Chapter 2 for the solution of BVPs can be here employed. The convergence of the method depends on the specific root-finding algorithm, on its setup, and on the given initial guess $\bar{z}^0$. To highlight the convergence region for each of the root-finding algorithms, all the points belonging to the uniform 51×51 grid defined over the set $D = [-10, 10]^2$ were considered as initial guesses. Results are presented in Figure 3.5: each point of the grid (hence initial guess) which leads to the optimal solution is indicated with a mark; points not leading to the optimal solution are left

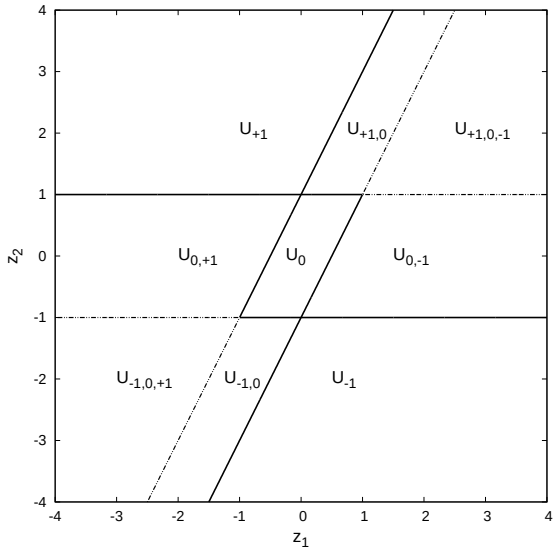

Figure 3.4: Subdivision of the search-space into regions with different control structures. Subscripts refer to the control structure that characterize each region.

unmarked. Hybrid-Powell method performs better than relaxed Newton method in this test, despite the relaxation factor values. However, increasing the relaxation (i.e., reducing the relaxation factor R_{min}) the convergence region widen.

3.3 Solution through a Multi-Bound approach

In this section the Multi-Bound approach, which has proven its capability of handling bang-bang control problems in many circumstances [13, 59], is described. First, the technique is introduced in an intuitive way; subsequently, a more rigorous and analytical development is performed. Afterwards, strengths and weaknesses of this method are enlightened in section [3.3.2] and verified in section [3.3.3] through the application at the illustrative example discussed in section [3.2.3].

3.3.1 Method description

In section [3.2.2] it was pointed out that many troubles connected to bang-bang control problems are linked to the solution of ODE system with discontinuous RHS. If all commutation instants (i.e., the switch on/off instants) were known, one could imagine

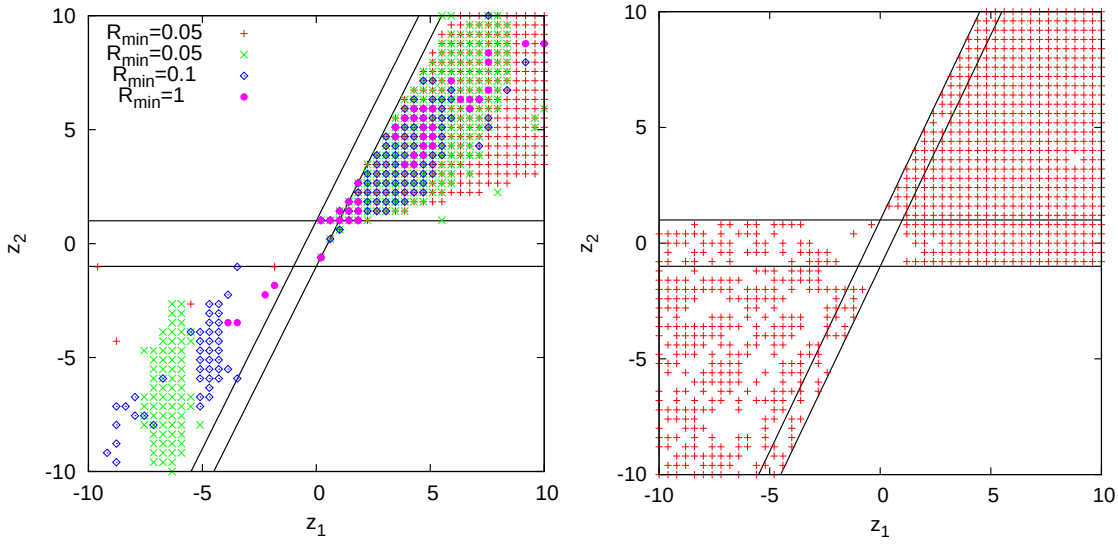

(a) Relaxed Newton Method (for several values of the relaxation parameter R_{min})

(b) Hybrid-Powell Method

Figure 3.5: Convergence map for the rocket sled problem: comparison between Relaxed Newton method and Hybrid Powell method.

to split the integration domain into many subsets where the control magnitude is alternatively null or maximum. The discontinuities would be moved at the edges of the integration intervals and only continuous, smooth, terms would be still present in the RHS. None of the shortcomings described above would have place. However, commutation instants are not known in advance in practical optimal control problems. To be precise, both their overall number and their values are unknown. In fact, these are often the most interesting information that comes out from optimization. Therefore, this transformation seems not to be possible at a first glance.

The crucial point is that, if the sequence of thrust and coast arc is known (and consequently the number of commutation points is known), it is possible to build an augmented optimal control problem where the control magnitude is no longer unknown but fixed and fulfills control constraint eq. (3.2), assuming either the minimum or maximum allowed values. The values of the independent variable at the switch instants are considered additional unknown parameters and become part of the BVP solution. The Multi-Bound approach is based on this assumption, which is better described in

the following.

Let B be an assumed mission structure (i.e., a sequence of burn and coast arcs). Each mission structure corresponds to a precise subdivision of the trajectory into a finite number n_{cmp} of arcs (or phases) and consequently a precise number of switch points n_{sw}. These two integer numbers are linked by the relation $n_{sw} = n_{cmp} - 1$. From a mathematical point of view, the mission structure B can be seen as a set of the values that the magnitude of the control assumes in each arc, therefore

$$B = \{\beta_i,\ i = 1, \ldots, n_{cmp}\}\,, \qquad \text{with } \beta_i = \{0, 1\} \tag{3.30}$$

A new independent variable t_ε is introduced. The purpose is to rescale each integration interval, so that independent variable always assumes known integer values at the edges:

$$t_\varepsilon = i - 1 + \frac{t - t|_{i-1}}{t|_i - t|_{i-1}}\,, \qquad i = 1 \ldots n_{cmp} \tag{3.31}$$

where $t|_i$ is the (unknown) value of the independent variable (i.e., the time) at the i-th boundary. Sometimes it may be useful to consider as unknowns the time-lengths τ_i of the original intervals instead of the switch instants. These two sets of unknown are related by the following equation:

$$\tau_i = t|_i - t|_{i-1}, \qquad i = 1 \ldots n_{cmp} \tag{3.32}$$

Eventually, the augmented MPBVP has $n_{sw} = n_{cmp} - 1$ additional unknowns, in comparison with the original problem. An equal number of sufficient optimality conditions is provided by the application of the transversality conditions (eqs. 2.18 to 2.21) at the internal bounds. State variables are all continuous at these boundaries and none is subject to other constraints. Therefore the corresponding adjoint variables are also continuous (c.f. section [2.3.1]):

$$\bar{x}|_{i-} - \bar{x}|_{i+} = 0, \qquad i = 1, \ldots, n_{sw} \tag{3.33}$$

$$\bar{\lambda}|_{i-} - \bar{\lambda}|_{i+} = 0, \qquad i = 1, \ldots, n_{sw} \tag{3.34}$$

Moreover, the time is continuous and free, thus the Hamiltonian is continuous:

$$t|_{i-} - t|_{i+} = 0, \qquad i = 1, \ldots, n_{sw} \tag{3.35}$$

$$H|_{i-} - H|_{i+} = 0, \qquad i = 1, \ldots, n_{sw} \tag{3.36}$$

The Hamiltonian can be expanded so that the command magnitude appears explicitly:

$$H = \bar{\lambda}^T \bar{f}(\bar{x}) + \bar{\lambda}^T \bar{\bar{g}}(\bar{x})\,\bar{u} - \|\bar{u}\| \tag{3.37}$$

By replacing control vector $\bar{u}$ with the optimal control expression found in section [3.2.1], it becomes:

$$\begin{aligned} H &= \bar{\lambda}^T \bar{f}(\bar{x}) + \beta\left(1 + \left\|\bar{\bar{g}}(\bar{x})^T \bar{\lambda}\right\|\right) \\ &= \bar{\lambda}^T \bar{f}(\bar{x}) + \beta S_F \end{aligned} \tag{3.38}$$

Thus, the optimality condition at the internal boundary is:

$$\bar{\lambda}\big|_{i-}^{\,T} \bar{f}\left(\bar{x}|_{i-}\right) + \beta_{i-} S_F|_{i-} - \bar{\lambda}\big|_{i+}^{\,T} \bar{f}\left(\bar{x}|_{i+}\right) + \beta_{i+} S_F|_{i+} = 0 \tag{3.39}$$

Recalling the continuity of state and adjoint variables at the switching boundaries, eqs. (3.33-3.34), one has $S_F|_{i-} = S_F|_{i+}$ and the optimality condition becomes:

$$\left(\beta_{i-} - \beta_{i+}\right) S_F|_i = 0 \tag{3.40}$$

being dropped the unnecessary plus and minus signs of the switch function. The sequence of arcs is characterized by an alternate of full-thrust and null-thrust arcs; therefore one of the two control magnitude values (β^{i-} or β^{i+}) is equal to zero, while the other is unitary. Thus, the additional boundary conditions, either in the case of a switch-on or a of switch-of boundary, can be written as:

$$S_F|_i = 0, \qquad i = 1, \ldots, n_{sw} \tag{3.41}$$

In general, it is possible to define several strategies, each one corresponding to a different augmented OCP. However, it is probable that some of them have a solution. Among all the physically acceptable solutions, those solving the original BVP are those which respect the Pontryagin Maximum Principle; the associated switch sequences are (locally) optimal. It is worthwhile to stress here that even the original BVP may have more than one physical solution. This is a common situation in real application (such as in the case of multi-revolution finite-thrust transfers). Anyway, for each physical solution of the original BVP there is just one solution of an augmented BVP which is both physical and PMP-respecting. Indeed, if the original BVP has only one solution, so will have the set of the augmented one.

The mathematical condition that ensures the respect of PMP is the same as eq. (3.14), but it is formulated in the inverse fashion:

$$S_F(t_\varepsilon)\begin{cases} < 0 & \text{if } \beta_i = 0 \\ > 0 & \text{if } \beta_i = 1 \end{cases}, \quad \forall t_\varepsilon \in]i-1, i[\,, \ \ \forall i \in [1, n_{cmp}] \tag{3.42}$$

In the framework of the Multi-Bound approach, this condition can be also referred to as PMP optimality criterion. Besides allowing to distinguish between (locally) "optimal" and "sub-optimal" solutions, the Pontryagin maximum principle will be used to address the research of the right switch sequence, whenever the assigned one produces a solution which does not satisfy eq. (3.42). In fact, by inspecting the switch function of the solution of an augmented BVP, one can devise many information on the basis of which the mission structure is changed (to achieve a better merit index).

A solution which respects the PMP optimality condition is represented in Figure 3.6(a). The switch function assumes negative values during the coast arcs (which is in the middle) and positive values in the burn arcs (at the left and right sides) $\beta|_i = 1$. The case of a non-PMP solution is shown in Figure 3.6(b). The switch function is positive inside a coast-arc. In this case it is easy to demonstrate that this solution can be improved by adding a propelled arc inside the coasting. In fact, by introducing an infinitesimal thrust in a point where $S_F > 0$, the Hamiltonian (eq. 3.38) increases, thus the merit index increases. The instants which correspond to points where the switch function crosses the zero, constitute a reasonable initial guess for the additional two unknowns introduced by splitting the original coast-arc into a three-arc sequence (coasting-thrust-coasting). An analogous procedure is advisable in the case shown in Figure 3.6(c), where a burn arc contains an interval with $S_F < 0$.

3.3.2 Remarks on Multi-Bound approach

Apart from the aforementioned cases, where it is quite evident how to modify properly the switch structure B, an all-embracing rule that indicates how to adjust the burn structure in order to satisfy PMP cannot be formulated. In fact, the switch function $S_F(t)$ depends in a pretty complex way on the thrust. Therefore, no one can ensure that adding/removing an arc will be sufficient to produce the desired effect. As a general rule, the first tried burn-structure should contain the minimum number of thrust arcs which is necessary to fulfill the constraints (e.g., to reach the desired final

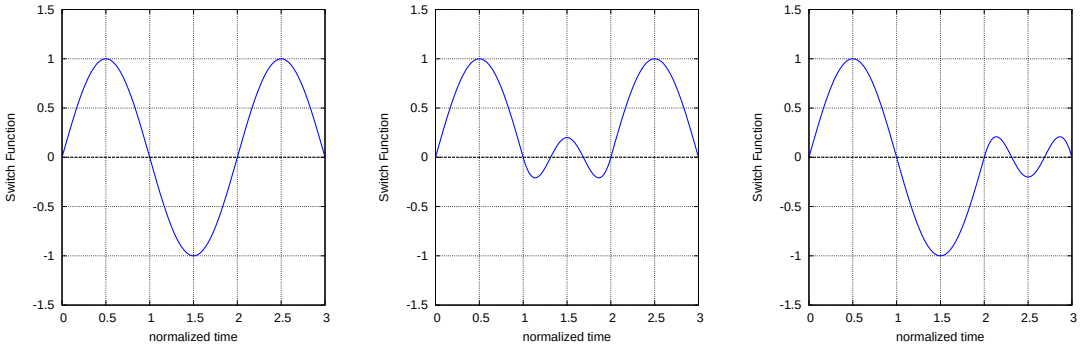

(a) PMP respected

(b) PMP not respected in a coasting arc

(c) PMP not respected in a burn arc

Figure 3.6: Some examples of Switching Functions.

conditions). In fact, if a solution with too many burn arcs is searched for, it may not exist or the root-finding method may converge to a solution that has no physical sense (i.e., time inversion may occur). Once a simple (sub-optimal) solution is found, further burns can be added (by looking at the switching function graph) in order to improve the mission. Note that by fixing the structure, the search space is "narrowed". Actually, the dimension of the unknown vector is greater, but the sensitivity of the trajectory to each unknown parameter is strongly reduced. This fact is extremely important as it means that crude estimate of the adjoint variables (whose optimal value is usually difficult to figure out) can be used without precluding the attainment of the convergence. As a final comment, the method cannot be fully automated. A user is needed in order to propose a reasonable switch structure and to correct it, whenever necessary. However, an experienced user can exploit his physical knowledge of the problem to produce an initial guess more suitable than the one produced using other general purpose methods. Therefore, even quite complex problems can be solved with this approach in a short amount of time [10].

3.3.3 Application of Multi-Bound Approach to the Rocket Sled problem

In this section the illustrative example shown in section [3.2.3] is solved by means of a Multi-Bound approach. The sequence of steps which are necessary to create the

augmented BVP and find the solution of the original problem are highlighted. Finally, some remarks are provided to make the reader aware of benefits and limitations of this approach.

Let OCP eq. (3.15) be the time-fixed rocket sled optimal control problem to be solved: First, the optimal control theory is applied, as usual, deriving:

- the Hamiltonian:

$$H = \lambda_x v + \lambda_v u - |u| \tag{3.43}$$

- Euler-Lagrange equations:

$$\dot{\lambda}_x = 0 \qquad\qquad \dot{\lambda}_v = -\lambda_x \tag{3.44}$$

- the switch function:

$$S_F(t) = |\lambda_v(t)| - 1 \tag{3.45}$$

The control $u(t)$ is split in into its magnitude $\beta(t)$ and "direction" $\omega(t)$[1], the latter being defined by eq. (3.10), that is:

$$\omega(t) = \lambda_v / |\lambda_v| \tag{3.46}$$

Observe that in this case the control is a scalar variable and the optimal direction is just the control sign. Instead of deciding the thrust magnitude on the basis of the switch function (e.g., as in equation 3.14), a mission structure B is introduced. The first (specific) step of the Multi-Bound approach consists in guessing a proper mission structure. Simple physical considerations push the user to choose a thrust-coast-thrust [T-C-T] control structure. This structure consists of 3 phases (that is $n_{cmp} = 3$, $n_{sw} = 2$) and the control magnitude is assigned as follows:

$$B = \{\beta_i,\ i = 1, \ldots, n_{cmp}\} = \{1, 0, 1\} \tag{3.47}$$

Two additional unknown variables t_1 and t_2 (which represent the commutation instants) have to be added to the problem. They must satisfy the condition:

$$0 \leq t_1 \leq t_2 \leq 2 \tag{3.48}$$

[1]For the sake of clearness, the symbol ω is employed in this section to denote the control direction, replacing the symbol $\hat{v}$, used in the previous ones, which here might be confused with the velocity component v.

A new independent variable t_ε is introduced as in eq. (3.31) and the time-lengths of the three arcs are:

$$\tau_1 = t_1, \qquad \tau_1 = t_2 - t_1, \qquad \tau_3 = 2 - t_2 \tag{3.49}$$

The augmented BVP is formulated as follows:

$$BVP^{Aug} = \begin{cases} \dfrac{dx}{dt_\varepsilon} = \tau v \\ \dfrac{dv}{dt_\varepsilon} = \tau \beta_i \dfrac{\lambda_v}{|\lambda_v|} \\ \dfrac{d\lambda_x}{dt_\varepsilon} = 0 \\ \dfrac{d\lambda_v}{dt_\varepsilon} = -\tau \lambda_x \\ s.t. \quad \begin{matrix} x(0) = 0 & S_F(t_1) = 0 & S_F(t_2) = 0 & x(2) = 1/2 \\ v(0) = 0 & & & v(2) = 0 \end{matrix} \end{cases} \tag{3.50}$$

with

$$\tau(t_\varepsilon) = \tau_i, \qquad \forall t_\varepsilon \in [i-1, i], \qquad i = 1, \ldots, n_{cmp} \tag{3.51}$$

The shooting function associated to the augmented BVP is:

$$\begin{aligned} S^{Aug} &: \quad \mathbb{R}^4 \rightarrow \qquad \mathbb{R}^4 \\ z^{Aug} = \begin{bmatrix} t_1 & t_2 & \lambda_{x_0} & \lambda_{v_0} \end{bmatrix} &\mapsto \begin{bmatrix} x|_3 & v|_3 & S_F|_1 & S_F|_2 \end{bmatrix} - \begin{bmatrix} 1/2 & 0 & 0 & 0 \end{bmatrix} \end{aligned} \tag{3.52}$$

Differently from the shooting function $S(\cdot)$ of the bang-bang control problem, $S^{Aug}(\cdot)$ admits many different roots. Table 3.1 collects all the four discovered roots.

Solution	t_1	t_2	λ_{x_0}	λ_{v_0}	J
A	0.292893	1.707107	1.414214	1.414214	0.585786
B	0.250000	2.250000	0.000000	1.000000	0.000000
C	-0.250000	1.750000	0.000000	-1.000000	0.000000
D	-0.224745	2.224745	-0.816497	-0.816497	-0.449490

Table 3.1: Discovered Roots for the Multi-Bound approach, assuming a TCT burn structure.

Solution "A" corresponds to the original OCP solution, found in section [3.2.3]. Solutions "B", "C", and "D" are not physically acceptable, due to one or even two time

inversions. the unphysical solutions are obtained even if the initial guess was physical (i.e., if the tentative values for t_1 and t_2 respect eq. (3.48). If none of the attained solution were physically acceptable or compatible with PMP, the mission structure would be properly modified and the solution process would be restarted. In a realistic scenario, in which the user does not know where the optimal solution is located, it is possible to extract useful information from the "false-root" solutions to move towards the optimal one: more difficult the problem, more useful this information. In practical cases, unlike the present example, it is not possible (or it is too expensive) to perform a complete exploration the whole search space. The convergence radius of the solutions is small, and a good initial guess is necessary to obtain the convergence to a solution (even sub-optimal) which should be used as springboard for the search of the optimal one.

In this example, if the solution B were attained, the user could envisage that the time inversion is equivalent to introduce a deceleration, even though $u(t)$ is positive inside the third arc. The suggestion that the user could draw is that braking is required in that part of the trajectory. An analogous reasoning could be done concerning the first arc of solution C; but in this case the negative time length suggests an acceleration at departure: a positive initial velocity adjoint λ_v should be chosen, so that $u(0) > 0$. Solution D presents simultaneously both situations, and both deductions hold. It is interesting to visualize the attraction basin of each root, as done with the original OCP in section [3.2.3]. In this case the dimension of the shooting function domain is greater than the original one ($z \in \mathbb{R}^2$, $z^{Aug} \in \mathbb{R}^4$); thus the analysis is more complex. Figure 3.7 presents 3 sections of the whole domain, obtained by fixing the time unknowns (t_1 and t_2) to some reasonable initial guess. The same 51×51 grid over the set $D = [-10, 10]^2$ is considered for the unknown initial adjoint variables.

The shooting function is made regular (i.e., the Jacobian matrix is non singular), but this is done at the expense of an increment of the system dimension and of the creation of "false-roots". The other strength point of the Multi-Bound approach, stressed in the previous section, is the improvement of the numerical behavior of the ODE system. This enhancement is hidden in the equations themselves, even though it may not be so evident. It can be observed using the optional output data released by the integration routine to measure its own performances. These data concern the number of steps employed to integrate all the trajectory, the number of RHS evaluation, and the number

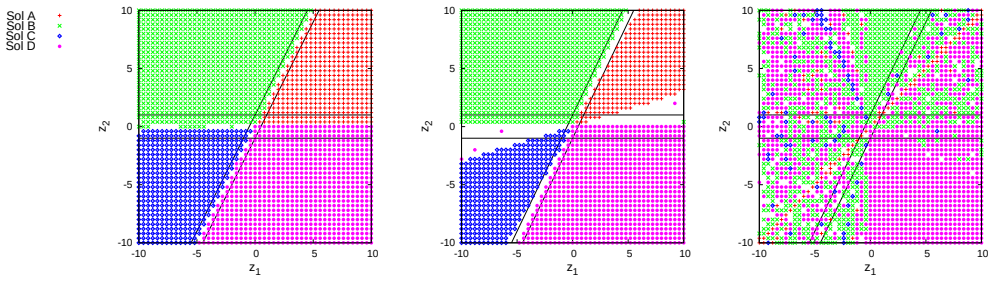

(a) $t_1 = 0.01, t_2 = 1.99$ (b) $t_1 = \left(2 - \sqrt{2}\right)/2,\ t_2 = \left(2 + \sqrt{2}\right)/2$ (c) $t_1 = 0.5, t_2 = 1.50$

Figure 3.7: Convergence Map with the Multi-Bound approach; three educated guesses for the time unknowns $\{t_1, t_2\}$.

of internal RHS Jacobian evaluations (and of matrix LU decompositions) in case a stiff problem is detected (and hence a stiff algorithm is used). Table 3.2 presents a comparison of the data provided by the integration code DLSODAR [60] for the two cases of the ODE system of the augmented BVP and the original one (they refer to the optimal trajectory, that is, the solution of the BVPs).

	No. steps	RHS-s No	J-s No
Multi-Bound	31	36	0
Bang-Bang	280	670	70

Table 3.2: Required number of Step, RHS and Jacobian evaluations for the integration of the rocket sled trajectory.

3.4 Solution through a Continuation-Smoothing technique

In this section a Continuation-Smoothing technique for handling bang-bang control problems is described. This method is quite general and it aims to improve the numerical solution process without involving any physical knowledge or specific behavior of the solution. The main principle is perturbing the objective function of the original problem in order to regularize (i.e., to smooth) the control law, by introducing a penalty or a barrier function, whose magnitude is scaled by a parameter ϵ. The solution of the

original problem is found by a gradual reduction (i.e., continuation) of the magnitude of the perturbing term. The original merit index is recovered for $\epsilon = 0$. Once again, the effectiveness of this method is shown in section [3.4.2] by applying it to the simple OCP problem previously described.

3.4.1 Method description

This section is dived in two parts. First, the continuation approach is stated in a clear and rigorous fashion. Necessary conditions for its convergence are also highlighted. Some implementation details which may improve the method, are here provided. Then, some useful perturbing function are considered and the associate control laws are derived. In order to simplify the notation, the vector sign will be dropped in this section.

3.4.1.1 Continuation Approach

The idea underlying a continuation method is to obtain the solution of a complex problem by building a sequence of (simpler) auxiliary problems which converge to the original one[1]. These auxiliary problems are characterized by the same set of differential equations, initial and final constraints, and control constraints as in original problem. The difference is made by the merit index, whose expression is:

$$J_\varepsilon = \int_{t_0}^{t_f} \left[\|u(t)\| - \varepsilon F\left(\|u(t)\|\right)\right] dt = \int_{t_0}^{t_f} h\left(u(t), \varepsilon\right) dt \tag{3.53}$$

The smoothing parameter ε belongs to the interval $]0, 1]$ and the function $h\left(u(t), \varepsilon\right)$ is supposed to be continuous. This approach is classified as penalty approach in case function $F(\cdot)$ has finite values in 0 and 1, whereas it is named barrier approach if $F(w) \to -\infty$ when w tends to 0 or 1.

The continuation procedure consists in:

- finding the solution of the auxiliary control problem associated with $\varepsilon = 1$ (that is, the BVP associated with this problem must be solved preliminarily);
- defining a sequence of decreasing values of ε ($\varepsilon_1 = 1 > \varepsilon_2 > ... > \varepsilon_n$);
- solving the BVP associated with $\varepsilon = \varepsilon_k$ ($k = 2...n$) using an initial guess "derived" by the solution at step $k - 1$.

[1] In our case the key point is not the complexity of the problem itself, rather than its regularity.

- the procedure ends when the desired precision on the objective function is reached, that is:

$$\left| J_{\varepsilon_{k+1}} \left(u^*_{\varepsilon_{k+1}} \right) - J_{\varepsilon_k} \left(u^*_{\varepsilon_k} \right) \right| \leq \Delta J_{\text{limit}}, \qquad \Delta J_{\text{limit}} > 0 \tag{3.54}$$

  where $u^*_{\varepsilon_k}$ is the optimal control which solve the auxiliary control problem associated to J_{ε_k}, while u^* corresponds to the optimal control of the original bang-bang control problem.

Beside this nominal stopping criterion, it may be useful to consider further ending criteria; for example the procedure may be stopped if ε becomes sufficiently small (i.e., $\varepsilon = \varepsilon_{end}$) or if a maximum step number $k_{\max}$ is reached.

In order to ensure that the sequence $J_{\varepsilon_k} \left(u^*_{\varepsilon_k} \right)$, $k \in \mathbb{N}$, converge to $J\left(u^*\right)$ the function $F\left(w\right)$ must be either non-negative or non-positive for all the w in its definition set (that is, from 0 to 1). In this way, the functions $h\left(u\left(t\right), \varepsilon\right)$ are monotonous in ε. In particular,

$$1) \quad F\left(w\right) \geq 0 \quad \Rightarrow \quad h\left(u\left(t\right), \varepsilon\right) = \left\| u\left(t\right) \right\| - \varepsilon F\left(\left\| u\left(t\right) \right\| \right) \quad \Rightarrow \quad h \text{ is decreasing in } \varepsilon \tag{3.55}$$

$$2) \quad F\left(w\right) \leq 0 \quad \Rightarrow \quad h\left(u\left(t\right), \varepsilon\right) = \left\| u\left(t\right) \right\| - \varepsilon F\left(\left\| u\left(t\right) \right\| \right) \quad \Rightarrow \quad h \text{ is increasing in } \varepsilon \tag{3.56}$$

The full convergence proof are given by Gergaud [61] for the first case and by Bell [62] for the second. The former will be use to justify the introduction of penalty function, for which it is required that $F\left(w\right) \geq 0 \ \forall w \in [0,1]$; the latter one to justify the introduction of barrier function, for which it is required that $F\left(w\right) \leq 0 \ \forall w \in]0,1[$. The open set in the second case does not constitute a problem.

A simple convergence Proof

A brief demonstration of convergence of the continuation procedure in case 2 - eq. (3.56) - is stated here. Assuming that $F\left(w\right) \leq 0, \ \forall w \in]0,1[$, it follows immediately that $h\left(u\left(t\right), \varepsilon\right)$ is increasing and hence the function $J_\varepsilon\left(u\right)$ is increasing w.r.t. ε; therefore:

$$J_{\varepsilon_k}\left(u\right) \leq J_{\varepsilon_l}\left(u\right) \qquad \forall \varepsilon_k < \varepsilon_l \tag{3.57}$$

By its definition, the optimal control u^*_α is the control which belongs to the admissibility set U which satisfies both algebraic and differential constraint imposed by the optimal control problem and that minimizes the index merit $J_\alpha\left(u\right)$. Let the set of all the

optimal control u^*_α associated to any index merit $J_\alpha(u)$ be U^*. It follows by definition that:

$$\min_{u \in U^*} J(u) = J(u^*) \tag{3.58}$$

and also

$$\min_{u \in U^*} J_{\varepsilon_k}(u) = J_{\varepsilon_k}\left(u^*_{\varepsilon_k}\right) \tag{3.59}$$

The following inequality chain can be stated:

$$J_{\varepsilon_k}\left(u^*_{\varepsilon_k}\right) = \min_{u \in U^*} J_{\varepsilon_k}(u) \leq J_{\varepsilon_k}\left(u^*_{\varepsilon_l}\right) \leq J_{\varepsilon_l}\left(u^*_{\varepsilon_l}\right) \tag{3.60}$$

The first $\leq$ comes from the definition, the second one by the eq. (3.57), thus

$$\Rightarrow \qquad J_{\varepsilon_k}\left(u^*_{\varepsilon_k}\right) \leq J_{\varepsilon_l}\left(u^*_{\varepsilon_l}\right), \qquad \forall \varepsilon_k < \varepsilon_l \tag{3.61}$$

which means that the sequence $J_{\varepsilon_k}\left(u^*_{\varepsilon_k}\right), k \in \mathbb{N}$ is decreasing. Recalling the hypothesis $F(w) \leq 0$:

$$\min_{u \in U} J_\varepsilon(u) = \min_{u \in U} \left\{ J(u) \underbrace{-\varepsilon \int_{t_0}^{t_f} F(\|u(t)\|)\, dt}_{\geq 0} \right\} \geq \min_{u \in U} J(u) = J(u^*) \tag{3.62}$$

so

$$J_{\varepsilon_k}\left(u^*_{\varepsilon_k}\right) \geq J(u^*) \qquad \forall k \in \mathbb{N} \tag{3.63}$$

which means that the sequence $J_{\varepsilon_k}\left(u^*_{\varepsilon_k}\right), k \in \mathbb{N}$ is bounded from below. Eventually, the sequence $J_{\varepsilon_k}\left(u^*_{\varepsilon_k}\right), k \in \mathbb{N}$ must converge to $J(u^*)$ since it is decreasing and bounded from below by the value $J(u^*)$ itself.

Implementation Details A crucial point in the continuation process is the definition of the ε_k sequence, that is the definition of the step length. In the author experience, the best solution is to use a decreasing geometric progression of common ratio γ:

$$\varepsilon_{k+1} = \gamma\, \varepsilon_k, \qquad \text{with } \gamma < 1 \tag{3.64}$$

A step-length $(\varepsilon_k - \varepsilon_{k+1})$ as long as possible is desired, in order to speed up the process. Unluckily, longer steps decrease the chance of convergence, or increase the risk of jumping from a family of solution to a different one. A good practice is to use an adaptive step method. Here a quite raw one is proposed: the common ratio

γ can be decreased (i.e. the step is increased) after m successive solutions are found consecutively, in order to speed up the process, until a limit value γ_{limit} is reached, thus:

$$\gamma_{k+1} = \max\left[\gamma'_{k+1}, \gamma_{\text{limit}}\right] \tag{3.65}$$

with

$$\gamma'_{k+1} = \begin{cases} (\gamma_k)^{1.5} & \text{after 5 successive solution are found consecutively} \\ \gamma_k & \text{otherwise} \end{cases} \tag{3.66}$$

In case the solution of an auxiliary problem could not be found (i.e., the root-finding method does not converge), the smoothing parameter is made closer to the previous one; for example

$$\varepsilon'_{k+1} = \frac{\varepsilon_{k+1} + \varepsilon_k}{2} \tag{3.67}$$

and the common ratio γ is increased:

$$\gamma_{k+1} = (\gamma_k)^{1/2} \tag{3.68}$$

The solution of the new auxiliary problem can be obtained using as initial guess the solution of the previous one (Fig. 3.11(a)). An improvement can be obtained by using a linear extrapolation:

$$p^0_{\varepsilon_{k+1}} = p^*_{\varepsilon_k} + \frac{p^*_{\varepsilon_k} - p^*_{\varepsilon_{k-1}}}{\varepsilon_k - \varepsilon_{k-1}} (\varepsilon_{k+1} - \varepsilon_k) \tag{3.69}$$

where $p^0_{\varepsilon_{k+1}}$ is the initial guess of the new problem, and $p^*_{\varepsilon_k}$ is the solution of the auxiliary problem with $\varepsilon = \varepsilon_k$. The advantages are pretty evident as it will be shown in section [3.4.2].

3.4.1.2 Creation of Smooth Control Laws

In this section some smooth control laws, obtained by the introduction of different perturbing function into the merit index, are presented. First a quadratic penalty term is proposed. Second, a logarithmic barrier approach is used, in order to achieve a more regular control law.

Quadratic Penalty Approach The most used approach is the quadratic one. The reader who desires to know different applications of this approach may refer for example to [52, 63, 64]. The main idea is introducing an energy related term (i.e., $\|u(t)\|^2$) into the objective function of the original problem, so that the merit index of the auxiliary problem with $\varepsilon_0 = 1$ is convex. Returning to the notation of the previous section, the merit index (to be *maximized*) becomes:

$$J_\varepsilon^q = \int_{t_0}^{t_1} \left[-\|u(t)\| + \varepsilon \|u(t)\| (1 - \|u(t)\|) \right] dt = \int_{t_0}^{t_1} h^q (u(t), \varepsilon)\, dt \tag{3.70}$$

which means that the perturbing function is:

$$F^q(w) = w(1-w) \geq 0, \qquad \forall w \in [0,1] \tag{3.71}$$

The convergence of the auxiliary problem sequence $(J_{\varepsilon_k}^q (u_{\varepsilon_k}^*), k \in \mathbb{N})$ towards $J(u^*)$ is thus guaranteed (because $F^q(w) \geq 0, \forall w \in [0,1]$). The optimal control law associated to the merit index (3.3) can be found by applying the optimal control equation (2.17). If the control vector $\bar{u}(t)$ is rewritten in order to make evident its magnitude β and its direction $\hat{v}$ as in eq. (3.7), the merit index becomes:

$$J_\varepsilon^q = \int_{t_0}^{t_1} \left[-\beta_\varepsilon^q + \varepsilon \beta_\varepsilon^q (1 - \beta_\varepsilon^q) \right] dt \tag{3.72}$$

therefore the Hamiltonian is:

$$\begin{aligned} H &= \lambda^T f(x) + \lambda^T g(x) u + h^q (u(t), \varepsilon) \\ &= \lambda^T f(x) + \beta_\varepsilon^q \left(1 + \left\| g(x)^T \lambda \right\| \right) + \varepsilon \beta_\varepsilon^q \left(1 - \beta_\varepsilon^1 \right) \\ &= \lambda^T f(x) + \beta_\varepsilon^q S_F + \varepsilon \left(\beta_\varepsilon^q - (\beta_\varepsilon^q)^2 \right) \end{aligned} \tag{3.73}$$

The optimal control magnitude is:

$$\frac{\partial H}{\partial \beta_\varepsilon^q} = 0 \Rightarrow S_F + \varepsilon (1 - 2\beta_\varepsilon^q) = 0 \Rightarrow \beta_\varepsilon^1 = \frac{1}{2} (1 + S_F/\varepsilon) \tag{3.74}$$

subject to the control constraint (3.2), that can be rewritten for convenience as:

$$0 \leq \beta_\varepsilon^q \leq 1 \tag{3.75}$$

Summarizing the last obtained result and those stated in section [3.2.1] concerning the optimal control direction, the optimal control law can be written as:

$$u_\varepsilon^q(t) = \begin{cases} 0 & \text{if } \left\| g(x(t))^T \lambda(t) \right\| = 0 \\ \beta_\varepsilon^q(t) \frac{g(x(t))^T \lambda(t)}{\left\| g(x(t))^T \lambda(t) \right\|} & \text{if } \left\| g(x(t))^T \lambda(t) \right\| \neq 0 \end{cases} \tag{3.76}$$

with

$$\beta_{\varepsilon}^{q}(t) = \begin{cases} 0 & \text{if } S_F(t) \leq -\varepsilon \\ \frac{1}{2}\left(1 + \frac{S_F(t)}{\varepsilon}\right) & \text{if } -\varepsilon < S_F(t) < \varepsilon \\ 1 & \text{if } S_F(t) \geq \varepsilon \end{cases} \tag{3.77}$$

where the expression for the switch function $S_F(t)$ is the same as in eq. (3.12). A way to "test" the convergence of the smooth control to the bang-bang one is to measure L^2 norm of their difference. Posing $S_F(t) = z$, then $\beta_{\varepsilon}^{q}(t) = \tilde{\beta}_{\varepsilon}^{q}(z)$ and $\beta(t) = \tilde{\beta}(z)$, $\forall z \in \mathbb{R}$, one has:

$$\left\| \tilde{\beta}_{\varepsilon}^{q}(z) - \tilde{\beta}(z) \right\|_2^2 = \int_{-\infty}^{+\infty} \left[\tilde{\beta}_{\varepsilon}^{q}(z) - \tilde{\beta}(z) \right]^2 dz = \frac{1}{6}\varepsilon \tag{3.78}$$

This implies that the function $\beta_{\varepsilon}^{q}(\cdot)$ converges in $L^2(\mathbb{R}, \mathbb{R})$ towards the function $\tilde{\beta}(\cdot)$ when ε tends to 0. Nonetheless, this control law is not differentiable because the function $\beta_{\varepsilon}^{q}(\cdot)$ is not. However, the regularity order of $u_{\varepsilon}^{*}(\cdot)$ is superior to that of original problem, which was discontinuous.

Logarithmic Barrier Approach The use of logarithmic barrier was inspired by the success of its application in the context of mathematical programming (both linear and quadratic programming). For example, a wide use of logarithmic barrier is made in interior point methods for nonlinear constrained optimization [65]. The use of the barrier concept in the optimal control context can be seen as a natural transposition. By definition, a bang-bang control assumes only values at the boundaries of its definition set (i.e., it switch alternatively from 0 to 1 and vice versa). The idea of the barrier approach is to introduce a perturbative term in the objective function in order to discourage (i.e. reducing the merit index) strongly the control magnitude from reaching its extremal values. Logarithmic functions are used here to prevent $\|u(t)\|$ to assume values 0 and 1. The barrier effect is more accentuated at the beginning of the continuation procedure, where $\varepsilon = 1$, and progressively vanishes as the smoothing parameter approaches zero. The merit index to *maximize* in this case is:

$$J_{\varepsilon}^{L} = -\int_{t_0}^{t_1} \left\{ \|u(t)\| - \varepsilon \left[\log\left(\|u(t)\|\right) + \log\left(1 - \|u(t)\|\right) \right] \right\} dt = \int_{t_0}^{t_1} h^{L}(u(t), \varepsilon)\, dt$$

$$J_{\varepsilon}^{L} = J + \varepsilon \int_{t_0}^{t_1} \left(\log\left(\|u(t)\|\right) + \log\left(1 - \|u(t)\|\right) \right) dt \tag{3.79}$$

The perturbing function $F^L(w)$ can be easily deduced:

$$F^L(w) = \log(w) + \log(1-w) \tag{3.80}$$

The following property can be easily demonstrated:

1. $F^L(w) \leq 0, \forall w \in]0,1]$
2. $\lim_{w\to 0} F^L(w) = \lim_{w\to 1} F^L(w) = -\infty$, i.e. $F^L(\cdot)$ is a barrier.

Notice that the definition set of the function $F^L(\cdot)$ is the open set $]0,1[$, thus the control cannot achieve its extreme values. The control constraint eq. (3.2) is automatically ensured (as far as $\varepsilon \neq 0$). Property 1) (c.f. section [3.4.1.1]) permits to ensure that the sequence of auxiliary problem $J^L_{\varepsilon_k}\left(u^*_{\varepsilon_k}\right)$, $k \in \mathbb{N}$ converges to $J(u^*)$. The optimal control law associated to the merit index eq. (3.3) can be found in the same way of the quadratic one: the control vector $\bar{u}(t)$ is rewritten in order to make evident its magnitude β and its optimal direction as in eq. (3.7). Thus, the index merit becomes:

$$J^L_\varepsilon = J + \varepsilon \int_{t_0}^{t_1} \left(\log\left(\beta^L_\varepsilon\right) + \log\left(1-\beta^L_\varepsilon\right)\right) dt \tag{3.81}$$

therefore the Hamiltonian is:

$$H = \lambda^T f(x) + \lambda^T g(x)\, u + h^L_\varepsilon\left(\beta^L_\varepsilon\right) \tag{3.82}$$

explicating the optimal thrust direction eq. (3.10), one has:

$$\begin{aligned} H &= \lambda^T f(x) + \beta^L_\varepsilon\left(1 + \left\|g(x)^T\lambda\right\|\right) + \varepsilon\left[\log\left(\beta^L_\varepsilon\right) + \log\left(1-\beta^L_\varepsilon\right)\right] \\ &= \lambda^T f(x) + \beta^L_\varepsilon S_F + \varepsilon\left[\log\left(\beta^L_\varepsilon\right) + \log\left(1-\beta^L_\varepsilon\right)\right] \end{aligned} \tag{3.83}$$

The optimal control magnitude is:

$$\frac{\partial H}{\partial \beta^L_\varepsilon} = 0 \Rightarrow \beta^2_\varepsilon(t) = \frac{2\varepsilon}{S_F(t) + 2\varepsilon + \sqrt{S_F(t)^2 + 4\varepsilon^2}} \tag{3.84}$$

Summarizing the last obtained results and those stated in section [3.2.1] concerning the optimal control direction, the optimal control law can be written as:

$$u^L_\varepsilon(t) = \begin{cases} 0 & \text{if } \left\|g(x(t))^T\lambda(t)\right\| = 0 \\ \beta^L_\varepsilon(t)\, \frac{g(x(t))^T\lambda(t)}{\left\|g(x(t))^T\lambda(t)\right\|} & \text{if } \left\|g(x(t))^T\lambda(t)\right\| \neq 0 \end{cases} \tag{3.85}$$

with

$$\beta_{\varepsilon}^{L}(t) = \frac{2\varepsilon}{S_F(t) + 2\varepsilon + \sqrt{S_F(t)^2 + 4\varepsilon^2}} \tag{3.86}$$

where the switch function $S_F(t)$ is still defined by eq. (3.12).

In the same fashion of the previous section, the L^2 norm of the difference between the smooth control law $\beta_{\varepsilon}^{2}(\cdot)$ and the bang-bang one $\tilde{\beta}(z)$ is calculated:

$$\left\| \beta_{\varepsilon}^{2}(z) - \tilde{\beta}(z) \right\|_2^2 = 4\varepsilon(1 - \log(2)) \tag{3.87}$$

The convergence for $\varepsilon \to 0$ is again proved. In this case, $\beta_{\varepsilon}^{2}(\cdot)$ is of class C^{∞}. However $u_{\varepsilon}^{*}(\cdot)$ is non continuous in case the vector $g(x(t))^T \lambda(t)$ is null. This fact does not represent a true problem from the practical point of view, as results from its use in both simple (Chapter 4) and difficult (Chapter 5) problems.

3.4.2 Application of Continuation-Smoothing Approach to the Rocket Sled problem

In this sections, the smoothed control laws just devised are applied to the illustrative example of section [3.2.3]. The aim is to confirm numerically the effectiveness of the Continuation-Smoothing approach. The root-finding algorithm used in these cases is the Hybrid-Powell one, which proved to be fast and reliable in previous tests. The problem is formally the same defined by eq (3.21); the difference is made by the control function, that now is a continuous function of the switching function: in the case of quadratic penalty, the control is expressed by eq. (3.77), whereas in the case of logarithmic barrier the control is given by eq. (3.86).

Quadratic Penalty Approach The problem is first solved using as perturbative term a quadratic penalty. Figure 3.8 presents a succession of optimal control laws for the auxiliary problem sequence $J_{\varepsilon}^{q}(u_{\varepsilon}^{*})$, for $\varepsilon \to 0$. First, one can notice that the control is actually continuous for any ε, as we expected. As the smoothing parameter is reduced, the corresponding control law becomes more sharp, and finally it becomes almost bang-bang. The convergence of the smoothed control law to the original one, demonstrated in section [3.4.1.1] is hence numerically confirmed.

It was stated that a more regular control law permits to enlarge the attraction basin of the root (i.e., the solution). To prove it, the convergence basin for the problem

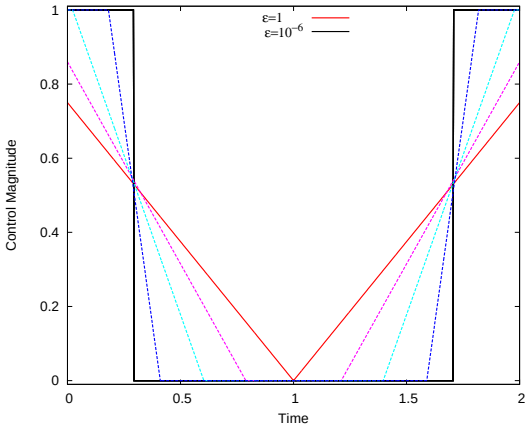

Figure 3.8: Control laws using the Quadratic Penalty approach, several values of the smoothing parameter.

with $\varepsilon = 1$ is searched for. As in section [3.2.3], an uniform 51×51 grid over the set $D = [-10, 10]^2$ is considered for the initial guess. The convergence domain is shown in Figure 3.9 (any grid point for which the solution is attained is marked with a cross).

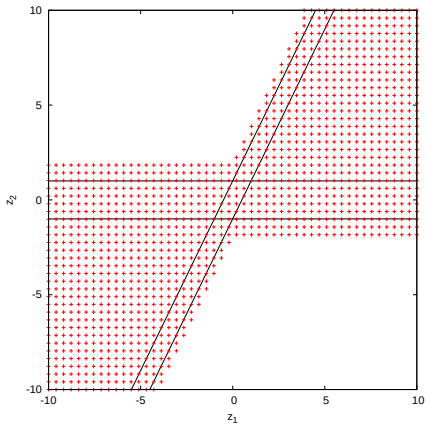

Figure 3.9: Convergence map for the rocket sled problem using a Quadratic Penalty approach.

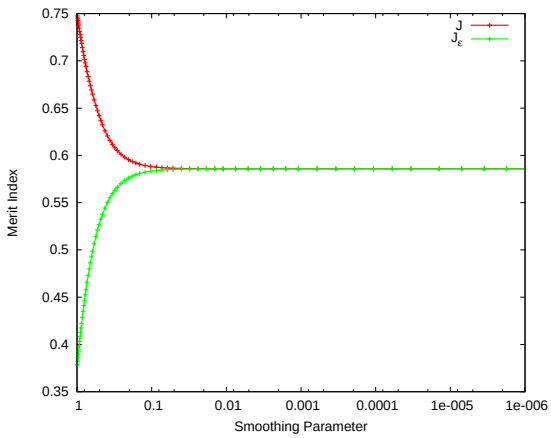

Figure 3.10: Original and Perturbed Merit index using a Quadratic Penalty approach.

The attraction basin is wider than the one of the original problem. This is due to the creation of a transition zone between the regions where the control is always on (U_{+1} and U_{-1}, top left and bottom right respectively) and the other regions. However, zones where the Jacobian matrix is singular still exist. Figure 3.10 shows the value

of the smoothed and original merit index in correspondence of each solved auxiliary problem (i.e., $J_{\varepsilon_k}\left(u^*_{\varepsilon_k}\right)$ and $J\left(u^*_{\varepsilon_k}\right)$ respectively). The two sequence are monotonous and converging to $J\left(u^*\right)$, as it was demonstrated in section [3.4.1].

To solve each auxiliary problem, the solution of the previous one is exploited. Figure 3.11 shows the prediction and correction steps all along the continuation path for the variable λ_{x_0} in case of a "zero-order" extrapolation and of a linear extrapolation (an analogous graph can be done for the other unknown variable). The effectiveness of the latter method is quite evident: the linear prediction (Figure 3.11(b)) permits to have smaller correction steps in comparison to the "zero-order" (Figure 3.11(a)), hence facilitating the work of the root-finding algorithm.

This is as more important as more complex are the problem faced: for difficult problems the convergence basin of the auxiliary problem is small; thus, being equal the correction-steps in either cases, linear extrapolation allows larger continuation-steps.

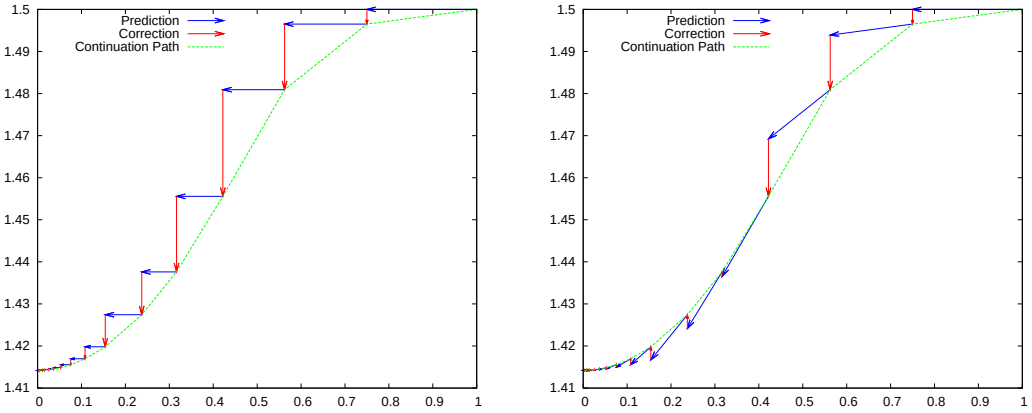

(a) "zero-order" extrapolation

(b) "linear" extrapolation

Figure 3.11: Continuation path with "zero-order" or "linear" extrapolation, quadratic penalty approach.

Logarithmic Barrier Approach

The same tests done for the quadratic penalty (on the control law regularization, the enlargement of the attraction basin, and the convergence of the auxiliary problem succession to the original one) can be performed using the second smooth control law that was derived by introducing a logarithmic barrier.

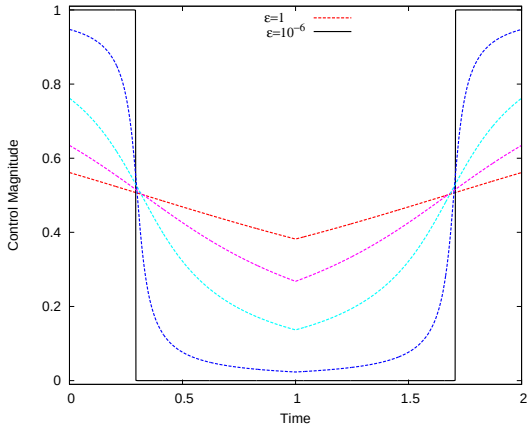

Figure 3.12: Control laws using the Logarithmic Barrier approach, several values of the smoothing parameter.

The resulting control is more regular then the previous one: it is continuous and even derivable, as made clear by Figure 3.12. The extremal values (i.e., 0 and 1) are never exactly achieved; therefore, there are not regions of the search space where the control is always on or always off. Consequently, no plateau is present in either surface of error components of the shooting function (see Figure 3.13). As the regions where the Jacobian matrix was singular have vanished, the convergence region is expanded. A proof is attained by replying the grid initialization performed for testing the quadratic control. Results shown in Figure 3.14 report that, actually, the convergence is obtained for any of the tried initial guesses.

The convergence speed of the quadratic and logarithmic approaches can be compared. Figure 3.15 presents the difference between the smoothed and original merit indexes for each perturbative term. The quadratic penalty approach converges to the optimal solution more rapidly than the logarithmic barrier one. This can be explained by recalling that the function $\beta_\varepsilon^1(\cdot)$ converges in norm $L^2(\mathbb{R},\mathbb{R})$ toward $\tilde{\beta}(\cdot)$ more rapidly than the function $\beta_\varepsilon^2(\cdot)$ (c.f. eqs. (3.78) and (3.87)). However, convergence speed is not the most important effect; rather, it is important the capability in finding the first solution (i.e., the one for $\varepsilon = 1$) and the overall improvement of the numerical behavior of the problem. The former point is probably in favor of the quadratic penalty, while the second goal is better achieved by the logarithmic barrier.

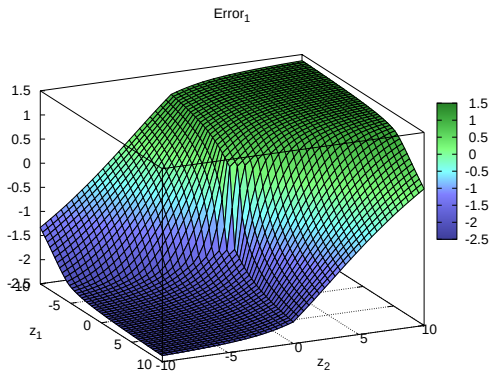

(a) First Error Component

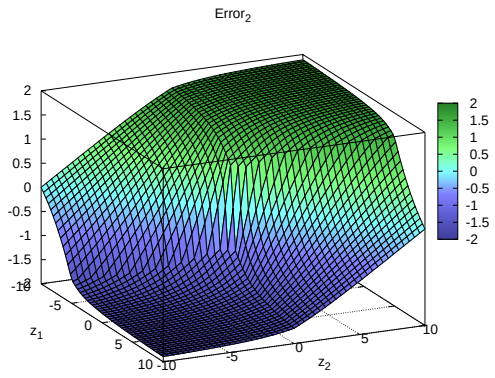

(b) Second Error Component

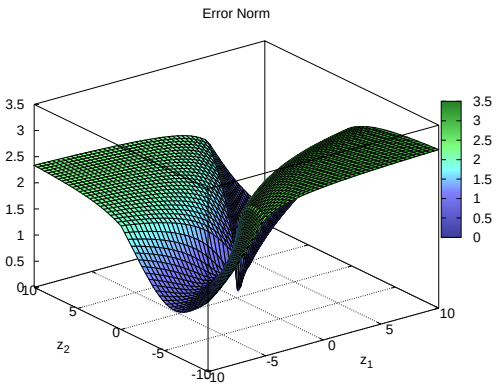

(c) Error Norm

Figure 3.13: Components and norm of the Shooting function for the rocket sled problem, using a Logarithmic barrier pertubation with $\epsilon = 1$.

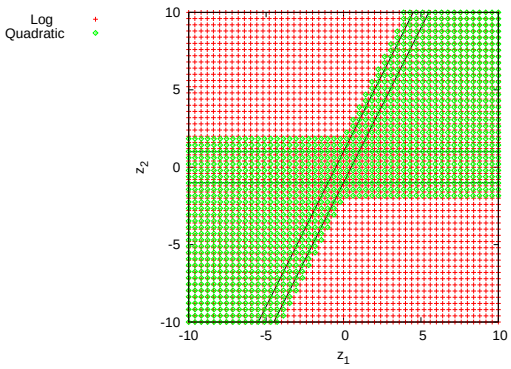

Figure 3.14: Convergence region: Quadratic penalty vs Logarithmic barrier approach.

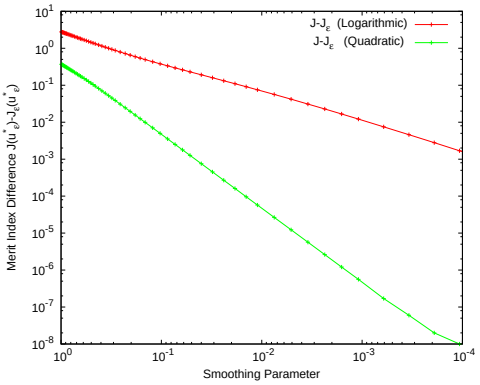

Figure 3.15: Convergence speed for the quadratic and logarithmic control laws.

3.4.3 An Automatic Initialization Procedure

Finding a good initial guess for the shooting procedure of indirect methods is often difficult. As far as the Multi-Bound approach is concerned, the burn structure can be explicitly assigned and the user can exploit its knowledge of the physical solution to attain a reasonable initial trajectory, by manually assigning sequence and duration of burn and coast arcs.

If the Continuation-Smoothing is applied, the user does not rely on an explicitly assigned burn structure. The choice of the initial guess becomes more tricky, as the whole control law depends only on the initial conditions (e.g., the values of state and adjoint variables). It is usually impossible to envisage a choice of initial values that will produce a desired burn strategy, hence the user knowledge is not of help. Therefore, unless the solution of a very similar problem is known, one has to find an "automatic" initialization procedure, that is, a way to initialize the shooting process without having to manually select a good initial guess.

A conceptually simple possibility is offered by the so called grid-initialization (or grid-shooting). The idea is to define a mesh of (usually) equally spaced points over a finite portion of search space and then use every point as an initial guess for the shooting method. The finer the shooting grid, the better the possibilities of finding out the optimal solution. This method is easy to understand and straightforward to implement, but it has a very low efficiency as the number of grid point increases

exponentially with the search space dimension. As this method is computationally too expensive, it will not be used in this thesis; instead, a different procedure to handle the initialization task is here suggested.

Whenever the Continuation-Smoothing formulation is used, the initialization task consists in finding the solution of a "Problem Zero", that is the problem with the highest smoothing parameter (usually $\varepsilon = 1$). This goal can be attained by continuation, that is by solving a sequence of problems which leads from an easy problem (or a problem whose solution is known) to the "Problem Zero". Each intermediate problem is solved by using as initial guess the solution of the previously solved one.

In space flight applications, a trivial problem concerns the time-fixed minimum-fuel transfer of a spacecraft between two fully-defined orbits that have the same orbital parameters; in this case, the optimal solution consists just of a coasting arc. Assuming that the spacecraft state is fully assigned at the departure, the initial adjoint variables are the only problem unknowns. The solution of this problem is simply given by posing all the adjoint variables at the departure equal to zero, except for the mass-adjoint which must be unitary.

Recalling eq. (3.13), a null constant thrust law is attained by setting null adjoint variables, because $\left\| g(x(t))^T \lambda(t) \right\| = 0$; moreover the switch function is constant along the trajectory:

$$S_F = \frac{0}{m} - \frac{1}{c} = -1/c \tag{3.88}$$

This solution holds whichever perturbative function is used to regularized the control. If the quadratic penalty is employed and $\varepsilon = 1$, one can notice that the smoothed control magnitude β_ϵ^q is also null, because:

$$\beta_\varepsilon^q(S_F) = \frac{1}{2}\left(1 + \frac{S_F}{\varepsilon/c}\right) \rightarrow \beta_{\varepsilon=1}^q\left(S_F = -\frac{1}{c}\right) = 0 \tag{3.89}$$

Therefore, in the special case of a quadratic control law, with $\epsilon = 1$, the control law u_ϵ^q, given by eq. (3.76), is a continuous function[1]. Being the control law regular for this solution (the one with null position-velocity adjoints, and unitary mass adjoint), the same holds for the shooting function; consequently the Jacobian of the shooting function is not singular (which is a necessary condition for the functioning of Newton-like methods).

[1]This special condition does not hold either if a logarithmic barrier is considered or if the smoothing parameter $\epsilon \neq 1$.

The idea for this automatic initialization procedure is to create a "starting problem" in which the spacecraft is initially on a "virtual" orbit whose parameters are the same of the final one. The sequence of problems which leads to the original one is obtained by changing only the "virtual" initial condition, until the "true" initial one is restored. A smoothed quadratic control law is assumed. We will refer to this process as "orbit-shape continuation". The virtual initial conditions that describe the sequence of auxiliary problems can be written as a linear convex combination of the true initial and final ones: $\bar{x}_\alpha = (1-\alpha)\,\bar{x}_0 + (\alpha)\,\bar{x}_f$ where α is the orbit-shape continuation parameter and $\bar{x}_0$ and $\bar{x}_f$ are the true initial and final conditions respectively. This continuation path starts with $\alpha = 1$ and ends with $\alpha = 0$.

After the continuation on the orbit-shape parameters has been successfully completed, the continuation on the smoothing parameter could be performed to reach, at least in theory, the problem solution, by using the quadratic control law eq. (3.77). In practice, it is quite difficult to complete the continuation process using this (quadratic) smoothed control law due to its poor numerical behavior; therefore, it is convenient to adopt a more regularized control law, such as the one produced by the logarithmic barrier, before starting the continuation on the smoothing parameter. The shift from a smooth control law to another implies a jump of the solution; the value of the smoothing parameter ε^L (relative to the logarithmic barrier problem) has to be chosen carefully, to avoid an abrupt change in the spacecraft trajectory, as it may lead to the impossibility of attaining the convergence. Which is the best value of ε^L to solve the new problem using as initial guess the solution of the quadratic problem is an open question, as it is problem-dependent. A direct relationship that links the two smoothing parameters was not envisaged; neither a way to move continuously from one perturbing function the other was found. In practice, a simple way obtain a good value is by a trial and error process: the convergence is attempted starting from $\varepsilon^L = 1$ and decreasing its value until a working one is obtained (usually this value lays between 10^{-1} and 10^{-2}). Usually, once a working value of ε^L has been found for a specific mission, that value is successfully adopted for all similar missions. Thus, the trial and error process can be performed just once.

This easy but powerful initialization technique can be used to create a self-consistent procedure (hereafter named Auto-CS algorithm) to solve this class of optimal control problems with the least effort. A scheme of the solution process is sketched below:

- define and solve a starting quadratic problem:
  the problem is associated to $\varepsilon = 1$, $\alpha = 1$, the solution is (usually) $\bar{\lambda}_x = 0$, $\lambda_m = 1$;

- orbit shape continuation:
  solve the sequence of problem for $\alpha : 1 \to 0$;

- control law shift:
  solve one problem regularized by using the logarithmic barrier, for an appropriate value of ε^L, using the last obtained solution as tentative guess;

- smoothing-parameter continuation:
  solve a sequence of problems for decreasing values of the smoothing-parameter, until a stopping criterion is met.

Albeit no convergence proof can be stated, in practice this initialization process demonstrated to be capable of achieving the optimal solution in most cases. Results will be shown in the Chapter 4.

3.5 Method Comparison

In this section, a comparison of the two solution methods for bang-bang control problems is presented. Relative strength and weakness points concern primarily their usage (e.g., if they are specific or all-purpose), the effort required to the user (e.g., if they can be automated or not), and the respective computational burden. The Multi-Bound approach stems from the idea of exploiting the user (past) knowledge of the control problem (and of its solution) in order to facilitate the optimization process. The previous statement clearly explains why the Multi-Bound approach cannot be fully automated. Nor this approach was derived to be used in this fashion; instead, it is focused on letting the user masters the situation (i.e., manually adjusting the first guess to obtain a reasonable solution). Conversely, the Continuation-Smoothing approach is much more general (in fact it is employed in many different application fields). Only a few parameters need to be set by the user (they usually are those variables which specify the continuation process: maximum step length, exit criteria, etc). Moreover, if it is coupled with a proper automatic initialization procedure, a "black-box" tool for

solving OCP can be created. This means that, in the case of not too complex problems, a good solution can be found almost immediately. From a numerical point of view, the BVPs produced by the Multi-Bound approach are "better" than those obtained by the Smoothing technique. In the former cases, the switch function acts only through the boundary conditions and does not influence directly the trajectory (which instead depends on the arc durations). The integration is less sensitive to the initial conditions; convergence radius is thus enlarged as coarser estimates of the initial conditions are permitted. Beside, in the Multi-Bound approach the ODE system contains only smooth terms, whereas in those related to the Continuation-Smoothing approach non-differentiable terms or, at least, fast time-varying terms are always present. Rapid variation of the control magnitude arises in correspondence of the switch points, where the optimal bang-bang control would experience its discontinuities. The ODE solver needs to perform smaller integration steps around these points, thus each shooting function evaluation is slower than those performed in the Multi-Bound approach. As the continuation advances, the "bad" numerical behavior of the original problem is restored: this means that the root attracting basin becomes smaller and smaller. Therefore, very small continuation steps are often necessary to achieve the convergence using as initial guess the previously found solution.

Another important strength point of the Multi-Bound approach is the possibility to perform "solution mining". The idea is that once that a first (parent) solution is found, it is possible to find a vein of solution by exploiting the continuous dependence of ODE solutions on the initial values. For instance, extensive parametric analysis can be done in this fashion. The solution of a slightly different problem can be found by using the previous solution as initial guess. This process works because the shooting function is regular in a "wide" neighborhood of the solution. On the opposite, in the case of a Continuation-Smoothing approach it is quite difficult, even for problems of medium complexity, to achieve the same result. A parametric analysis cannot be performed by exploiting the solution of the last obtained auxiliary problem (i.e., the one with the lowest value of the smoothing parameter). Usually, solution mining can be performed only on $\varepsilon = 1$ problems.

In summary, the Multi-Bound approach is more difficult to set up properly than the Continuation-Smoothing approach, and it requires usually a preliminary study of the optimal control problem to solve. However, this extra time is rewarded by a more

regular and numerically "easy to solve" BVP. The best feature of the Continuation-Smoothing approach is that no hypothesis on the switch sequence is needed in order to solve the problem. This feature is really valuable whenever the switch sequence is difficult to forecast, as it is highly dependent on the initial conditions. This is exactly the case of the applicative problem presented in Chapter 5.

Although in this Chapter the two methods were presented one in opposition to the other, they are not necessarily alternative. They have both good qualities and troubles. A way to join the two methods is proposed in Chapter 5. Initially, use is made of the Continuation-Smoothing approach to find out the optimal switching structure; the smoothing parameter does not have to reach its lowest value, so numerical issues are limited. Once the optimal switching structure is "revealed", the fixed-structure Multi-Bound approach is employed to produce the final solution (thus avoiding the last hard steps of the continuation process).

Chapter 4

A Cooperative Rendezvous Mission

Introduction

In this chapter, the peculiar approaches (namely the Multi-Bound approach and the smoothing technique) outlined in Chapter 3 to handle bang-bang optimal control problems will be employed in the optimization of a typical space flight mission.

The two-spacecraft rendezvous problem is well-known in astrodynamics. Many researchers dealt with it in the past years; therefore, literature concerning this topic is wide. Usually the problem concerns one maneuvering spacecraft whose aim is to chase for a passive target. Results for impulsive-thrust missions [66–72] and for finite-thrust cases [73] have been presented. The cooperative rendezvous mission, that is the problem of two maneuvering spacecraft that simultaneously chase one for the other, is a much more complex problem and few papers can be found on this topics; besides, most of them assume just impulsive thrust [74].

In this chapter, a finite-thrust time-constrained cooperative rendezvous will be studied. A simple two-body dynamical model is considered. The aim is twofold. From one side, this problem is a reasonable benchmark for the techniques previously described: it is representative of space flight applications, thus it has all the features that one expects to find in a real problem (multiplicity of solutions, change of the burn structure according to the available flight time, etc..); at the same time, it is a well conditioned problem, whose numerical behavior is not a problem "per se". In particular, it is interesting to

evaluate the performance of the automatic initialization procedure (described in the previous chapter), which exploits some peculiarities of the Continuation-Smoothing techniques. Solutions found in this way will be checked against with those found manually. To make the latter task easier, the Multi-Bound formulation will be adopted as the resulting shooting problem is easier to be hand-driven to convergence. From the other side, the problem has specific interest in this thesis, as it appears a simpler case of the formation deployment that will be studied in the next chapter. It allows to foresee the possibility of saving propellant if a cooperative strategy is adopted instead of the classical chaser/target one; also the limits of this approach will be stressed.

The chapter is organized in this way: first, a comprehensive description of the rendezvous problem is provided in section [4.1]; the two mission strategies (cooperative and non-cooperative) will be enunciated. Section [4.2] presents the non-cooperative (leader/follower) strategy, whereas section [4.3] presents the cooperative rendezvous. Eventually, a comparison of the numerical results obtained in either cases is provided.

4.1 Problem Statement

A complete statement of the problem under investigation will be provided in this section, illustrating the choice of the state variables, the merit index to maximize, the spacecraft dynamics, and the constraints on initial and final states.

Two spacecraft fly on the same circular orbit of radius $\tilde{r}_0$, separated each other of 180° (that is, they are in opposition). Both spacecraft can maneuver and have identical propulsive features (i.e., initial mass, maximum thrust, specific impulse). At an assigned final time $\tilde{t}_f$, they must have reached a circular orbit of assigned radius $\tilde{r}_f$ (greater than the initial one) and they must have completed their rendezvous. For the sake of simplicity the initial and final orbits are assumed to be coplanar, hence the problem geometry is two-dimensional. The goal is to find the trajectory, and the associated control law, that minimizes the overall amount of exhausted propellant.

According to the objective of this study, the two spacecraft can be assumed to be point-mass objects; the state of each one is fully described by its position, velocity, and mass. Variables are normalized with respect to the initial radius, the corresponding circular velocity and the single spacecraft initial mass. The position of each satellite with respect to an inertial frame is given by a set of polar coordinates r, ϑ. The reference

frame $\left\{\hat{i};\hat{j}\right\}$, chosen to describe the spacecraft velocity, is a topocentric rotating one, which follows the spacecraft during its motion, keeping the axes pointed in the radial $\hat{i}$ and transverse $\hat{j}$ directions. The two unit vectors $\hat{i}$, $\hat{j}$ are defined with respect to the

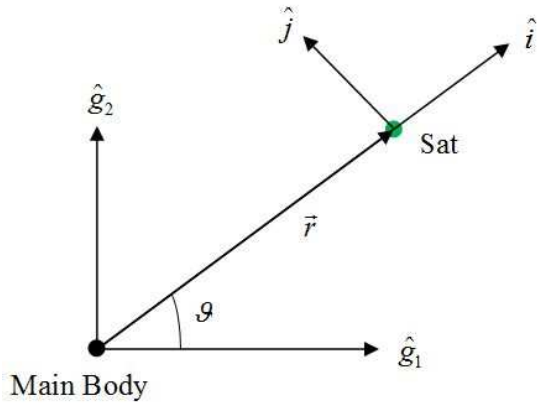

Figure 4.1: Reference Frame for planar missions.

inertial reference frame $\{\hat{g}_1;\hat{g}_2\}$ by the following equations:

$$\begin{aligned}\hat{i} &= \cos\vartheta\,\hat{g}_1 + \sin\vartheta\,\hat{g}_2\\ \hat{j} &= -\sin\vartheta\,\hat{g}_1 + \cos\vartheta\,\hat{g}_2\end{aligned} \tag{4.1}$$

The velocity is expressed by means of the radial u and transverse v components respectively. A simple two-body dynamical model is considered; thus the motion of each spacecraft is described by the following set of differential equations:

$$\dot{\bar{x}}_j = \bar{f}\left(\bar{x}_j, \bar{u}_j, t\right) = \begin{cases} \dot{r}_j = u_j \\ \dot{\vartheta}_j = v_j/r_j \\ \dot{u}_j = -1/r_j^2 + v_j^2/r_j + T_{j,u}/m_j \\ \dot{v}_j = -u_j v_j/r_j + T_{j,v}/m_j \\ \dot{m}_j = -T_j/c_j \end{cases}, \qquad j = I, II \tag{4.2}$$

where $\bar{u}_j = \vec{T}_j = \begin{pmatrix} T_{j,u} & T_{j,v} \end{pmatrix}$ is the control vector of the j-th spacecraft, whose component are

$$T_{j,u} = T_j \sin\alpha \quad , \quad T_{j,v} = T_j \cos\alpha \tag{4.3}$$

The thrust magnitude of both spacecraft is limited to a maximum value T_{max}. The mission performance is evaluated with respect to the overall propellant consumption,

that is, the sum of the spacecraft consumptions. Equivalently, the merit index to maximize can be stated as the sum of the final masses of the two spacecraft:

$$J = m_I|_f + m_{II}|_f \tag{4.4}$$

The boundary constraints can be easily formulated in terms of the chosen state variables. The initial state of both spacecraft is completely known and can be expressed in terms of the initial radius:

$$r_I|_0 = \tilde{r}_0 \qquad \vartheta_I|_0 = 0 \qquad u_I|_0 = 0 \qquad v_I|_0 = \sqrt{1/\tilde{r}_0} \qquad m_I|_0 = 1 \tag{4.5}$$

$$r_{II}|_0 = \tilde{r}_0 \qquad \vartheta_{II}|_0 = \pi \qquad u_{II}|_0 = 0 \qquad v_{II}|_0 = \sqrt{1/\tilde{r}_0} \qquad m_{II}|_0 = 1 \tag{4.6}$$

A the end of the transfer the following rendezvous conditions hold:

$$r_I|_f - r_{II}|_f = 0 \tag{4.7}$$

$$\vartheta_I|_f - \vartheta_{II}|_f = 2k_{rev}\pi \tag{4.8}$$

$$u_I|_f - u_{II}|_f = 0 \tag{4.9}$$

$$v_I|_f - v_{II}|_f = 0 \tag{4.10}$$

Moreover the two spacecraft are required to reach the assigned final circular orbit:

$$r_I|_f = \tilde{r}_f \qquad u_I|_f = 0 \qquad v_I|_f = \sqrt{1/\tilde{r}_f} \tag{4.11a-c}$$

in an assigned time:

$$t|_f = \tilde{t}_f \tag{4.12}$$

Numerical data for the example problem, in nondimensional units, are:

$$\tilde{r}_0 = 1 \qquad \tilde{r}_f = 1.2 \qquad T_{\max} = 0.1 \qquad c_I = c_{II} = 1$$

The proposed problem can be handled by planning a sequential deployment or a cooperative strategy. In the sequential deployment, the flight of the two spacecraft is analyzed separately (i.e., in sequence). One spacecraft, the *Leader*, flies along an optimal "unconstrained" trajectory to reach the assigned final orbit, minimizing its propellant consumption without caring about the rendezvous constraint. The other spacecraft, the *Follower*, chases for the leader while aiming at minimizing its own propellant consumption. In the cooperative strategy, the two spacecraft are peer: there

are no leader and follower roles, but both spacecraft equally operate to accomplish the final constraints. The deployment is more complex to envisage, as the two spacecraft maneuver simultaneously and, depending on the available time, their propulsive strategies may change drastically. The higher complexity is rewarded by better overall performances.

4.2 The Leader / Follower Strategy

In this section of the Leader/Follower strategy will be outlined, highlighting different mission scenarios. The optimal control problems related to either spacecraft will be stated; for each one, optimality conditions will be derived and employed to form a Hamiltonian boundary value problem. Numerical results will be shown.

4.2.1 Strategy overview

The first step is deciding which spacecraft is the Leader and which one is the Follower. The Leader is privileged, as it flies an independent minimum-fuel transfer, while the follower alone bears the entire phasing duty, hence the associated cost. For the peculiar problem under investigation, choosing either spacecraft as the leader is the same: the spacecraft are almost indistinguishable, because identical from a propulsive point of view and in opposition one respect the other. Arbitrarily, Sat 2 has been chosen to be the Leader spacecraft and Sat 1 the Follower. The formation deployment problem is split into two distinct "basic" optimal control problems: a time-fixed orbit transfer between two completely defined orbits and a time-fixed rendezvous problem. The deployment of the Leader spacecraft is a self-consistent problem, as the relevant spacecraft is constrained only to reach the final circular orbit into a given time.

The deployment of the Follower, instead, depends on the Leader trajectory, as the Follower is constrained to reach the same final circular orbit, but, in addition, at the final instant it has to attain the same angular position as the Leader. Thus, the Leader transfer is optimized first, in order to provide the final conditions to define the Follower mission.

For a given (assigned) flight time, the optimal solution of the Leader deployment is not unique. Under the assumption that the thrust level is reasonably high and the available time sufficiently long, the Leader minimize its propellant consumption by

performing a Hohmann-like transfer, with one burn at the perigee of the transfer orbit and a second at the apogee[1]. Indeed, for any assigned final time $\tilde{t}_f$ greater than the duration t^* of the Hohmann-like transfer, there is a whole family of trajectories that have the same merit index and differ only by the duration of the coasting arcs on the initial and final orbits.

Once that the solution of Hohmann-like transfer is found, one can devise all the mission possibilities of the Leader spacecraft, for any assigned final time, by varying the time length of the coasting arcs on the initial or final orbits. The family of optimal trajectory of the Leader for any assigned flight duration $\tilde{t}_f$ can be parameterized in terms of length of the initial coasting arc τ_0. Thus, it is possible to calculate the angular position of the leader at the end of the trajectory algebraically:

$$\vartheta_{L_f} = \vartheta_{L_0} + \omega_0 \tau_0 + \vartheta^* + \omega_f \left(\tilde{t}_f - t^* - \tau_0 \right) \tag{4.13}$$

where:

- ω_0, ω_f are the angular velocity of the spacecraft on the initial and final orbits;
- ϑ_{L_0} is the right ascension of the leader spacecraft at the departure;
- τ_0 is the time-length of the initial coasting (subject to $0 \leq \tau_0 \leq \tilde{t}_f - t^*$);
- t^*, ϑ^* are, respectively, the flight time and the angular distance covered during the Hohmann-like transfer.

Knowing the numerical values for t^* and ϑ^*, it is possible to reduce the formation deployment problem just to the Follower deployment problem. In fact, the final Leader angular position ϑ_{L_f} is the only further element necessary to define completely the the rendezvous mission.

The Follower spacecraft may accomplish the rendezvous condition eq. (4.8) in two ways: by recovering phase (i.e., reducing the initial phase angle) or by losing phase (i.e., increasing the initial phase angle). In the first case, the Leader spacecraft has to be slower than the Follower, so that the initial phase angle may decrease along the trajectory; the phase constraint is verified with $k_{rev} = 0$. In the second case, the Leader

[1] If the available time is high, the optimal deployment of the Leader may be not an two-burn transfer, but it may consist of a sequence of many perigee and apogee burns. However, for the sake of clarity, we neglect this possibility and we assume that the leader only performs a two burn Hohmann-like transfer.

spacecraft has to be faster than the Follower, in order to permit that the initial phase angle increases. Eventually, the chaser spacecraft will perform half revolution less than the leader spacecraft and the phase constraint will be verified with $k_{rev} = -1$. For each of the two cases, a correct choice of duration τ_0 of the Leader initial coasting permits to minimize the rendezvous cost without altering the propellant consumption of the Leader deployment. In practice, the optimal value of τ_0 is at the extreme of its definition set ($\tau_0 \in \left[0, \tilde{t}_f - t^*\right]$). In the first case ($\tau_0 = 0$), the best mission opportunity is achieved by forcing the Leader spacecraft to start the Hohmann transfer soon and waiting on the final (slower) orbit. The chaser spacecraft flies along an inner orbit, therefore the phase angle decreases more rapidly if the Leader reaches sooner the final (higher) orbit. Conversely, in the second case ($\tau_0 = \tilde{t}_f - t^*$) the best option is given by forcing the Leader to wait as much as possible on the initial (fast) orbit before leaving for the Hohmann transfer. The Follower has to fly over an orbit exterior to the Leader's one in order to lose phase, and it needs to reach less high (and less expensive) altitude if the Leader stays on the initial orbit. Therefore, only these two strategies will be investigated: the first or *Interior* strategy is obtained by imposing $k_{rev} = 0$ and $\tau_0 = 0$; the second or *Exterior* strategy is defined by $k_{rev} = -1$ and $\tau_0 = \tilde{t}_f - t^*$.

4.2.2 The Leader Deployment

In this section the optimal control problem of the leader spacecraft (which leads to the one revolution Hohmann-like transfer) will be stated and its solution addressed by means of the indirect method described in the two previous chapters. The spacecraft state variables and dynamics were presented in section [4.1]: The spacecraft motion is described by a set of differential equation given by eq (4.14), that can be summarized synthetically by:

$$\dot{\bar{x}} = \bar{f}\left(\bar{x}, \bar{u}, t\right) = \begin{cases} \dot{\vec{r}} = \vec{V} \\ \dot{\vec{V}} = \vec{G}\left(\vec{r}\right) + \vec{T}/m \\ \dot{m} = -T/c \end{cases} \tag{4.14}$$

where $\vec{r} = r\,\hat{i}$ is the position vector and $\vec{V} = u\,\hat{i} + v\,\hat{j}$ is the velocity vector in the local reference frame $\bar{u} = \vec{T}$ is the control vector, and $\vec{G}\left(\vec{r}\right)$ is the gravitational acceleration vector. The transfer goal is to minimize the propellant consumption of the maneuvering spacecraft; or conversely, to maximize the final mass for an assigned initial value, that

is $J = m|_f$. At departure, the spacecraft state is fully assigned by eq. (4.5). At arrival, the spacecraft must be on the target circular orbit of radius $\tilde{r}_f$, hence eqs. (4.11a-c) hold. The flight time is here considered free; however only the solution lasting less than one revolution is searched for.

The optimal control problem, briefly described above, can be solved by an indirect method, that is by applying the procedure described in Chapter 2. First order necessary conditions must be derived and the Hamiltonian boundary value problem which arises can be addressed by means of a simple shooting technique. The adjoint variables $\bar{\lambda}_x = (\lambda_r, \lambda_\vartheta, \lambda_u, \lambda_v, \lambda_m)$ and the Hamiltonian $H = \bar{\lambda}_x^T \dot{\bar{x}}$ are introduced. Adjoint variables can be regrouped to highlight the adjoint position vector $\vec{\lambda}_r = \begin{pmatrix} \lambda_r & \lambda_\vartheta/r \end{pmatrix}^T$, and the adjoint velocity vector $\vec{\lambda}_V = \begin{pmatrix} \lambda_u & \lambda_v \end{pmatrix}^T$, hence the Hamiltonian can be written concisely as:

$$H = \vec{\lambda}_r^T \vec{V} + \vec{\lambda}_V^T \vec{G} + \vec{\lambda}_V^T \vec{T}/m - \lambda_m T/c \tag{4.15}$$

Euler-Lagrange equations provide the time-derivatives of the adjoint variables, are calculated according to eq. (2.16). Their analytical expression can be found, as an example, in [13]. The system dynamics is affine in the control whose magnitude is bounded; therefore the problem which arises is a bang-bang optimal control problem like those dealt with in Chapter 3. Recalling section [3.2], the optimal thrust direction is provided by eq. (3.10) or equivalently by Lawden primer vector theory. It follows that:

$$\vec{T} = \beta T_{\max} \vec{\lambda}_V \tag{4.16}$$

where $\vec{\lambda}_V$ is the adjoint velocity vector previously defined, also named "Primer Vector". For the sake of clarity, the Hamiltonian is here rewritten in order to highlight explicitly the switching function:

$$\begin{aligned} H &= \vec{\lambda}_r^T \vec{V} + \vec{\lambda}_V^T \vec{G} + \beta T_{\max} S_F \\ S_F &= \left|\vec{\lambda}_V\right|/m - \lambda_m/c \end{aligned} \tag{4.17}$$

Pontryagin Maximum Principle indicates whether the spacecraft has to maneuver or not. The Hamiltonian is linear in the thrust value, the control has a bang-bang structure: maximum thrust ($\beta = 1$) is exploited when the Switch Function S_F is positive, otherwise the engine is turned off ($\beta = 0$). Both the Multi-Bound approach and the Continuation-Smoothing technique discussed in Chapter 3 can be employed to avoid troubles linked to this formulation.

Since the burn structure of the desired solution is known (burn-coast-burn) a Multi-Bound approach can be easily applied. The trajectory is split into $n_{cmp} = 3$ arcs, joined by $n_{sw} = n_{cmp} - 1 = 2$ switching points. A mission structure $B = \{1, 0, 1\}$ is enforced and assigns the values of the magnitude of the control β in each arc. An auxiliary independent variable t_ε is introduced, linked to the time t by the equation:

$$t_\varepsilon = i - 1 + \left(t - \sum_{k=1}^{i-1} \tau_k \right) / \tau_i \ , \qquad i = 1, \ldots, n_{cmp} \tag{4.18}$$

where τ_i is the time length of the i-th arc. At the two internal boundaries the switching condition holds:

$$S_F|_i = 0 \ , \qquad i = 1, \ldots, n_{sw} \tag{4.19}$$

As far as the boundary conditions are concerned, all the adjoint variables are free at departure point because the spacecraft state is completely defined; instead, by applying the transversality conditions at the arrival point one obtains:

$$\lambda_\vartheta|_f = 0 \tag{4.20}$$

$$\lambda_m|_f = 1 \tag{4.21}$$

$$H|_f = 0 \tag{4.22}$$

The Hamiltonian boundary value problem can now be stated concisely as:

$$\begin{cases} \dfrac{d\bar{y}}{dt_\varepsilon} = \tau_i \bar{F}\left(\bar{y}, t_\varepsilon\right), \qquad \forall t_\varepsilon \in [i-1, i] \ , \ \ i = 1, .., 3 \\ s.t. \\ \qquad \beta = \{\beta_i, i = 1, .., 3\} = \{1, 0, 1\} \\ \qquad \bar{\Psi}_0\left(\bar{y}\left(0\right)\right) = 0 \\ \qquad S_F\left(\bar{y}\left(i\right)\right) = 0, \ \ i = 1, 2 \\ \qquad \bar{\Psi}_f\left(\bar{y}\left(3\right)\right) = 0 \end{cases} \tag{4.23}$$

$\bar{y} = \begin{pmatrix} \bar{x} & \bar{\lambda}_x & \bar{\tau} \end{pmatrix}^T$ is a vector which collects all the state and adjoint variables, plus the unknown arc time-length; $\bar{y} = \begin{pmatrix} \dot{\bar{x}} & \dot{\bar{\lambda}}_x & \dot{\bar{\tau}} \end{pmatrix}^T$ collects the differential equations associated to the state and adjoint variables, plus a vector of zeros ($\dot{\bar{\tau}} = 0$) for the constant

unknowns. $\bar{\Psi}_0$ is the vector of the initial condition and $\bar{\Psi}_f$ those the final conditions:

$$\bar{\Psi}_0(\bar{y}) = \begin{pmatrix} r - \tilde{r}_0 \\ \vartheta - \tilde{\vartheta}_0 \\ u - \tilde{u}_0 \\ v - \tilde{v}_0 \\ m - \tilde{m}_0 \end{pmatrix} \qquad \bar{\Psi}_f(\bar{y}) = \begin{pmatrix} r - \tilde{r}_f \\ \lambda_\vartheta \\ u \\ v - \sqrt{1/\tilde{r}_f} \\ \lambda_m - 1 \\ H \end{pmatrix} \tag{4.24}$$

The problem dimension is 13, but 5 variables are explicitly assigned at the initial point (i.e., the spacecraft state). Therefore, the actual problem has just 8 unknowns: 3 time-lengths τ_i, plus all the 5 initial values of the adjoint variables, hence

$$\bar{z} = \begin{pmatrix} \tau_1 & \tau_2 & \tau_3 & \lambda_{r0} & \lambda_{\vartheta 0} & \lambda_{u0} & \lambda_{v0} & \lambda_{m0} \end{pmatrix}^T$$

4.2.2.1 Numerical Results

The Hohmann-like transfer takes in total a time equal to $t^* = \tau_1 + \tau_2 + \tau_3 = 4.0416855$ (nondimensional unit: a time unit is equal to the period of the initial orbit divided by 2π). The spacecraft covers an angular distance $\vartheta^* = 3.5109880$ radians. The required propellant is $m^* = 0.0832786$ (as a fraction of the initial mass). The thrust direction, here expressed by the angle φ_T in Figure 4.3, is almost parallel to the velocity direction (given in terms of the flight path angle φ_V) during both burns.

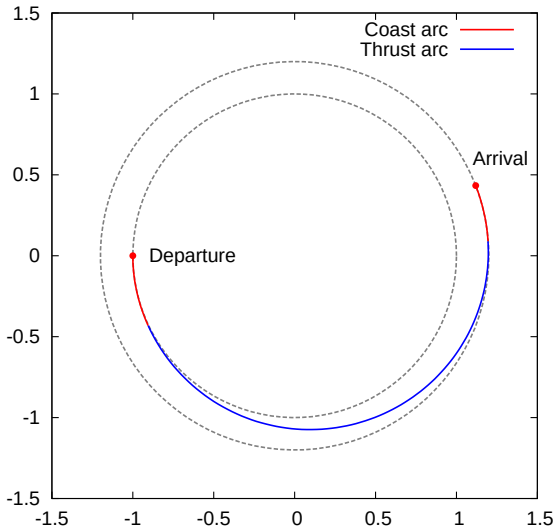

Figure 4.2: Trajectory of Leader Hohmann-like optimal transfer.

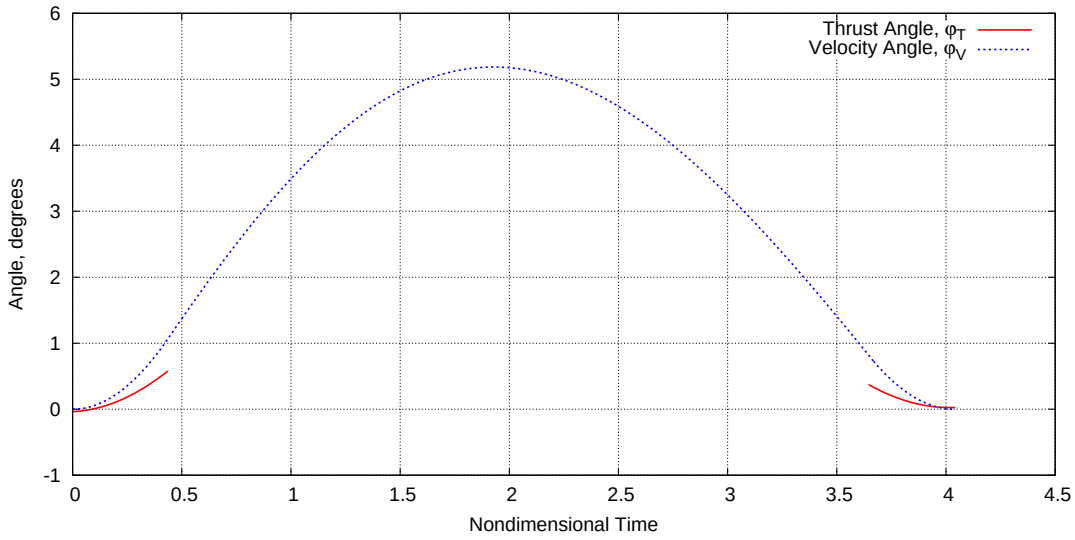

Figure 4.3: Thrust and Velocity angles of the Leader Hohmann-like optimal transfer.

4.2.3 The Follower Deployment

In this section the optimal control problem of the follower spacecraft will be stated and its solution addressed by means of the indirect method that exploits a Continuation-Smoothing technique. The spacecraft state variables and dynamics are the same as in Leader deployment; hence the same Euler-Lagrange equations (2.16) hold. The optimal control direction is still provided by eq (3.10), whereas the control magnitude β is given by eq. (3.77) or (3.86), whether the perturbing term introduced to regularize the control law is a quadratic penalty function or a logarithmic barrier, respectively. Boundary conditions are formally different with respect to the Leader deployment, mainly due to the presence of a phase constraint at the end of the trajectory, but also because the flight time is assigned. At departure, the spacecraft state is fully assigned: equations (4.5-4.6) hold and the adjoint variables are free. At arrival the spacecraft is constrained to reach the target circular orbit:

$$r|_f = \tilde{r}_f \qquad u|_f = 0 \qquad v|_f = \sqrt{1/\tilde{r}_f} \tag{4.25}$$

and to accomplish a phase constraint, which ensure the rendezvous with the leader:

$$\vartheta_1 = \vartheta_{L_f} + 2k_{rev}\pi, \qquad k_{rev} \in \mathbb{Z} \tag{4.26}$$

with $\vartheta_{L_f} = \vartheta_{L_f}\left(\tilde{t}_f, \tau_0\right)$ defined by eq (4.13) in section [4.2.1]. The flight time is also assigned:

$$t_f = \tilde{t}_f \tag{4.27}$$

By applying the transversality conditions eqs. (2.18-2.21) one obtains the conditions that close the Hamiltonian boundary value problem:

$$\lambda_m = 1 \tag{4.28}$$

The Hamiltonian boundary value problem can now be stated concisely as:

$$\begin{cases} \dfrac{d\bar{y}}{dt} = \bar{F}\left(\bar{y}, t\right), & \forall t \in \left[0, \tilde{t}_f\right] \\ s.t. \\ \bar{\Psi}_0\left(\bar{y}\left(0\right)\right) = 0 \\ \bar{\Psi}_f\left(\bar{y}\left(\tilde{t}_f\right)\right) = 0 \end{cases} \tag{4.29}$$

where:

- $\bar{y} = \begin{pmatrix} \bar{x} & \bar{\lambda}_x \end{pmatrix}^T$ collects state and adjoint variables;
- $\bar{F} = \begin{pmatrix} \dot{\bar{x}} & \dot{\bar{\lambda}}_x \end{pmatrix}^T$ their time-evolution, which encompasses the thrust law $\vec{T}$ defined as $\vec{T} = \beta\, T_{\max} \vec{\lambda}_V$, with $\beta = \beta_\varepsilon^L\left(\bar{y}\left(t_\varepsilon\right)\right)$, $\forall t \in \left[0, \tilde{t}_f\right]$;
- $\bar{\Psi}_0$ is the vector of the initial condition and $\bar{\Psi}_f$ the one of the final conditions:

$$\bar{\Psi}_0\left(\bar{y}\right) = \begin{pmatrix} r - \tilde{r}_0 \\ \vartheta - \tilde{\vartheta}_0 \\ u - \tilde{u}_0 \\ v - \tilde{v}_0 \\ m - \tilde{m}_0 \end{pmatrix} \qquad \bar{\Psi}_f\left(\bar{y}\right) = \begin{pmatrix} r - \tilde{r}_f \\ \vartheta - \vartheta_{L_f} - 2k_{rev}\pi \\ u \\ v - \sqrt{1/\tilde{r}_f} \\ \lambda_m - 1 \end{pmatrix} \tag{4.30}$$

The problem unknown are just the 5 initial adjoint variables, hence:

$$\bar{z} = \begin{pmatrix} \lambda_{r0} & \lambda_{\vartheta 0} & \lambda_{u0} & \lambda_{v0} & \lambda_{m0} \end{pmatrix}^T$$

The automatic initialization procedure described in section [3.4.3] can be adapted to the rendezvous problem under investigation, with only a slight modification to the orbit-shape continuation process. In particular, virtual initial condition $\bar{x}_\alpha$ (that are a

linear combination of true initial values $\bar{x}_0$ and final true values $\bar{x}_f$) should be written as:

$$\begin{aligned} r_\alpha &= (1-\alpha)\,\tilde{r}_0 + \alpha\,\tilde{r}_f \\ \vartheta_\alpha &= (1-\alpha)\,\vartheta_0 + \alpha\left(\vartheta_{L_f} - \omega_f \tilde{t}_f\right) \\ u_\alpha &= (1-\alpha)\,\tilde{u}_0 + \alpha\,\tilde{u}_f \\ v_\alpha &= (1-\alpha)\,\tilde{v}_0 + \alpha\,\tilde{v}_f \end{aligned} \tag{4.31}$$

In this way, the solution of the starting problem (i.e., the one characterized by a quadratic control law, a smoothing parameter $\varepsilon = 1$, and an orbit-shape parameter $\alpha = 1$), is simply:

$$\lambda_{r_0} = 0 \qquad \lambda_{r_0} = 0 \qquad \lambda_{u_0} = 0 \qquad \lambda_{v_0} = 0 \qquad \lambda_m = 1 \tag{4.32}$$

Starting from this solution, the continuation on the orbit-shape parameter and, subsequently, on the smoothing parameter can be performed, leading eventually to the optimal solution for any assigned flight time $\tilde{t}_f$.

4.2.3.1 Numerical Results

Depending on the assigned flight time, the rendezvous mission varies remarkably. Indeed a limit time t_{limit} exists: beyond this value the optimal trajectory is simply given by an Hohmann-like transfer, identical (from a propulsive point of view) to the one performed by the leader spacecraft, but shifted in time. The actual value of limit time can be calculated by replacing into the phase constraint (4.8) the right ascension of Sat 1 and Sat 2 calculated as sum of the angle covered during the Hohmann-like transfer plus the angle covered by coasting on the initial or final orbit respectively:

$$\begin{aligned} \vartheta_1\left(t_{\text{limit}}\right) &= \vartheta_1\left(0\right) + \omega_0\left(t_{\text{limit}} - t^*\right) + \vartheta^* \\ \vartheta_2\left(t_{\text{limit}}\right) &= \vartheta_2\left(0\right) + \omega_f\left(t_{\text{limit}} - t^*\right) + \vartheta^* \end{aligned} \tag{4.33}$$

with

$$\vartheta_2\left(0\right) - \vartheta_1\left(0\right) = \pi \tag{4.34}$$

thus:

$$\tilde{t}_{\text{limit}} = t^* + \pi / \left(\omega_0 - \omega_f\right) \tag{4.35}$$

The same value of the limit time t_{limit} holds whether the Interior or Exterior strategies are considered.

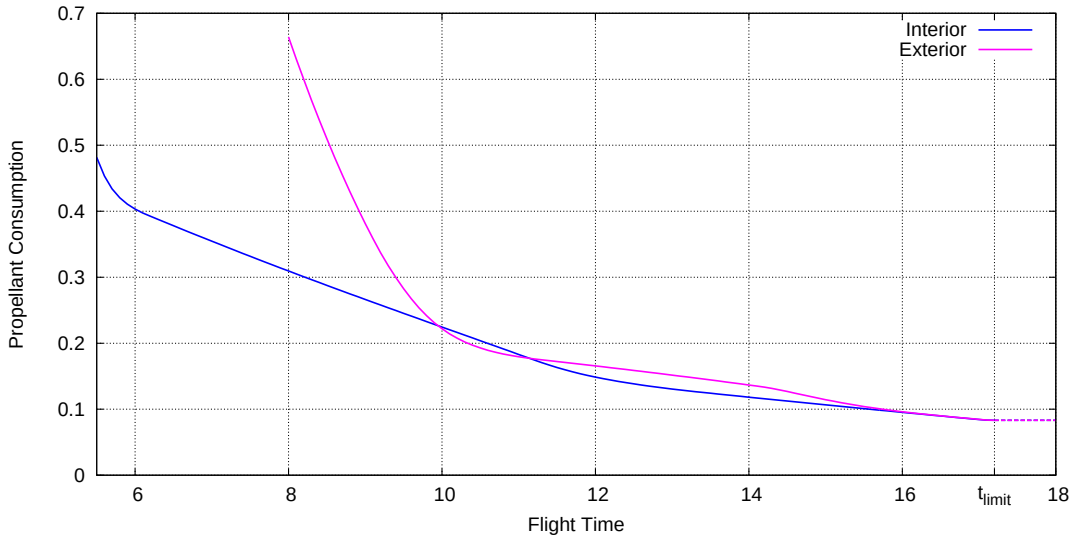

Figure 4.4: Performance comparison between Interior and Exterior strategies for the Follower transfer.

Performance of the Interior and Exterior strategies (introduced in section [4.2.1]) are shown in Figure 4.4. The propellant consumption of the Follower, expressed as a fraction of the its initial mass, is plotted versus the available flight time. The interior option ($k = 0$, $\tau_0 = 0$) proves to be more economic in almost any case, while the exterior option is preferable only if $\tilde{t}_f$ belongs to the time interval $(10 \div 11.2)$.

In either case, the burn structure of the solutions changes according to the available time $\tilde{t}_f$ The burn structure of the *Interior* solutions presents a sequence of 5 regions (for increasing t_f) with 2, 3, 4, 3, and eventually 2 burns. The same happens for the *Exterior* solution. A more detailed description is here provided for the Interior strategy, as it is almost always better than the other one.

If the available time to complete the rendezvous is very short (e.g. $\tilde{t}_f = 5.4$, Figure 4.5(a)), the Follower moves towards the inner regions in order to increase hastily its angular velocity, and to recover rapidly the phase difference with the target satellite. If the available time is a bit greater ($5.6 < \tilde{t}_f < 6.2$), the Follower can raise the perigee of its transfer orbit, hence reducing the propellant expenditure; a 3-burn strategy becomes optimal (Figure 4.5(b)). For longer mission ($6.3 < \tilde{t}_f < 11$) a 4-burn strategy proves to be the best. The first burn always aims to put the spacecraft into a faster (i.e., smaller)

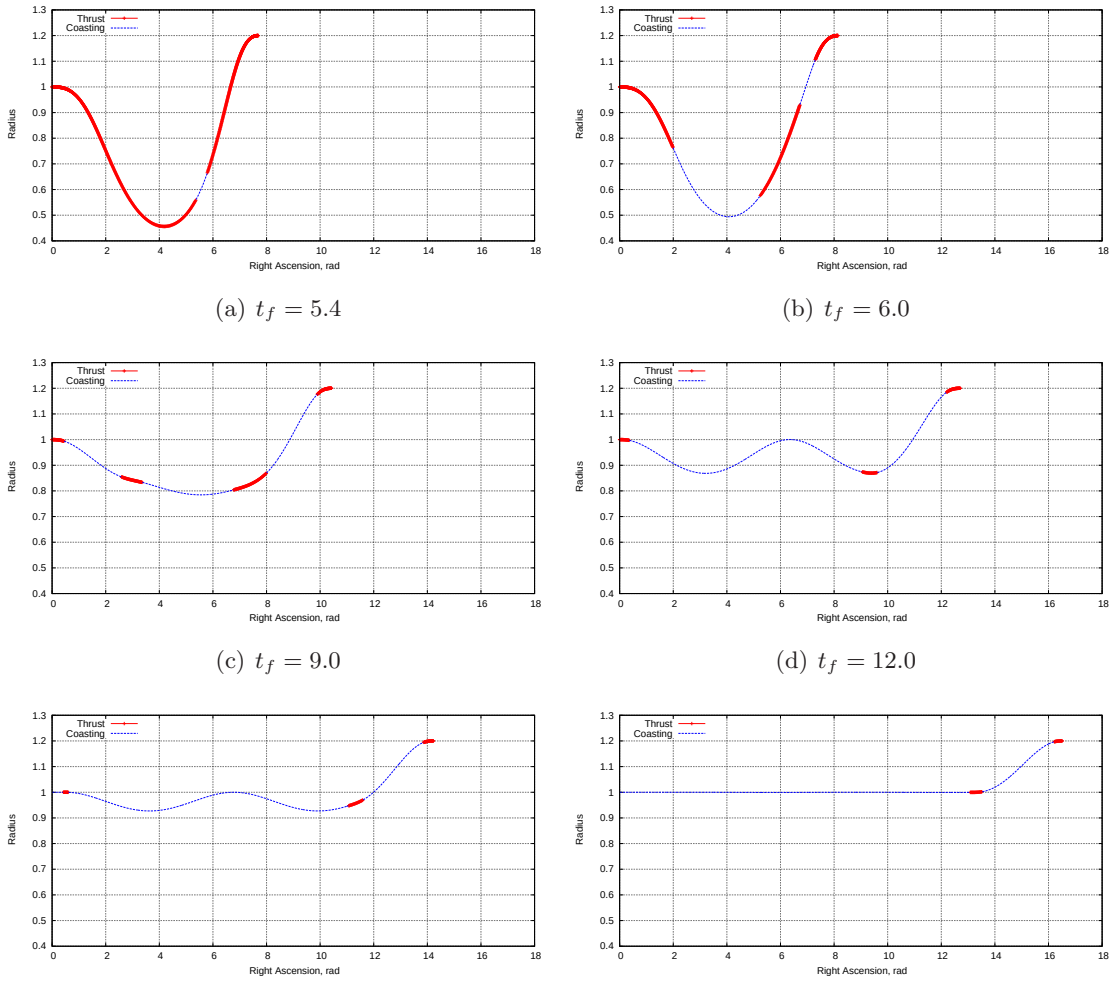

(a) $t_f = 5.4$

(b) $t_f = 6.0$

(c) $t_f = 9.0$

(d) $t_f = 12.0$

(e) $t_f = 14.0$

(f) $t_f = 17.0$

Figure 4.5: Follower trajectory in the r-ϑ plane, for several assigned flight times.

orbit and the last burn serves to complete the rendezvous. The two internal burns are employed to adjust the period of the interior orbit. The shape of the interior orbit change according to the mission duration. An interesting situation arises for $\tilde{t}_f = 9$ (Figure 4.5(c)): here the Follower employs the first burn to move inside and the second to (almost) circularize its trajectory. After roughly half revolution over this smaller orbit, a third burn is used to raise the apoapsis to the final circular orbit, and the last burn finalizes the rendezvous. For longer flight times, the Follower does not need to circularize the orbit, but it just wait on an elliptical orbit with a periapsis radius not too lower than the one of the initial circular orbit. The burn structure reduces to 3-burns (Figure 4.5(d)). As the available time increases, the periapsis increases, and an initial coasting arc arises ($t_f = 14$, Figure 4.5(e)). Eventually, when the limit time is reached, no interior waiting ellipse is needed and the trajectory is composed only of a coasting and a Hohmann transfer (Figure 4.5(f)).

4.3 The Cooperative Strategy

In this section the cooperative strategy for the rendezvous problem will be analyzed. The problem was comprehensively described in section [4.1] and, differently from the Leader/Follower case, no other assumption on the spacecraft trajectories has to be made in order to achieve the solution. Optimality conditions needed to form the Hamiltonian Boundary value problem will be derived in section [4.3.1]. Two different formulations, corresponding to the use of the Multi-Bound or the Continuation-Smoothing technique, will be discussed. The latter will exploit once more the automatic initialization algorithm described in section [3.4.3], and also adopted in the Follower mission (section [4.3.1]). However, since the problem is more tangled, its solutions will be checked by comparing them with those obtained manually using the Multi-Bound formulation. After that, the optimal cooperative solutions, just obtained, will be analyzed and compared to those achieved by the Leader/Follower strategy, highlighting the respective pros and cons.

4.3.1 Problem optimization

In the cooperative strategy there are no “Leader” or “Follower” satellites but both spacecraft operate to reach the rendezvous. As the mission is not halved into two

distinct problems, involving one spacecraft at once, the motion of both satellites has to be considered simultaneously. Therefore, the state of the overall "system" is given by a collection of the state variables of the two satellites:

$$\bar{x} = (\bar{x}_I, \bar{x}_{II}) = (r_I, \vartheta_I, u_I, v_I, m_I, r_{II}, \vartheta_{II}, u_{II}, v_{II}, m_{II}) \tag{4.36}$$

The corresponding adjoint vector (collection of adjoint variables) can be introduced:

$$\bar{\lambda}_x = \left(\bar{\lambda}_{x_I}, \bar{\lambda}_{x_{II}}\right) = (\lambda_{r_I}, \lambda_{\vartheta_I}, \lambda_{u_I}, \lambda_{v_I}, \lambda_{m_I}, \lambda_{r_{II}}, \lambda_{\vartheta_{II}}, \lambda_{u_{II}}, \lambda_{v_{II}}, \lambda_{m_{II}}) \tag{4.37}$$

The equations of motion of each spacecraft remain unchanged with respect to the single spacecraft problem, but obviously their number doubles:

$$\frac{d\bar{x}}{dt} = \bar{f}\left(\bar{x}, \bar{u}, t\right) = \left(\bar{f}_I\left(\bar{x}_I, \bar{u}_I, t\right), \bar{f}_{II}\left(\bar{x}_{II}, \bar{u}_{II}, t\right)\right) \tag{4.38}$$

where even the control vector $\bar{u}$ can be partitioned into two thrust vectors $\bar{u}_I = \vec{T}_I$ and $\bar{u}_{II} = \vec{T}_{II}$, each one acting on a different spacecraft. Both vectors are limited in magnitude to a maximum, finite thrust value $T_{\max}$.

As always, the Hamiltonian is defined as $H = \bar{\lambda}_x^T \bar{f}$. However, in this case it can be written as the sum of the two Hamiltonians corresponding to each spacecraft (by exploiting the natural partition of both adjoint vector and differential equation system).

$$H = H_I + H_{II} = \bar{\lambda}_{x_I}^T \dot{\bar{x}}_I + \bar{\lambda}_{x_{II}}^T \dot{\bar{x}}_{II} \tag{4.39}$$

Easily, one can reduce the Euler-Lagrange equations of this system to those of the two single spacecraft. As far as the control is concerned, due to the peculiar partition of the Hamiltonian, the equations that define the optimal thrust laws of the two spacecrafts are analogous. In particular, by applying the Pontryagin Maximum Principle, it is simple to verify that the optimal thrust direction for each spacecraft, is collinear to the Primer Vector of that spacecraft, that is $\vec{\lambda}_{V_j} = \begin{pmatrix}\lambda_{u_j} & \lambda_{v_j}\end{pmatrix}^T$ with $j = I, II$ in case of Sat 1 and Sat 2 respectively. Thus:

$$\vec{T}_j = T_{\max}\beta_j \vec{\lambda}_{V_j}, \qquad j = I, II \tag{4.40}$$

By replacing the latter equation in the Hamiltonian, one highlights the presence of two distinct switching functions S_{F_I}, $S_{F_{II}}$ each one related to one spacecraft:

$$\begin{aligned} H = &\vec{\lambda}_{r_I}^T \vec{V}_I + \vec{\lambda}_{V_I}^T \vec{G}\left(\vec{r}_I\right) + T_{max} S_{F_I} \beta_I + \\ &\vec{\lambda}_{r_{II}}^T \vec{V}_{II} + \vec{\lambda}_{V_{II}}^T \vec{G}\left(\vec{r}_{II}\right) + T_{max} S_{F_{II}} \beta_{II} \end{aligned} \tag{4.41}$$

By applying again PMP, one finds out that the optimal thrust modulus β of each spacecraft only depends on the magnitude of the relevant switching function: maximum thrust ($\beta = 1$) is exploited when the switching function is positive, otherwise the engine is turned off ($\beta = 0$). The optimal control is therefore bang-bang.

Depending on the technique adopted to handle the bang-bang control, one has a different formulation. Here, we consider the Continuation-Smoothing technique (the Multi-Bound formulation will be shown later). When the Continuation-Smoothing technique is employed, the thrust magnitude β for each spacecraft can be directly calculated by using equation eq.(3.77) or (3.86), depending on the choice of a quadratic or logarithmic term for the regularization, respectively. One needs just to replace the generic switch function value S_F of the formulas with that of the relevant spacecraft. As each spacecraft has its own switch function at any time, the thrust magnitude will be usually different between them.

Boundary conditions are mostly the same presented in the Leader/Follower deployment problem, because all the problem physical constraints (listed in section [4.1]) have to be fulfilled, no matter which approach is used. The only degree of freedom is the right ascension of the arrival point (which is free at the rendezvous).

At departure, the state of each spacecraft is fully assigned: equations (4.5-4.6) hold and all the adjoint variables are free. At the end of the transfer, both spacecraft are constrained to reach the target circular orbit with the same angular position. Equations (4.11a-c) and (4.7-4.10) hold respectively. The flight time is also assigned. By applying the transversality conditions (2.18-2.21) one obtains the conditions that close the Hamiltonian boundary value problem:

$$\lambda_{\vartheta_I}|_f + \lambda_{\vartheta_{II}}|_f = 0 \qquad \lambda_{m_I}|_f = 1 \qquad \lambda_{m_{II}}|_f = 1 \tag{4.42}$$

The resulting Hamiltonian Boundary Value Problem can now be stated as:

$$\begin{cases} \dfrac{d\bar{y}}{dt} = \bar{F}\left(\bar{y}, t\right), \qquad \forall t \in \left[0, \tilde{t}_f\right] \\ s.t. \\ \qquad \bar{\Psi}_0\left(\bar{y}\left(0\right)\right) = 0 \\ \qquad \bar{\Psi}_f\left(\bar{y}\left(\tilde{t}_f\right)\right) = 0 \end{cases} \tag{4.43}$$

where:

- $\bar{y} = \begin{pmatrix} \bar{x} & \bar{\lambda}_x \end{pmatrix}^T$ collects state and adjoint variables;
- $\bar{F} = \begin{pmatrix} \dot{\bar{x}} & \dot{\bar{\lambda}}_x \end{pmatrix}^T$ their time-evolution, which encompasses the thrust law $\vec{T}_j$ defined as $\vec{T}_j = \beta_j T_{\max} \vec{\lambda}_{V_j}$ and $\beta_j = \beta_\varepsilon \left(S_{F,j} \right)$, where the subscript "$j$" indicates quantities related to the j-th spacecraft.
- $\bar{\Psi}_0$ is the vector of the initial conditions:

$$\bar{\Psi}_0 \left(\bar{y} \right) = \begin{pmatrix} \begin{pmatrix} r_I - \tilde{r}_0 & \vartheta_I - \tilde{\vartheta}_0 & u_I - \tilde{u}_0 & v_I - \tilde{v}_0 & m_I - \tilde{m}_0 \end{pmatrix}^T \\ \begin{pmatrix} r_{II} - \tilde{r}_0 & \vartheta_{II} - \tilde{\vartheta}_0 & u_{II} - \tilde{u}_0 & v_{II} - \tilde{v}_0 & m_{II} - \tilde{m}_0 \end{pmatrix}^T \end{pmatrix} \tag{4.44}$$

- $\bar{\Psi}_f$ is the vector the final conditions

$$\bar{\Psi}_f \left(\bar{y} \right) = \begin{pmatrix} \begin{pmatrix} r_I - \tilde{r}_f & u_I & v_I - \sqrt{1/\tilde{r}_f} & \lambda_{m_I} - 1 \end{pmatrix}^T \\ \begin{pmatrix} r_{II} - \tilde{r}_f & u_{II} & v_{II} - \sqrt{1/\tilde{r}_f} & \lambda_{m_{II}} - 1 \end{pmatrix}^T \\ \begin{pmatrix} \vartheta_I - \vartheta_{II} & \lambda_{\vartheta_I} + \lambda_{\vartheta_{II}} \end{pmatrix}^T \end{pmatrix} \tag{4.45}$$

The problem unknown are just the 10 initial adjoint variables, hence $\bar{z} = \begin{pmatrix} \bar{\lambda}_{x_{I,0}} & \bar{\lambda}_{x_{II,0}} \end{pmatrix}^T$.

As for the Follower deployment mission, the Continuation-Smoothing formulation can be coupled with a simple automatic initialization procedure based on an "orbit-shape" continuation. This is made to relieve the user from having to manually look for a proper initial guess at the solution of the BVP. With respect to the algorithm presented in section [4.2.3], minimal changes of the orbit-shape continuation are needed to adapt it to the two-spacecraft cooperative case.

$$r_{I\alpha} = (1-\alpha)\,\tilde{r}_0 + \alpha\,\tilde{r}_f \qquad r_{II\alpha} = (1-\alpha)\,\tilde{r}_0 + \alpha\,\tilde{r}_f \tag{4.46}$$

$$\vartheta_{I\alpha} = (1-\alpha)\,\vartheta_{I0} + \alpha\tfrac{\vartheta_{I0}+\vartheta_{II0}}{2} \qquad \vartheta_{II\alpha} = (1-\alpha)\,\vartheta_{II0} + \alpha\tfrac{\vartheta_{I0}+\vartheta_{II0}}{2} \tag{4.47}$$

$$u_{I\alpha} = (1-\alpha)\,\tilde{u}_0 + \alpha\,\tilde{u}_f \qquad u_{II\alpha} = (1-\alpha)\,\tilde{u}_0 + \alpha\,\tilde{u}_f \tag{4.48}$$

$$v_{I,\alpha} = (1-\alpha)\,\tilde{v}_0 + \alpha\,\tilde{v}_f \qquad v_{II,\alpha} = (1-\alpha)\,\tilde{v}_0 + \alpha\,\tilde{v}_f \tag{4.49}$$

The solution of the starting problem ($\alpha = 1$), assuming a quadratic merit index (i.e., a quadratic penalty function, smoothing parameter $\varepsilon = 1$) is simply:

$$\lambda_{r_{I,0}} = 0 \qquad \lambda_{\vartheta_{I,0}} = 0 \qquad \lambda_{u_{I,0}} = 0 \qquad \lambda_{v_{I,0}} = 0 \qquad \lambda_{m_{I,0}} = 1 \tag{4.50}$$

$$\lambda_{r_{II,0}} = 0 \qquad \lambda_{\vartheta_{II,0}} = 0 \qquad \lambda_{u_{II,0}} = 0 \qquad \lambda_{v_{II,0}} = 0 \qquad \lambda_{m_{II,0}} = 1 \tag{4.51}$$

To attain the solution of the original problem, the orbit-shape continuation for $\alpha : 1 \to 0$ is performed, keeping the same regularization term for the control law. Next, a second continuation is performed on the smoothing parameter assuming a logarithmic barrier regularization, for $\varepsilon \to 10^{-6}$.

4.3.2 Formulation with the Multi-Bound Technique

If the Multi-bound approach is used to handle the bang-bang control laws of the two spacecraft, the magnitude β of the control is not provided any longer by eq. (3.77) or (3.86). Instead, the trajectory has to be divided in phases and either a null or unit value of β is enforced in any arc for each spacecraft; hence, at any instant, thrust magnitudes are not directly linked to the current value of the switching functions at that instant. The remainder of the problem (i.e., differential equations, initial and final boundary conditions) remain unchanged.

To indicate whether Sat 1 and Sat 2 has to maneuver or not, a pair of thrust magnitude values (β_I, β_{II}) must be assigned to any arc. The mission structure B_M is therefore given by the collection of the pair (β_I, β_{II}) for every arc:

$$B_M = \left\{ (\beta_I, \beta_{II})|_1, \ldots, (\beta_I, \beta_{II})|_{n_{cmp}} \right\} \tag{4.52}$$

At any internal boundary, the switching condition applies (usually) to one spacecraft only. This formulation is pretty uncomfortable to be used. In fact, it requires not only to assign the burn structures of both spacecraft, but also the relative sequence of switch on/off of the two spacecraft. The latter requirement is the most difficult one to match, as it is usually unknown whether Sat 1 would start thrusting before Sat 2 or vice versa, and a wrong assumption would lead for sure to convergence issues (i.e., arcs with negative time lengths). This problem can be overcome by using two different, independent time-scales for the two spacecraft; in this way the mission structure B_M is formally divided into two independent spacecraft burn structure B_I and B_{II}, related

to Sat 1 and Sat 2. The two time scales t_I, t_{II} of the two spacecraft are obtained by introducing an auxiliary independent variable t_ε, linked to the time t_j of the j-th spacecraft by the equation:

$$t_j = \tau_i \left(t_\varepsilon - i + 1\right) + \sum_{k=1}^{i-1} \tau_{j,i}, \qquad t_{j,i-1} \leq t \leq t_{j,i} \tag{4.53}$$

with $t_{j,i} = \sum_{k=1}^{i} \tau_{j,i}$ and $j = I, II$ for Sat 1 and Sat 2 respectively.

The burn structures of the two spacecraft may require, in general, a different number of coast and thrust arcs. To improve the numerical solution algorithm, it is convenient to articulate both trajectories into the same number of arcs; moreover the statement of the internal boundary conditions is simplified by "aligning" thrust and coast arcs of the two spacecraft, so that corresponding arcs are thrust or coast phases for both spacecraft and a burn arc is always followed by a coasting (and vice versa). For example, one assumes an odd number of arcs: the first and the last are thrust arcs, the others are defined accordingly. This useful scheme can be always fulfilled by choosing a number of arcs n_{cmp} sufficiently high to match the number of burn and coasting arcs required by the longest burn structure, and adding a proper number of null-length arcs to the other.

The aligned burn structures of the two spacecraft can be reduced to "over-structures" where one needs to declare only if a certain burn is "activated" (i.e., true: the arc-lengths are not zero) or "deactivated" (i.e., false, meaning that there is a pair - a coast and a burn phase - of null-length arcs). The overstructure OB of each spacecraft has the form $OB = \{b_1, ..., b_{n_b}\}$, with (for example) $b_i = 1$ if the burn is activated or $b_i = 0$ if it is not.

For each spacecraft, internal boundary conditions are different if the burn is activated or not. If all burns are active, at any internal boundary the switching conditions eq. (3.41) hold. If the first (or last) burn of a spacecraft is deactivated, the switching condition at the first (last) internal boundary is replaced by a null-length condition on the first (last) arc duration (that is $\tau_1 = 0$ or $\tau_{n_{cmp}} = 0$). Instead, whenever the i-th internal burn is deactivated, the switching conditions at the boundaries $2(i-1)$ and $2(i-1)+1$ are replaced with null-length conditions on the duration of arcs $2(i-1)$ and

$2(i-1)+1$[1]. By using this escamotage, one can handle two complex and different burn structures at the same time, with a minimal effort. In the present problem, the longest spacecraft burn structure is TcTcTcT, which has $n_b = 4$ burns, therefore it is sufficient to split the trajectory into $n_{cmp} = 2n_b - 1 = 7$ arcs, with $n_{sw} = n_{cmp} - 1 = 6$ switching points. With respect to the Continuation-Smoothing formulation, the number of unknowns grows. In particular, in the case mentioned above, the additional unknowns are n_{cmp} for each spacecraft, that is 14 all together. Some example of burn structures and corresponding over-structures are:

$$\begin{aligned}
\text{TcT} &\rightarrow \ OB = \{1,0,0,1\} \\
\text{TcTc} &\rightarrow \ OB = \{1,0,1,0\} \\
\text{cTcT} &\rightarrow \ OB = \{0,1,0,1\} \\
\text{cTcTc} &\rightarrow \ OB = \{0,1,1,0\} \\
\text{TcTcTc} &\rightarrow \ OB = \{1,1,1,0\} \\
\text{cTcTcT} &\rightarrow \ OB = \{0,1,1,1\} \\
\text{TcTcTcT} &\rightarrow \ OB = \{1,1,1,1\}
\end{aligned}$$

4.3.3 Numerical Results

Numerical solution obtained either via Multi-Bound and Auto-initialized Continuation-Smoothing approach are presented in this section. The Multi-Bound approach is employed first, to explore the solution space.

Departing from the solution of a specific mission (i.e., corresponding to a certain flight-time), solutions for different mission flight-times can be achieved by extension, that is, by slowly varying the mission duration and using the previous solution as initial guess for the next one.

A branch is followed as long as the solution fulfills PMP. Whenever an unfeasible/unphysical or non-PMP solution is attained, the burn structure must be modified accordingly. The extension procedure is resumed, but this time it follows a new, different, branch.

[1] If all the burns are deactivated, the only non-null coasting arc is the $n_{cmp} - 1$.

When the extension procedure is interrupted, the burn structure has to be manually adjusted, according to the detected event.[1] Usually, three event may occur:

1. The switching function becomes negative in a burn arc; thus one has to split the burn arc in two and to add a coasting arc;

2. The switching function becomes positive in a coasting arc; thus one has to split the coasting arc in two and to add a burning arc;

3. A coasting or burning arc duration becomes negative; thus one has to remove that arc and to join the two adjacent ones.

The extension process is very efficient in case of the Multi-Bound approach. The burn structure is preassigned, hence a solution branch can be followed easily (e.g., with longer steps) without fear of losing it (i.e., jumping on a different one). Also, this procedure can be employed to follow a solution branch even when it does not respect PMP.

Collecting all the solution found, one can produce an overall picture, which is depicted in Figure 4.6. Continuous lines refer to the PMP solutions, while dotted lines refers to the non-PMP ones. This picture reveals that the cooperative rendezvous problem has a multitude of optimal and sub-optimal solutions, which belongs to the variety of burn structures that each spacecraft might adopt to complete its own transfer. One can notice that there are two families of locally optimal solutions, which respect all the first order optimality conditions; several sub-optimal (non-PMP) branches of solutions depart from these two families. The global optimal solution of the problem belongs alternatively to one of the two families of PMP solutions. A single transition point (beyond which a family stops being globally optimal and the other one starts) can be detected.

The cooperative rendezvous problem can also be faced using the Auto-CS algorithm described in section [4.3.1], which make use of a combination of a simple initialization procedure and the Continuation-Smoothing approach. Its solutions can be checked against those found previously using the Multi-Bound approach. A comparison is presented in Figure 4.7. As far as the solutions found using the Multi-Bound approach are concerned, only those respecting PMP are shown, for the sake of clearness. The

[1] These adjustments have to be made manually, cannot be fully-automated, because in general two events might take place simultaneously.

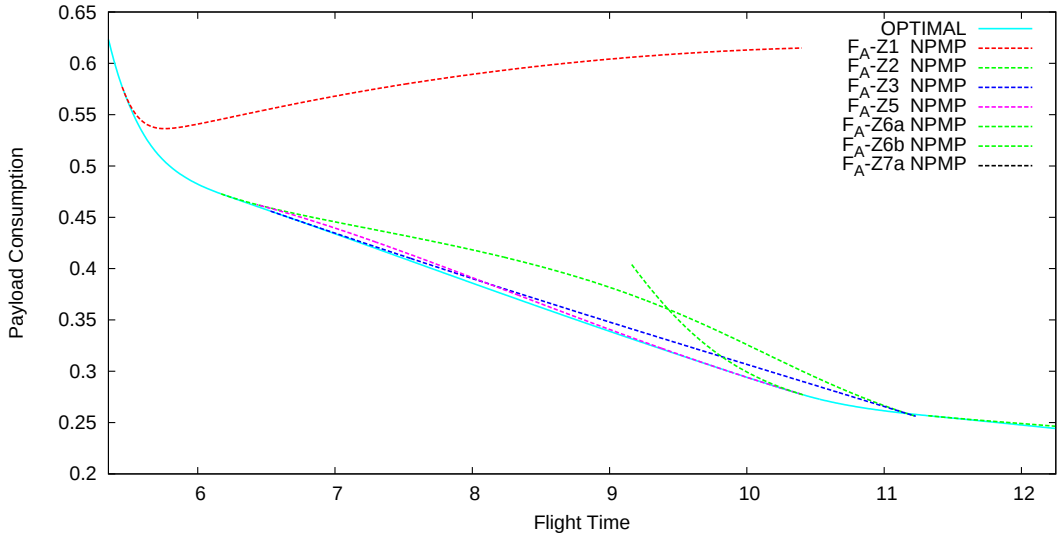

(a) Family F_A

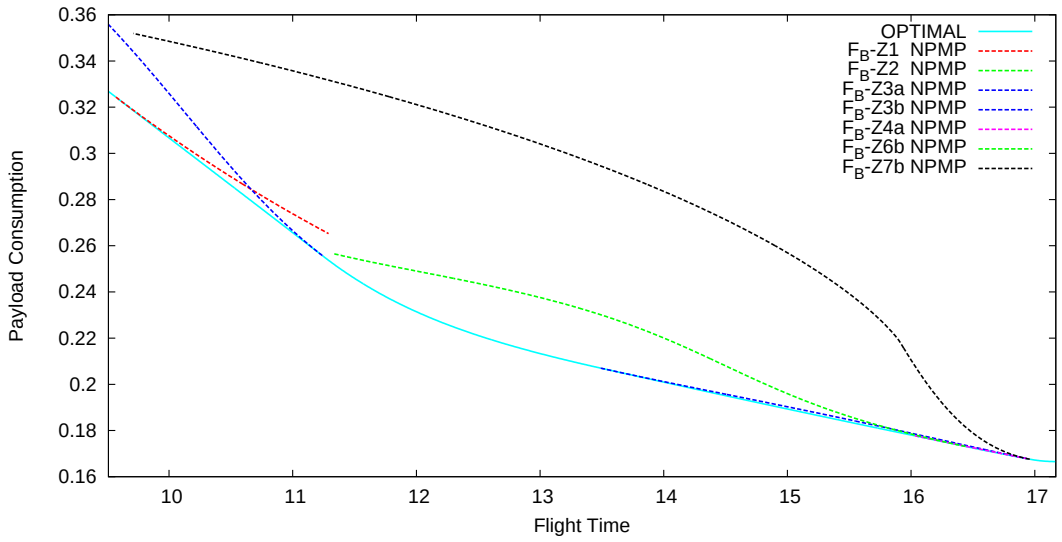

(b) Family F_B

Figure 4.6: Optimal and Sub-optimal solutions for the cooperative rendezvous.

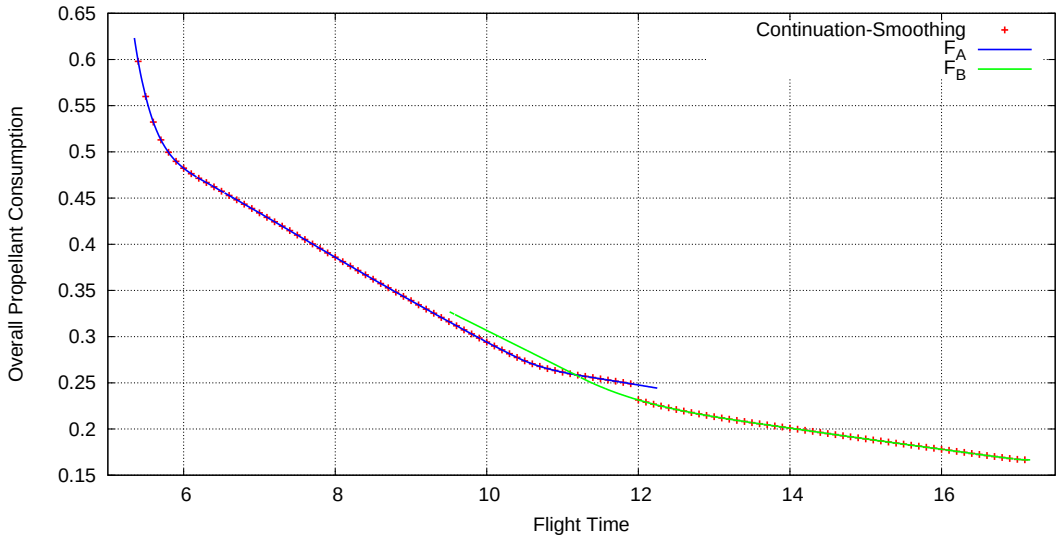

Figure 4.7: Comparison between the solutions found either via Multi-Bound or Auto-CS approach.

Auto-CS algorithm converges to the optimal solution in most of the cases, despite the presence of many optimal and sub-optimal solutions, which might prevent an automated method from convergence. All the solutions found respect PMP; only in a small region just after the transition point, the Auto-CS algorithm attains a group of solutions which fulfill PMP but are only locally optimal. However, the overall judgment about the proposed algorithm is very positive. As a general remark, the algorithm shows difficulties in capturing the correct solution when there are two, or more, flight profiles that differ for more than a complete revolution (that is, when the number of revolutions can change of an integer round by varying to the control law, with a small additional fuel consumption). In that case the orbit-shape initialization (which is performed assuming as merit index the energy of the control) leads to the minimum-energy solution, which may or may not have the same number of revolutions of the minimum-fuel solution.

The attention will be now pointed towards the optimal solution itself (regardless how it is obtained). The two families of PMP solutions, their burn structures, relative performance and region of existence, are analyzed. Figure 4.7 shows that, for an assigned mission duration, the solutions corresponding to the two "PMP-families" do not always exist "simultaneously". In particular, one can notice that solutions belonging to the family labeled "F_B" are present in the right part of the graph (that is, for

longer missions), while solutions that belong to the "F_A" family exist in the left part of the graph (shorter missions). Both kinds of solution are attainable in an intermediate region ($9.51 \leq \tilde{t}_f \leq 12.25$).

In either case, the burn structure of the two spacecraft changes with to the assigned flight time. The region of existence of both families can be split into different zones according to the burn structure. The actual subdivision is presented in Table 4.1 and 4.2. The (globally) optimal solution belongs to either family, depending on the flight time. The "switch" from optimality of family F_A to F_B is for $\tilde{t}_f \approx 11.165$.

F_A - Zone 1	TcT	TcTc	5.35	5.45
F_A - Zone 2	TcTcT	TcTc	5.46	6.17
F_A - Zone 3	TcTcTcT	TcTc	6.18	6.53
F_A - Zone 4	TcTcTcT	TcTcT	6.54	9.91
F_A - Zone 5	cTcTcT	TcTcT	9.92	10.40
F_A - Zone 6	cTcT	TcTcT	10.41	11.32
F_A - Zone 7	cTcT	TcTcTc	11.33	12.25

Table 4.1: Family F_A.

F_B - Zone 1	TcTcTcT	TcTcT	9.51	9.57
F_B - Zone 2	TcTcTcT	TcTc	9.58	11.23
F_B - Zone 3	TcTcT	TcTc	11.24	13.49
F_B - Zone 4	cTcTcT	TcTc	13.50	16.03
F_B - Zone 5	cTcTcT	TcTcT	16.04	16.43
F_B - Zone 6	cTcT	TcTcT	16.44	16.95
F_B - Zone 7	cTcT	TcTc	16.96	17.17

Table 4.2: Family F_B.

The two families of solutions may be distinguished (and also named) on the basis of the number of revolutions performed by the spacecraft. In particular, Family F_A is characterized by solutions where the slower spacecraft performs (more or less) one revolution and always less than two. Solutions that belongs to Family F_B are characterized by almost two complete revolutions of Sat 1 and Sat 2, and always more than

one. As the final right ascension is tightly linked to the available time, the existence of only one family of solutions for very short or very long times is easily explained. However, there is an intermediate range of times for which both solutions are possible: in the first case the preceding spacecraft flies over a slower (external) orbit while the other spacecraft wait on the initial orbit; in the other case the following spacecraft flies over a faster (internal) orbit and the other spacecraft wait on the final orbit.

Looking at Figures 4.8 and 4.9, one can observe the behavior of the solutions as the available time grows, and notice the regions of higher (or lower) cooperation. For the lowest times (e.g. for $t_f = 5.5$, Figure 4.8(a)), only family F_A exists. The phasing duty is completely born by Sat 1, which performs a very internal trajectory to recover phase angle. Sat 2 does not help Sat 1, as the available time permits to perform a Hohmann-like transfer, but it is too short to allow a further half revolution on a "waiting orbit". Other possibilities would exist, but are not optimal, as the thrust would not be parallel to the velocity, hence causing severe velocity losses. When the time increases (e.g. for $t_f = 7$, Figure 4.8(b)) Sat 2 is capable of helping Sat 1 by raising its transfer orbit and performing two half revolutions: one from the departure orbit to an apogee higher than 1.2, the other to "come back" on the arrival orbit. Henceforward Sat 2 will always perform about one complete revolution before reaching the final orbit.

If the time increases further (e.g. $t_f = 8$ or 9, Figure 4.8(c)), Sat 1 can avoid to reach the low altitudes needed in the cases of the lowest flight times. This happens because, when the time increases, Sat 1 can recover the same phase angle more slowly, and also due to the help of Sat 2 that manages to raise the apogee of its waiting orbit. The phasing duty is being shifted from Sat 1 to Sat 2. The perigee of Sat 1 internal orbit increases progressively. At first, a coasting on the initial orbit arises at the beginning of the trajectory; subsequently, the internal orbit reduces to a long coasting on the initial orbit: the shift of the phasing duty from Sat 1 to Sat 2 is complete ($t_f = 10.5$, Figure 4.8(d)). Henceforward Sat 1 performs substantially a Hohmann-like transfer. For longer times (more than 10.5) Sat 2 reduces the altitude of its intermediate apogee (since the available time to lose the same phase angle is greater). For even longer missions, Sat 2 continues to perform almost a complete revolution, by adjusting its trajectory, and, when it cannot lower its apogee anymore, its trajectory is modified by adding a coasting on the final orbit. Soon after (for $t_f = 12.25$), the family F_A dies (no solution can be attained).

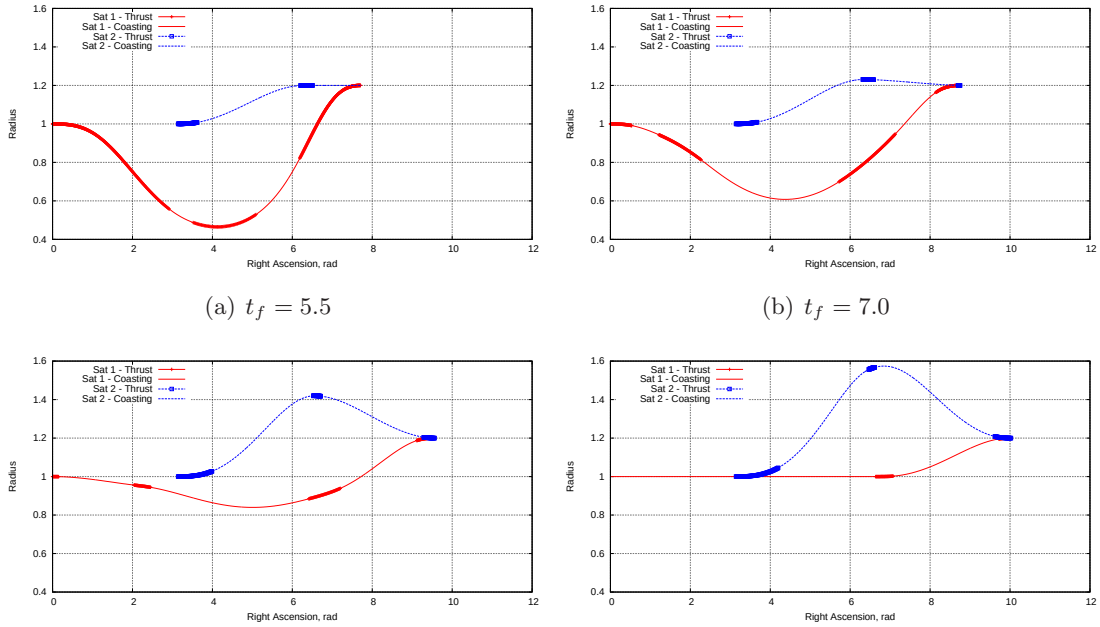

(a) $t_f = 5.5$ (b) $t_f = 7.0$

(c) $t_f = 9.0$ (d) $t_f = 10.5$

Figure 4.8: Cooperative Rendezvous Family F_A: Sat 1 and Sat 2 trajectories in the r-ϑ plane, for several assigned flight times.

Before the F_A solution branch extinguishes, family F_B arises. At the beginning (e.g., $t_f = 9.8$, Figure 4.9(a)), the phasing duty is again taken by Sat 1. This spacecraft covers one and half revolution on an internal orbit, and then almost half revolution to reach the final orbit. It starts its transfer braking (therefore at an apogee) and when it is at the second periapsis it accelerates to rise the apogee to the arrival orbit at r=1.2; Sat 2 does not have sufficient time to perform two complete revolutions over an orbit with period greater than the final one, hence it perform a trajectory very close to the optimal unconstrained one. As the time increases, the perigees of Sat 1 intermediate orbit raise. At first the intermediate orbit is almost circular (and 4 burns are exploited); subsequently, for longer flight times (e.g., for $t_f = 11.8$, Figure 4.9(b), and $t_f = 14.0$, Figure 4.9(c)), it reduces to a unique elliptic orbit with one burn located near the second apogee (and one burn vanishes). Sat 2 continues to perform a Hohmann-like transfer followed by a coasting on the final orbit. When the time is sufficiently high ($t_f = 16.3$, Figure 4.9(d)) Sat 2 manages to complete two revolutions on a waiting orbit

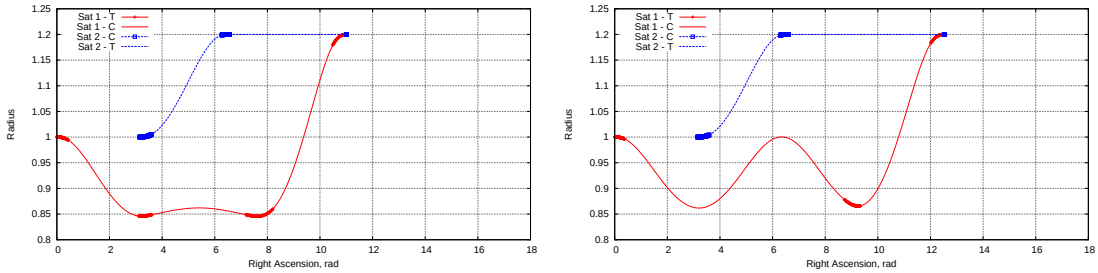

(a) $t_f = 9.8$ (b) $t_f = 11.8$

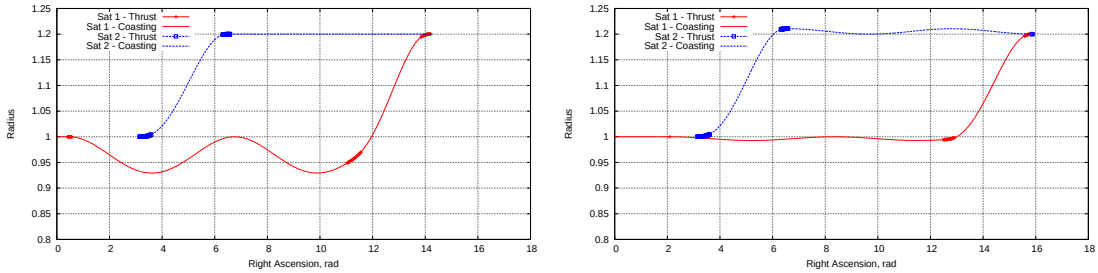

(c) $t_f = 14.0$ (d) $t_f = 16.3$

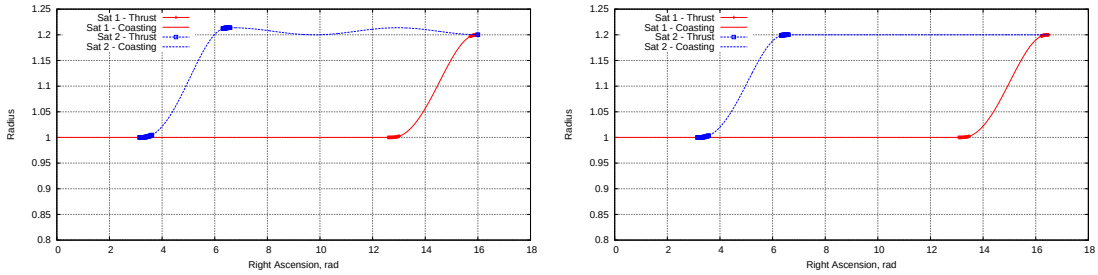

(e) $t_f = 16.5$ (f) $t_f = 17.0$

Figure 4.9: Cooperative Rendezvous - Family F_B: Sat 1 and Sat 2 trajectories in the r-ϑ plane, for several assigned flight times.

with period greater that the final orbit, therefore it can relieve Sat 1 from a piece of the phasing duty. In a very tight range of times, the overall duty is moved from one spacecraft to the other, and the intermediate orbit of Sat 1 progressively reduces just to a costing over the initial one ($t_f = 16.5$, Figure 4.9(e)). Finally the available time reaches the limit value $t_{\text{limit}} = 17.1713$, and both spacecraft can perform their optimal "unconstrained" transfers.

Comparison between Cooperative and Leader/Follower Performances

The propulsive effort related to the (optimal) cooperative solution can be compared to that required by the Leader/Follower strategy. Numerical results are shown in Figure 4.10. The difference between the overall mass consumption of the optimal

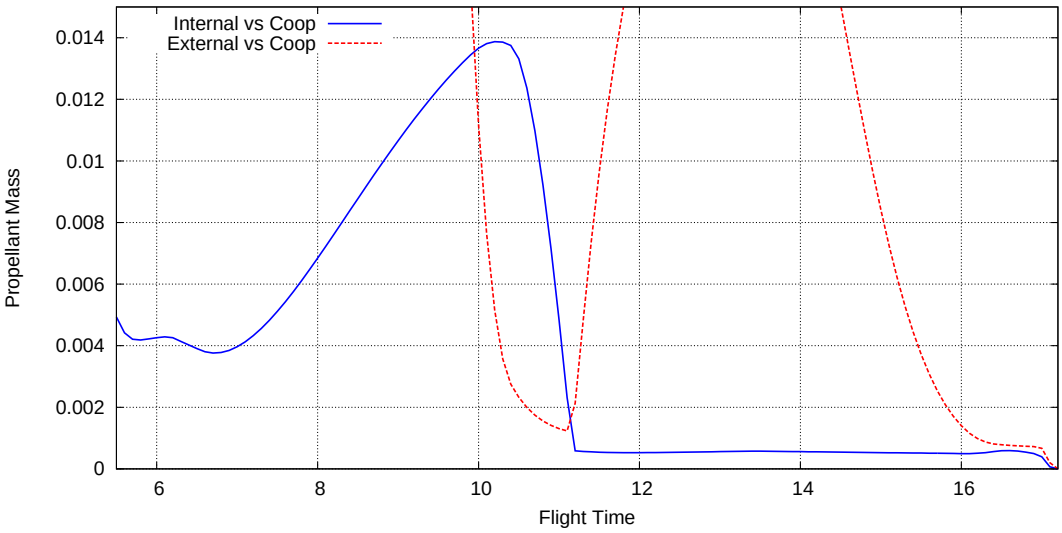

Figure 4.10: Payload increment related to the use of the Cooperative strategy w.r.t. the Internal and External Leader/Follower strategies.

cooperative and the "Internal" strategy is drawn in blue, the difference with respect to the "External" solution is in red. The propellant mass is made nondimensional with respect to the initial mass of a single spacecraft. As the cooperative rendezvous permits the optimal split of the phasing duty, one expects, at any time, a lower overall propellant consumption with respect to the Leader/Follower strategy. The external Leader/Follower wtrategy is useful only for $10 \leq \tilde{t}_f \leq 11.2$ (as highlighted in section [4.2.3]). Outside this range, the internal strategy provides much better solutions. With

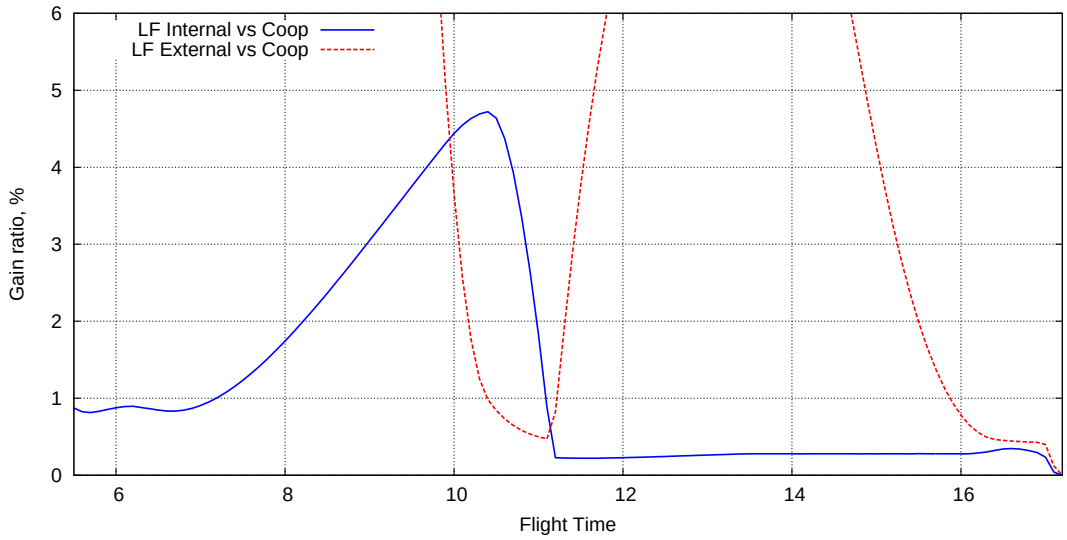

Figure 4.11: Percent of propellant saved using the Cooperative strategy with respect to the propellant consumed using the Leader/Follower strategy.

respect to the best of the Leader/Follower options, the gain at the peak is about 1.4% of the initial mass of one spacecraft. In general, the gain is more consistent for short missions: as the available time increases, the cost of the phasing decreases and it can be shifted almost entirely to one spacecraft. Therefore the cooperative solution becomes more similar to the Leader/Follower solution and the gain is much lower.

The passage between a region of higher cooperation (ratio of spacecraft phase duty near 0.5) and a region of more "individualistic" solution (ratio of spacecraft phase duty near 0 or 1) happens suddenly at the point of transition between the two families of solutions, that is for $\tilde{t}_f = 11.165$. Henceforward, the cooperative and the internal Leader/Follower solutions are almost indistinguishable and the phasing duty diminishes, hence the gain is quite lower. Finally the gain is null for mission longer then the limit time $t_{\text{limit}} = 17.17$. A more appropriated measure of the gain that could be attained by using the cooperative strategy is given by the percent of propellant saved with respect to the one consumed in the Leader/Follower strategy. The gain is quite consistent (always greater than 1%, with a maximum about 4.5%) in the left half of the figure, that is before the transition point; whereas it is much lower in the other part.

We can imagine to divide the cost (i.e., propellant spent) of the deployment of each spacecraft into two terms: the first is related to the increment of semi major-axis is an

"energy duty", the other is a "phasing duty" which is related to acquiring the proper angular position to achieve the rendezvous. The "energy duty" Δm^E is a fixed quantity, whose value can be calculated by considering the optimal "unconstrained" transfer of a single spacecraft between the initial and final orbits. Its value can be measured as the propellant spent to realize the Hohmann-like transfer (section [4.2.3]) for each spacecraft independently from the other. The "phasing duty" Δm^ϕ is a quantity which varies with the mission flight time: it is maximum for the minimum time and zero for the limit time and henceforward. It can be measured "a posteriori" as the difference between the actual mission consumption and the energy duty (of both spacecraft).

$$\Delta m^\phi = \Delta m_I + \Delta m_{II} - 2\Delta m^E \tag{4.54}$$

In the Leader/Follower case, the "phasing duty" is carried completely by the Follower satellite; instead, in the cooperative case the phasing duty is split between the two spacecraft, but the better subdivision of the phasing effort leads to a lower overall propellant consumption. One can define the phasing duty for each spacecraft as:

$$\Delta m_I^\phi = \Delta m_I - \Delta m^E \qquad\qquad \Delta m_{II}^\phi = \Delta m_{II} - \Delta m^E \tag{4.55}$$

and also a ratio of phasing duty:

$$\rho_I^\phi = \frac{\Delta m_I - \Delta m^E}{\Delta m^\phi} \qquad\qquad \rho_{II}^\phi = \frac{\Delta m_{II} - \Delta m^E}{\Delta m^\phi} \tag{4.56}$$

Plotting the ratio of phasing duty on a graph (Figure 4.12), one can immediately visualize the regions of higher cooperation and the zones of lower cooperation. One can observe that, for the family F_A, the region where the cooperation is higher corresponds roughly to the region of maximum gain. The situation repeats for the family F_B, but in this case overall phase duty is so low that the saving is hardly noticeable. Eventually, the phasing duty becomes zero for a flight time longer than the limit time, hence the definition of phasing duty ratio becomes meaningless.

The better mission performance of the cooperative strategy are achieved at the expense of longer computational times, w.r.t. the Leader/Follower strategy. Substantially, the latter strategy reduce the overall mission just to the Follower transfer: the optimal leader transfer is the same for any assigned flight time and it has to be calculated only once. The number of equations to be integrated at any iteration of Newton's method is half that of the cooperative problem and the same holds for the number of

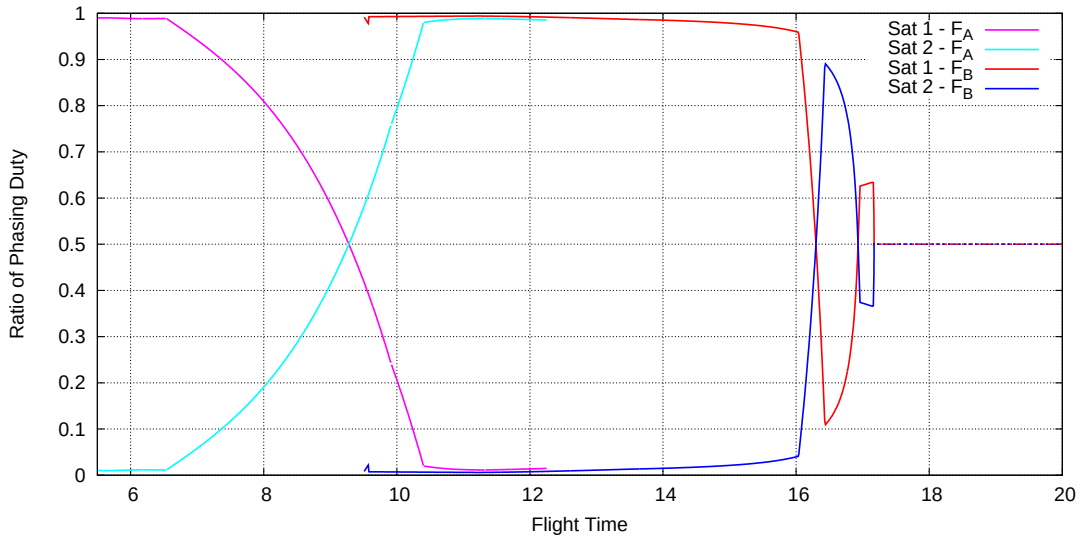

Figure 4.12: Ratio of phasing duty born by each spacecraft.

unknown initial values. Recalling that, for this kind of problems, the difficulty grows roughly with the square of the unknowns' number, it is easy to understand that the computational requirements of the Leader/Follower strategy are much lower than those of the cooperative strategy. Tests performed on an Intel Core i7 920 @ 2.67 GHz testify that: the measured time require for solving the two problems (assuming an identical automatically initialized Continuation-Smoothing formulation) is about 10-13s in case of a Follower deployment and 40-60s in case of a cooperative one.

Chapter 5

Deployment of the Simbol-X Formation

In this chapter the problem of the optimal deployment of a spacecraft formation in a practical and really complex mission is faced. The now-canceled SIMBOL-X mission [12, 75, 76], a joint collaboration of ASI and CNES agencies, is chosen. The main features of this mission will be presented. The choice of operative and injection orbits is explained, in order to motivate the initial and final conditions of the deployment maneuver. Then, the problem, which consists in moving two spacecraft from the injection condition to the pre-link (i.e., preoperative) condition, will be formulated as an optimal control problem. An analysis of the perturbative effects related to different sources (Lunisolar gravitational attraction, Solar radiation pressure, Earth asphericity) on Highly Elliptical Orbits (HEOs) is proposed in section [5.2.2], explaining which ones should be considered and which ones could be neglected. The investigation of optimal (cost-effective) deployment strategies constitutes the core of this chapter. An indirect method is used to attain the solution; proper optimality conditions are derived. The problem is first solved by assuming a two-body dynamics for the spacecraft (that is, by neglecting all the perturbations), in order to facilitate the convergence process and to permit a simpler analysis of the phasing strategies. Next, the Earth oblateness is included in the dynamical model; corresponding solutions are obtained. Subsequently, the problem is solved once again, but assuming a more realistic environment which also

embeds the Lunisolar attraction. The role of the perturbing forces on the deployment is investigated as well as the choice of the departure date. Some results are presented to show the difficulties faced. and the effectiveness of the proposed solution method.

To the author knowledge, no result concerning the deployment problem for a mission similar to Simbol-X (that is, a problem involving two spacecraft flying in high elliptical orbits and accounting for multiple significant perturbative forces) is available in literature. In this thesis, the solution of a such complex problem has been obtained and verified by using in a coordinate way several techniques, that, separately, are often adopted. The Multi-Bound approach is able to find a batch of solutions that can be considered trustworthy as the approach has been tested many times in the past years on several optimization problem; convergence needs a careful choice of the initial guess. The Continuation-Smoothing technique, described in Chapter 3, is exploited to overcame the need of pre-assigning the mission burn structure, which cannot be easily forecast for this intricate problem. The modified equinoctial elements have been introduced in order to improve the numerical stability of the shooting algorithm.

By means of these tools a fully automatic procedure has been envisaged to solve the problem for any departure date and any mission length, without requiring any user action or choice of a proper initial guess. In particular, a suitable initial guess for any mission of interest is provided by a proper initialization procedure which exploits an "orbit-shaping continuation" and relies uniquely on a fixed (trivial) initial guess. In the most difficult cases, when the automated procedure is capable of achieving the solution but with errors greater than the prescribed tolerance, the Multi-Bound approach is used to refine the found solution, hence improving the effectiveness of the proposed solution method.

5.1 An overview of the Simbol-X Mission

The SIMBOL-X project was proposed in 2004 by a consortium of European laboratories as a bilateral collaboration between CNES and ASI. The original idea was to create a powerful X-ray telescope which would have permitted advances in high energy astrophysics and cosmology sciences; at the same time, it would have demonstrated the feasibility of a mission using multiple spacecraft flying in close formation. The mission

completed successfully the Phase A of it development, but now it has been stopped due to budget restriction imposed to the agencies.

To work at its best, the X-ray telescope must have a focal length (i.e., the distance between the focusing and the detecting elements) approximately equal to 20-30 m. Since this size cannot fit in a single spacecraft, due to the limited size of fairings, it was thought to load the mirror and detector elements on two separate spacecrafts which flew in close formation at a distance equal to the desired focal length. To make possible the "reconstruction" of the images captured by this kind of telescope, very stringent requirements are posed on the formation flying stability: the distance between the two spacecraft (along the telescope axis) must be kept at the focal length value within about $\pm$ 10 cm, whereas the intersection of the telescope axis must be at the center of the focal plane within about $\pm$ 20 arcsec. The image reconstruction process also requires that the relative positions of the two spacecrafts are known with a very high level of accuracy.

With respect to the other X-ray telescopes, that rely on a single satellite, a dramatic improvement in the investigation of key issues in high energy astrophysics (e.g. Black Holes physics and Particle acceleration mechanisms) could be attained by this innovative distributed solution. Due to its novel technology Simbol-X would offer superior angular resolution and sensitivity in the X-ray range, hence the possibility of studying a very wide range of sources, such as Galactic and extra-galactic compact sources, supernovae remnants, cluster of galaxies, or young stellar objects. Very long uninterrupted observations (100 ks or more) on the same target are needed to attain these results. In view of the various scientific domains that will be covered by Simbol-X, and of the corresponding very large number of targets, Simbol-X was designed to offer two/three full years of scientific data taking, with sufficient propellant resources to accommodate over 1000 different targets.

The pressing requirements made by its scientific payload conditioned strongly the choice of the operational orbit, as much as the need of containing the overall costs did. Many different options were studied during Phase A. All of them were motivated by the need of attaining an altitude high enough to ensure that the radiation-belt induced background was as low as possible and that the best compromise was found between the perturbations (gravity gradient) and the propellant needed to control a spacecraft on a forced orbit.

According to the experience gained with a previous experiment (the XMM-Newton mission), it is considered useful to scientific purposes the orbit portion above 75000 km of altitude. Over this height, the presence of a background noise due to the Earth radiation-belt particles becomes negligible, hence the reliability of the science observations is guaranteed. Intuitively, since long uninterrupted observations are desired, the simplest solution would be using a circular orbit, choice that would also permit to simplify dramatically the formation flying control. A first configuration based on a 91,000 km altitude circular orbit was proposed, but it was discovered soon that the gravity gradient (and hence the consumption of the control system) was too big at that altitude, and higher heights were needed. Higher circular orbit might be used in principle, but the deployment cost would be greater. Among all the opportunities, a HALO orbit around lunar L1 point would be appealing, but out of budget.

High Elliptical Orbits (HEOs) seem to provide a good compromise between cost and performance. Due to their shape, the useful time for observations is a relevant fraction of the orbital period, while the cost associated to the spacecraft deployment is surely lower than that of a circular orbit of equal semi-major axis. Moreover, most of the flight time is spent near the apogee (that is away from the earth perturbation), hence the control budget necessary for a correct pointing is low.

Selected configuration

The result of these, and many other, compromises is the operational High Elliptical Orbit sketched in Figure 5.1 and summarized in Table 5.1. It has a perigee of about 20.000 km, an apogee of about 180.000 km, and a period of four days. Considering the 75.000 km altitude as the limit under which the observation in nominal condition[1] cannot be performed, this orbit permits, for each revolution, an uninterrupted window of about 290 ks available for observations, which correspond to about 80.56 hours or 3.35 days (almost 83.92% of the orbital period).

The envisioned launch vehicle was a Soyuz with a Fregat upper stage, to be launched from the Kourou Space Centre, the European spaceport located in French Guiana. The fairing offers ample space for fitting both spacecraft, with two different options. One is to mate the two spacecrafts together, as a single composite spacecraft, for the launch

[1] observations might still have a low background at lower altitudes depending on magnetospheric activity.

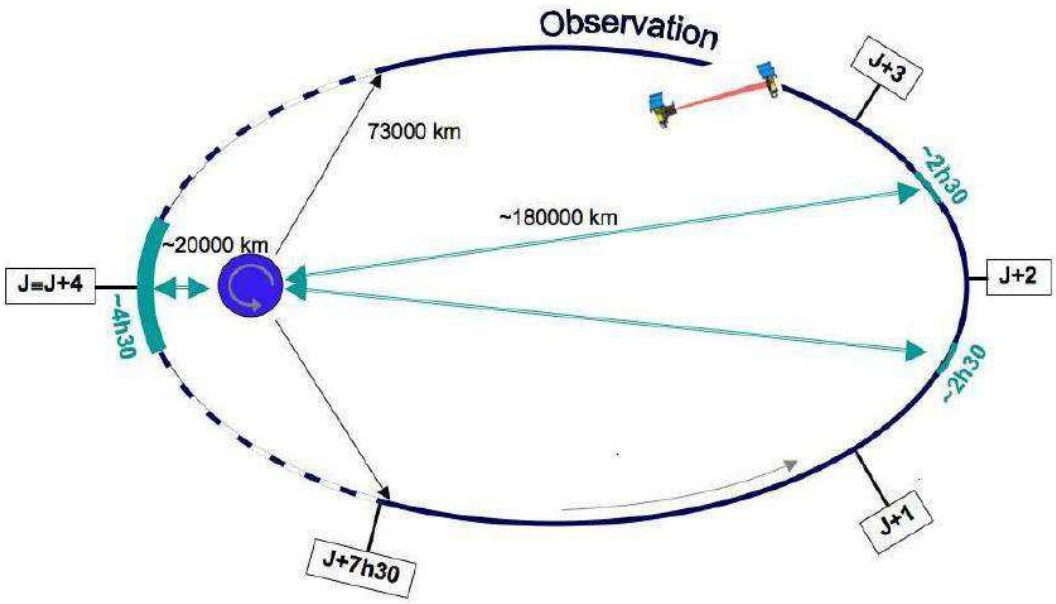

Figure 5.1: Simbol-X orbit. The observation period and the nominal contacts with the Malindi ground station are indicated.

operations up to the time when the composite reaches the operational orbit; the detector and mirror spacecrafts would then separate. The other option is a dual launch of the two spacecraft, each of them reaching the operational orbit independently. This second option is preferable as it offers the advantage of simplifying all mechanical interfaces between the two spacecrafts, and it is studied in this thesis.

Table 5.1: Spacecraft initial and final orbits in the J2000 inertial frame.

Orbit	Initial Sat 1	Initial Sat 2	Final
Semi-Major Axis (km)	99185.351	98922.000	106246.9753
Eccentricity	0.933791	0.931985	0.798788
Inclination (deg)	5.2	5.2	free
Argument of Perigee (deg)	180.0	180.0	free
RAAN (deg)	90.0	90.0	free

In the next section the problem of choosing the best departure date and control law for the transfer of the two satellite from the injection point to a pre-link condition is dealt with. The goal is to minimize the fuel consumption necessary for the formation

Table 5.2: Spacecraft features.

	Sat 1	Sat 2
Mass		
Launch Mass (kg)	960	1250
Propellant Mass (kg)	150	200
Thruster		
Thrust Magnitude (N)	1÷8	1÷8
Isp (s)	220	220

deployment, avoiding collision between the two spacecraft.

5.2 A Preliminary Analysis

The task of bringing the two satellites from their injection point at 350 km of altitude to roughly 200000 km, few kilometers apart from each other, exploiting the perturbation forces due to Moon and Sun in order to minimize the propellant effort, is very challenging. A complete statement of the optimal control problem is provided in section [5.2.1], which highlights the choice of the state variables, the merit index to maximize, the spacecraft dynamics, the (supposed) initial conditions, the (desired) final conditions and all the other path constraints.

A preliminary analysis of perturbation effects for High Elliptic Orbits is carried out in section [5.2.2]. The relative importance of lunar and solar gravity attraction and Earth asphericity will be assessed. The analysis ends with a few considerations that point out the need of envisaging deployment strategies where the two spacecraft stay as close as possible to reduce the deployment costs (which would be increased by different effects of the perturbations), thus neglecting the possibility of splitting the deployment in two well-separated phases.

5.2.1 Problem Statement

The formation deployment consists in performing an orbit raising of both spacecraft towards the operational orbit, and phasing them in order to reach the pre-link configuration.

According to the objective of this study, the two spacecraft can be assumed as point-mass objects; the state of each one is fully described by its position, velocity, and mass. The Earth equatorial radius, the corresponding circular velocity, and 1000 kg have

been chosen as reference values (independently of the specific case under investigation) for distances, velocities and masses to make any variable involved in the calculus non-dimensional. The satellite position with respect to an inertial frame is given by a

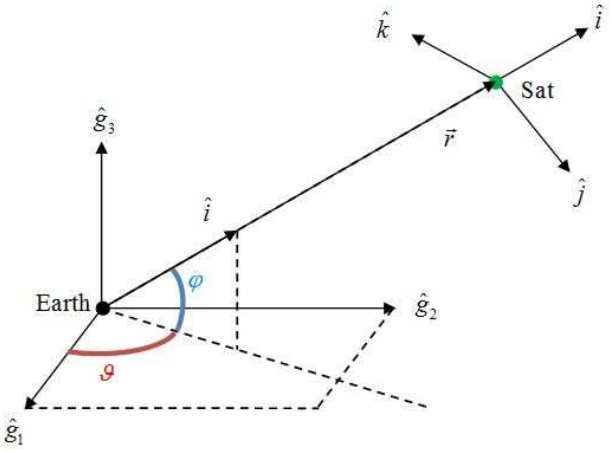

Figure 5.2: Reference Frame 3D.

set of polar coordinates (r, ϑ, φ). The reference frame, which is chosen to describe the spacecraft velocity, is a topocentric rotating frame that is based on the horizontal plane and follows the spacecraft during its motion. The velocity is therefore expressed by means of the components in the radial u, eastward v and northward w directions. This formulation, which is apparently complex, permits to describe the dynamics of each spacecraft trough a simple set of differential equations.

$$\dot{\bar{x}}_j = \bar{f}\left(\bar{x}_j, \bar{u}_j, t\right) = \\ = \begin{cases} \dot{r}_j = u_j \\ \dot{\vartheta}_j = v_j / \left(r_j \cos\varphi_j\right) \\ \dot{\varphi}_j = w_j / r_j \\ \dot{u}_j = -1/r_j^2 + \left(v_j^2 + w_j^2\right)/r_j + T_{j_u}/m_j + \left(a_p\left(\bar{x}_j, t\right)\right)_u \\ \dot{v}_j = \left(-u_j v_j + v_j w_j \tan\vartheta\right)_j / r_j + T_{j_v}/m_j + \left(a_p\left(\bar{x}_j, t\right)\right)_v \\ \dot{w}_j = -\left(u_j w_j + v_j^2 \tan\vartheta_j\right)/r_j + T_{j_w}/m_j + \left(a_p\left(\bar{x}_j, t\right)\right)_w \\ \dot{m}_j = -T_j / c_j \end{cases} \quad , \qquad j = 1, 2 \qquad (5.1)$$

where:

- $\bar{u}_j = \vec{T}_j = \begin{pmatrix} T_{j,u} & T_{j,v} & T_{j,\mathrm{w}} \end{pmatrix}$ is the control vector of the j-th spacecraft, that is the thrust vector, whose magnitude is bounded by T_{max};
- $\vec{a}_p\left(\bar{x}_j, t\right)$ is the overall perturbing acceleration[1] acting on the j-th spacecraft.

The performance of the deployment is evaluated with respect to the overall propellant consumption, that is, the sum of the single spacecraft consumptions. Equivalently, the merit index to maximize can be stated as the sum of the final masses of the two spacecraft:

$$J = m_{f_1} + m_{f_2} \tag{5.2}$$

Mission specifics are enforced through boundary and path constrains. As remarked in the previous section, the two spacecraft are thought to be carried together by the launch vehicle and injected at the perigee of the insertion orbit (whose characteristic are stated in Table 5.1). The satellites are separated one from the other at the time of injection on the transfer orbit. The on-orbit position of both satellites is the same at the separation instant, but the semi-major axes (and the eccentricities) are slightly different because of a small ΔV (0.5 m/s magnitude) produced by the launcher at separation. The ΔV is applied to Sat 1 (the mirror spacecraft) and, assuming no separation errors, it is parallel to the spacecraft inertial velocity; an increment of the apogee altitude (calculated neglecting the perturbation) of nearly 5400 km is produced. The injection orbit of both spacecraft is thought to be fixed in a geocentric "inertial" reference frame (J2000), whereas the departure date is left free. The resulting initial conditions in terms of the considered stated variables are given in Table 5.3.

The choice of the departure date represents an important aspect of the deployment problem, thus of its optimization. For high elliptical orbits, Moon and Sun produce relevant perturbations on the spacecraft trajectory. These effects depend on the relative position of the perturbing bodies, the spacecraft and the Earth. A variation in the initial date changes the relative positions all along the trajectory, hence it may lead to significant changes in the overall consumption.

[1] One should refer to Appendix A for a detailed description of the perturbing accelerations due to Earth Asphericity and Lunisolar attraction.

Table 5.3: Dimensional initial values of the two spacecraft state.

	Sat 1	Sat 2
r, km	6728.16	6728.16
ϑ deg	270.00	270.00
φ, deg	0.00	0.00
u, km/s	0.000	0.00
v, km/s	10.65496	10.65446
w, km/s	-0.96968	-0.96963
m, kg	960	1250

The purpose of the transfer is to reach the "pre-link" condition, which consist in placing the two spacecraft on the operational orbit, separated by a phase angle that permits to attain an intersatellite distance of 10 km when the first (leader) spacecraft reach the apogee. As result, at the end of the transfer the two spacecraft have to share the same orbital elements, with the exception of the true anomaly. This require that the following conditions hold at the final boundary:

$$a_1 = \tilde{a} \tag{5.3}$$

$$e_1 = \tilde{e} \tag{5.4}$$

$$\nu_1 = \pi \tag{5.5}$$

$$a_1 - a_2 = 0 \tag{5.6}$$

$$e_1 - e_2 = 0 \tag{5.7}$$

$$i_1 - i_2 = 0 \tag{5.8}$$

$$\omega_1 - \omega_2 = 0 \tag{5.9}$$

$$\Omega_1 - \Omega_2 = 0 \tag{5.10}$$

$$\|\vec{r}_1 - \vec{r}_2\| - \tilde{D} = 0 \tag{5.11}$$

where $\tilde{a}$ and $\tilde{e}$ are the assigned values of semi-major axis and eccentricity of the final orbit (c.f. Table 5.1).

Notice that a certain "freedom" is given to design the transfer: only semi-major axis and eccentricity of the operational orbit are assigned (their choice was motivated

in section [5.1]), whereas inclination, longitude of the ascending node, and argument of the perigee are left free. In fact, the scientific payload does not require that these orbital parameters have a particular value in order to work correctly.

A path constraint is also present: a minimum (security) distance d_s, equal to 1 km, has to be guaranteed between the two spacecraft all along the trajectory in order to avoid any collision risk. This constraint can be posed formally as:

$$\|\vec{r}_1(t) - \vec{r}_2(t)\| \geq d_s, \qquad \forall t \in [t_0, t_f] \tag{5.12}$$

Practical operation requirements forbid the use of the engines around both departure and arrival points. The ΔV separation maneuver performed at departure is against the goal of acquiring a tight formation and the optimization procedure may suggest to contrast it; nevertheless the separation is necessary to avoid collision risks at the begin of the deployment, hence the prohibition of maneuvering during the first revolution. On the other side the pre-link configuration has to be achieved during a coast arc. In this way, the closer approach (i.e., the link condition) can be attained safely: at the last apogee it is possible to exploit freely the thrust only to account for any deviation from the nominal transfer trajectory that might have been occurred, without having to use it for perigee raise.

5.2.2 Perturbation effects on HEO Orbits

> Perturbations are deviations from a normal, idealized, or undisturbed motion. The actual motion will vary from an ideal undisturbed path (two-body) due to perturbations caused by other bodies (such as the Sun and Moon) and additional forces not considered in Keplerian motion (such as a non-spherical central body and drag).
>
> - David A. Vallado

When dealing with highly elliptical orbits, many perturbative forces have to be taken into account; moreover, due to the fact that such orbits cover a wide range of altitudes, the hierarchy of the perturbations acting on the satellite changes with the position on the orbit. At low altitude, the oblateness of the Earth (the so called J2 effect) is the dominant perturbation, while at high altitude the Lunisolar gravitational perturbations greatly exceed J_2 acceleration.

Table 5.4: Perturbing acceleration comparison, normalized w.r.t. Earth gravity at $r = r_E$, i.e., 9.79829 m/s^2.

	Initial Orbit perigee	Final Orbit Apogee
spherical Earth Gravity	0.899	$0.11 \cdot 10^{-2}$
J_2 effect	$0.11 \cdot 10^{-2}$	$0.20 \cdot 10^{-8}$
$J_{2,1}$ to $J_{8,8}$ effect	$0.42 \cdot 10^{-5}$	$0.30 \cdot 10^{-12}$
Moon's gravity	$0.32 \cdot 10^{-5}$	$0.11 \cdot 10^{-4}$
Sun's gravity	$0.63 \cdot 10^{-3}$	$0.63 \cdot 10^{-3}$
Moon's grav. perturbation	$0.11 \cdot 10^{-6}$	$0.83 \cdot 10^{-5}$
Sun's grav. perturbation	$0.57 \cdot 10^{-7}$	$0.16 \cdot 10^{-5}$
Solar radiation Pressure	$0.49 \cdot 10^{-8}$	$0.49 \cdot 10^{-8}$

Numerical values for these perturbative effects at the lowest and highest point of the initial and final orbits respectively, are presented in Table 5.4. Other effects (such as drag, tides, albedo) seems instead negligible and were not considered.

In order to better understand the effects of different perturbation sources on the spacecraft trajectories involved in this mission, a simplified analysis is carried out to show their qualitative behavior; extensive numerical simulations (which take into account the Earth asphericity and the third-body perturbation of Moon and Sun either singularly or all together) provide a more precise quantitative evaluation. The most important results are summarized in this section.

A first important aspect to investigate concerns the analysis of the effects of perturbations on the spacecraft injection orbit after a complete revolution. In particular, the attention is focused on the altitude at the perigee passage, quite low at the beginning of the mission, since a further reduction (due to "adverse" perturbation) could lead the spacecraft to re-enter into the atmosphere.

After, the effects of the perturbations over a longer time horizon are studied. The attention is now drawn to the evolution of the orbital plane, which is subject to variations of inclination and direction of the line of nodes, which depend on the orbital parameters (mainly semi-major axis and eccentricity). Results of this analysis suggest not to split the deployment in two well-separated maneuvers, not to increase the propulsive effort.

Test 1 - Injection Orbit / Perigee An analysis of the evolution of the initial orbit after a complete ballistic revolution is very mandatory from a mission-analysis point of view to understand the effect of the perturbations over the perigee altitude. The initial altitude is quite low; therefore the spacecraft might plunge into the atmosphere if perturbations decrease significantly the velocity at the apogee (because it would lower the perigee altitude even more). In those cases, an apogee maneuver would be mandatory during the first revolution to avoid the re-entry by counteracting the perturbation effect, thus resulting in additional costs. On the other side, if the starting date is particularly favorable, the perturbations can produce a "free" perigee raising, with a positive effect on the overall propellant consumption.

To understand qualitatively the effects of the various perturbations, a simplified analytical analysis can be performed. For what concerns perturbations due to the Earth asphericity, many analytical results exist. If effects other than the Earth Oblateness (J_2) are neglected, the variation of semi-major axis and eccentricity are null over a whole revolution. Therefore, even though high order harmonics are considered, the perigee variation will be pretty small, being the other terms at least two order of magnitude smaller. (NB: in turn, the apogee radius is lower than the value calculated at the departure using the parameter of the osculating orbit at perigee).

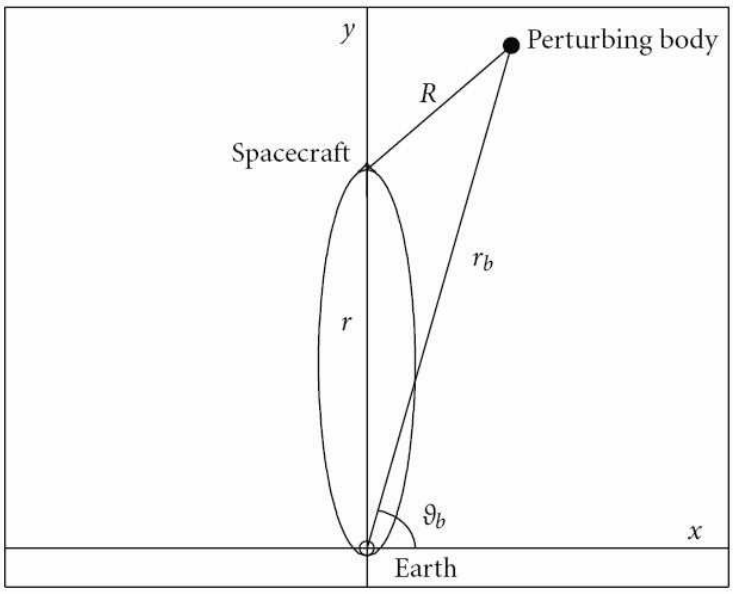

Figure 5.3: Schematic geometry of gravitational perturbations.

A qualitative estimation of the effect of the third body gravitation on the spacecraft perigee height, as a function of the perturbing body position can also be performed. To simplify the calculus, the perturbative acceleration exerted by the 3rd body over a whole revolution is supposed to be concentrated at the apogee, and here applied impulsively. This assumption is reasonable because, for highly elliptic orbits, the spacecraft spends most time at the apogee ($\nu = 180°$, $\vartheta = 90°$) where, in addition, the perturbing acceleration is larger due to the greater Earth-spacecraft distance. Therefore, the perturbing acceleration can be evaluated by considering only the apogee. The acceleration component parallel to the apogee velocity, i.e., the tangential component a_t, is the main cause of the perigee variation. If coplanar orbits are assumed (see Figure 5.3), one easily determines that this component is:

$$a_t = -\frac{\mu_b}{r_b^2}\left[(r_b/R)^3 - 1\right]\cos\vartheta_b \tag{5.13}$$

with the spacecraft distance from the perturbing body expressed as

$$R^2 = r_b^2 + r^2 - 2r_b r\sin\vartheta_b \tag{5.14}$$

When the Sun is the perturbing body, $r << r_b$ and only first order terms are retained to obtain

$$(r_b/R)^3 \approx 1 + 3(r/r_b)\sin\vartheta_b \tag{5.15}$$

and

$$a_t \approx -\frac{\mu_b}{r_b^2}\frac{3}{2}\sin(2\vartheta_b) \tag{5.16}$$

with maximum positive values at $\vartheta_b = 135°$ and $315°$ (the most favorable positions of the Sun), and maximum negative values at $\vartheta_b = 45°$ and $225°$ (the most unfavorable positions).

When the Moon is considered, the spacecraft distance from the Earth becomes comparable to the Earth-Moon distance ($r/r_b \approx 0.5$) and the previous simplification does not hold. The symmetry of the result with respect to the x axis (here orthogonal to the line of apses) and the effects of the third-body perturbation are enhanced when Moon and spacecraft apogee are on the same side with respect to the Earth, that is when $\sin\vartheta_b > 0$. The maximum benefit occurs when $\vartheta_b \approx 115°$ (with a less pronounced beneficial effect at $\vartheta_b \approx 330°$), whereas the largest negative effect is at $\vartheta_b \approx 65°$ (with a less remarkable effect at $\vartheta_b \approx 210°$).

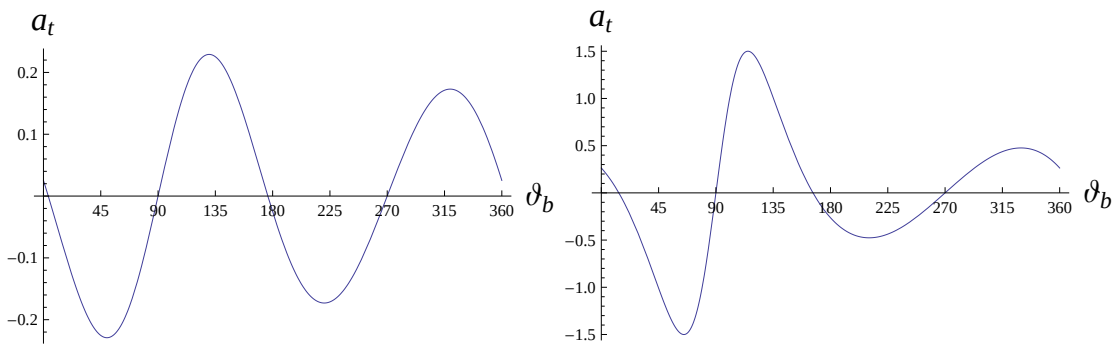

(a) Sun gravity perturbation

(b) Moon gravity perturbation

Figure 5.4: Approximation of the perturbing acceleration at the apogee of HEO, due to a third body gravity attraction.

An analysis on the initial ballistic orbit has been carried out, in order to verify numerically the simplified analysis just performed and to assess quantitatively/evaluate precisely the effects of each perturbation on the spacecraft trajectory. For every departure date between 1/12/2015 and 1/12/2016, a complete revolution of a spacecraft is simulated and the final perigee radius is recorded.

Earth Asphericity (8x8 model) Earth Asphericity (8x8 model) The Earth asphericity does not play a significant role on the perigee variation, while it can rise/lower the actual apogee radius (i.e., the maximum spacecraft radius) of ±70 km. These effects change with the departure date, with a daily periodicity.

Sun Perturbation Taking only the solar perturbation into account, one observes that the effects have a half year period even though the Earth makes one revolution per year around the Sun. This can be explained simply by recalling that the perturbing acceleration is linked to the difference between the pull exerted by the perturbing body (i.e., the Sun) on the primary body (the Earth) and on the S/C. Thus, since the dimension of the S/C orbit is much smaller than the Earth sphere of influence, the opposition and conjunction effects are nearly identical and this results in a semi-annual periodicity (Figure 5.5). The perigee variation due to the solar perturbation is about ±70 km: maximum and minimum effects occur when the third body has a phase angle

$\pm 45°$ from the line of apses. In particular the maxima occur for $-45°$ and $+135°$ and the minima for $-135°$ and $+45°$.

Moon Perturbation The same reasoning does not hold for the lunar perturbation, because the apogee altitude of the S/C orbit is comparable to the Earth-Moon distance. As a result (Figure 5.6), the perturbing effect has a period of about 27 days, corresponding to a complete Moon period (instead of half-period as in case of the Sun perturbation). The Moon moves remarkably during a S/C revolution, but one can relate the overall perigee variation to the Moon position when the S/C is at the apogee, because there the spacecraft both spends most of its time and experiments most of the third-body perturbation. The perigee variation due to the lunar perturbation shows two maxima and two minima During each Moon revolution. Maxima and minima do not correspond to the conjunction or opposition points, but rather to points at $\pm 30°$ (the more prominent peaks) and $\pm 120°$ (the less sharp ones); maximum variation is bounded between ± 300 km. Summarizing the results, one can notice that the spacecraft enters the atmosphere (an arbitrary value of 200 km has been chosen as the upper limit to the atmosphere) if the Moon phase at the departure is between $8°$ and $53°$, thus about 3.5 days during each lunar period cannot be used as departure date.

Table 5.5 summarizes the variations on the perigee height due to each perturbation as function of the right ascension of the perturbative body at the departure $\vartheta_b(t_0)$ or of the apogee of the S/C orbit ϑ_b. Moreover, for each perturbation the perigee height is plotted versus the departure date (Figures 5.5(a) and 5.6(a)) and versus the phase at the apogee γ_b (Figures 5.5(b) and 5.6(b)) which is related to the right ascension of the third body at the apogee passage by the relation $\gamma_b = \vartheta_b - \pi/2$. This change of variable highlight the symmetry of the third-body effects. Finally the graph, which is obtained taking the Lunisolar perturbation and the Earth asphericity into account, is given (Figure 5.7).

Test 2 - Evolution of the Orbital Plane Beside the study of the apogee altitude, the evolution of orbital plane is analyzed over a longer time horizon. At the end of the deployment, the two spacecraft are constrained to be on the same plane; even though it is not specifically assigned, it is worthwhile to understand how the planes of the

Table 5.5: Maximum and minimum variations of the Perigee radius due to lunar and solar perturbations.

Sun	Δr_p, km	$\vartheta_b(t_0)$, deg	ϑ_b, deg	t_0, MJD
Max 1	76.53	-44.03	-45.91	57422.41
Min 1	-66.25	39.19	40.96	57509.85
Max 2	70.31	134.95	136.78	57604.69
Min 2	-69.65	-139.68	-137.88	57697.00
Moon	Δr_p, km	$\vartheta_b(t_0)$, degrees	ϑ_b, degrees	t_0, MJD
Max 1	301.01	90.37	116.12	57381.27
Min 1	-299.06	33.33	59.05	57377.33
Max 2	128.78	-54.27	-29.74	57370.88
Min 2	-102.50	-169.09	-148.54	57361.92

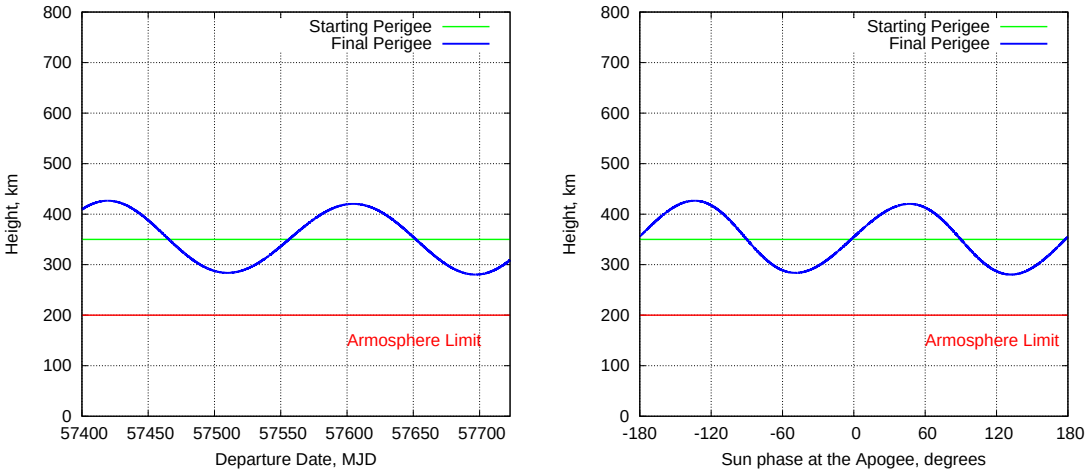

(a) Sun perturbation effects vs Departure Date (b) Sun perturbation effects vs Apogee Phase Angle

Figure 5.5: Sun perturbation effects on perigee height after one revolution.

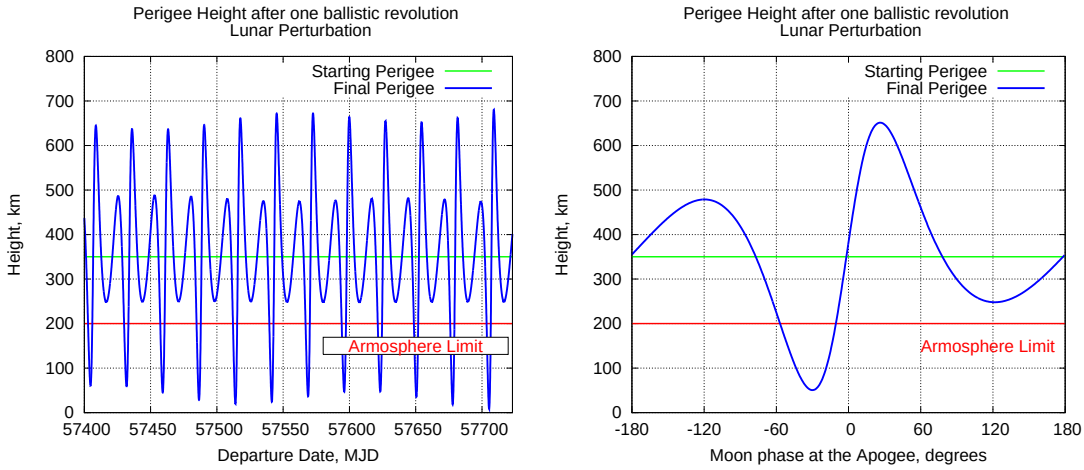

(a) Moon perturbation effects vs Departure Date (b) Moon perturbation effects vs Apogee Phase Angle

Figure 5.6: Moon perturbation effects on perigee height after one revolution.

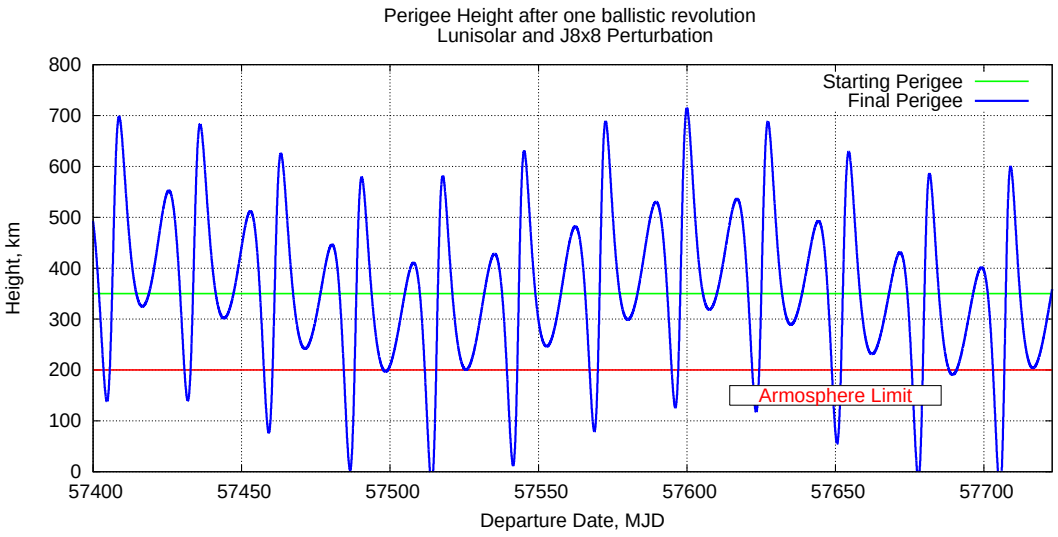

Figure 5.7: Overall perturbation effects on perigee height.

two spacecraft rotate in space due to perturbations and how much this rotation differs between the initial or final orbits.

The Earth asphericity produces a regression of the line of nodes and a rotation of the line of apsides. Inclination, eccentricity and semi-major axis are not altered by the Earth oblateness. Analytical results exist if the J_2 effect is the only one considered:

$$\Delta\Omega = -3\pi J_2 \left(\frac{r_\oplus}{p}\right)^2 \cos(i) \tag{5.17}$$

$$\Delta\omega = \frac{3}{2}\pi J_2 \left(\frac{r_\oplus}{p}\right)^2 \left(5\cos^2(i) - 1\right) \tag{5.18}$$

Moon and Sun effects on the plane inclination are more difficult to handle analytically.

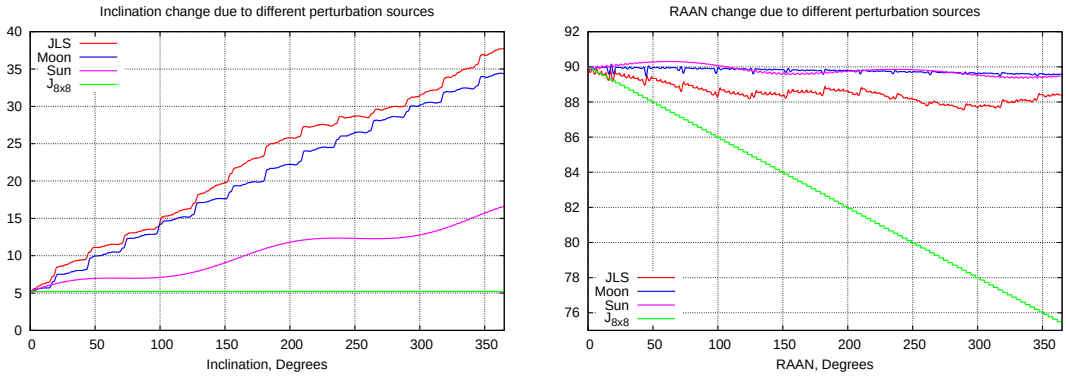

(a) Inclination Change

(b) RAAN Change

Figure 5.8: Variation of inclination and RAAN for the Simbol-X injection orbit over a year.

Numerical simulations considering a more detailed Earth gravitational model (up to J_{8x8}) and the effects of Lunisolar gravitation were performed. The variation of inclination and RAAN starting from the injection orbit are shown in Figure 5.8. Analogous results can be obtained by considering the operational orbit, initially.

The parameters of injection and operative orbits have rate of change different from each other. Assuming that at a given time the two orbits are coplanar and differ only in semi-major axis and eccentricity, the different perturbative effects will move apart the

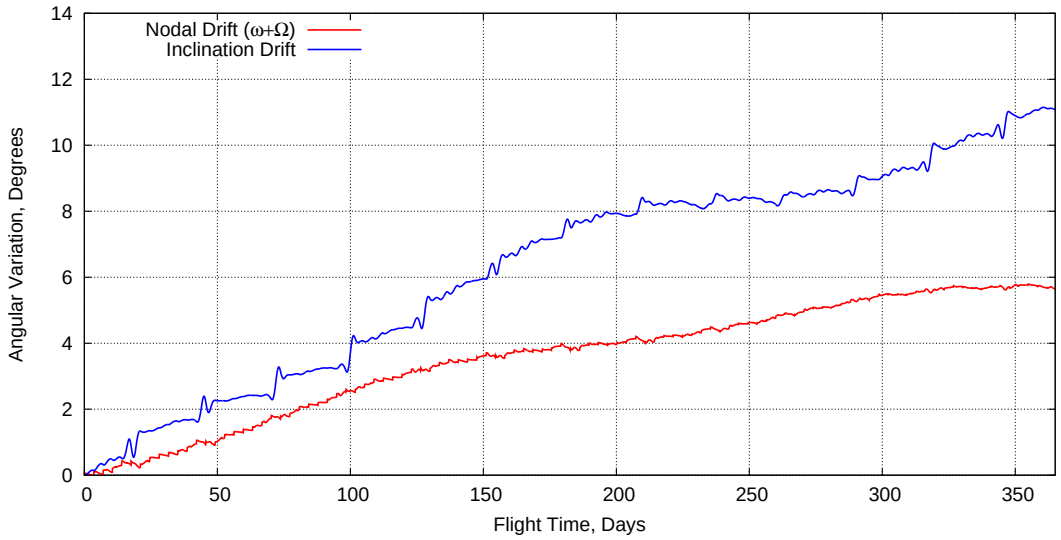

Figure 5.9: Inclination and nodal drifts between initial and final orbit.

two orbital planes. The relative variation (i.e., drift) of their inclination and direction of the line of nodes over one year is shown in Figure 5.9.

The mechanism that creates the drift is quite subtle: differences in the semi-major axis and inclination between the two satellites create a nodal drift. Lunisolar perturbations, which are different between the injection orbit and the final orbit, also depend on the phase angle between the perturbing body and the spacecraft line of nodes, produce a drift in inclination.

These simulations point out the necessity of envisaging deployment strategies where the two spacecraft stay as close as possible. If, on the contrary (e.g., due to a failure), one spacecraft remains on the injection orbit while the other reaches the operational orbit, the two spacecraft would experience the separation of the orbital planes just described, which increases as long as the two spacecraft fly on different orbits. For example, if a spacecraft spends a month one on the injection orbit and the other on the operative one, the inclination drift is about 1.5° . Assuming an impulsive correction maneuver at the apogee of the final orbit, and neglecting the change of the line of nodes, the ΔV required for such plane change is:

$$\Delta V = 2V_a \sin\left(\frac{\Delta i}{2}\right) = 16.96\,\mathrm{m/s} \tag{5.19}$$

and a hydrazine mass of about 7.5 kg is required (given the characteristic of the available

engines). This simple evaluation underestimate the true cost of recovering the coplanar condition, as the correction of the line of nodes requires a further propulsive effort.

5.3 Coordinated Strategy for the Simbol-X deployment: an Optimal Control Approach

This section presents solutions of the Simbol-X formation deployment mission obtained by using an indirect method. Two different deployment strategies are envisaged; for each one, the first order necessary conditions are derived. A clear and detailed formulation of the resulting Hamiltonian boundary value problems is provided in section [5.3.1]. Section [5.3.2] presents some numerical results concerning a simplified deployment problem obtained by assuming only a two-body dynamical model (i.e., an unperturbed, Keplerian, environment). The aim is to highlight the aspects related to the phasing constraint and show an easy but effective way to attain the respect of the security distance constraint. The full perturbation model is restored in section [5.3.2]. The attention here is pointed toward the remarkable effects that perturbations cause to the optimal control law, hence to the overall consumption. The relationship between the burn structure and the perturbing effects (hence the departure date) is complex and the optimal structure cannot be forecasted by means of elementary physical reasonings. Thus, the application of the Multi-Bound approach becomes difficult, especially to perform a parametric analysis (as those required to understand the effects of departure date). A self-consistent algorithm, which relies on the smoothing\continuation technique, is proposed to find the optimal solution of the deployment problem for an assigned departure, with almost none manual (user) effort. Its validity is confirmed by comparing its results with those obtained by the Multi-Bound approach for a set of the single satellite missions. Eventually, formation deployment results for departure date ranging over a whole month are presented, with some remarks about odd burn structures that arise in rare cases.

5.3.1 Strategies and Optimality conditions for the formation deployment

As the title may suggest, in this section feasible strategies for the formation deployment are individuated. For each one, optimality conditions are derived and employed to form

an Hamiltonian boundary value problem, whose solution provides the optimal control law for the two spacecraft.

The strategies differ according to the way the phasing constraint is conceived. In fact, that is the only condition that couples the dynamics of the two spacecraft, that otherwise will be independent (and so could be independently optimized). Two different, conceptually antithetic, ways to look at at the deployment (hence to handle this constraint) were envisaged: one is to see the problem as a monolithic block that has to be solved all at once; the other tries to solve the problem optimizing only a spacecraft transfer at once. These thoughts resulted in the formulation of a parallel or "Cooperative Approach" (the former one) and of a serial or "Chaser/Target Approach" (the latter one).

To attain a simpler formulation, it is convenient to rewrite the phasing constraint, which is given under the form of an inter-satellite distance between the two spacecraft in the close proximity of the apogee of the final orbit, as a time-constraint on the two spacecraft dates of passage at the apogee of the final orbit, that is:

$$t_2 - t_1 = \Delta t_{\tilde{D}} \tag{5.20}$$

where $\Delta t_{\tilde{D}}$ is a time delay which depends on the imposed intersatellite distance $\tilde{D}$ and on the spacecraft velocity at the apogee of the final orbit V_a. Since the Earth-spacecraft distance is very high and the intersatellite distance very low, it can be calculated approximately as:

$$\Delta t_{\tilde{D}} = \tilde{D}/V_a \tag{5.21}$$

The "Chaser/Target Approach" and the "Cooperative Approach" can now be enunciated. In the serial approach there is a clear separation between the optimization of the deployment of each spacecraft, that is done in sequence and corresponds to solving two separate, distinct optimal control problems. First, one chooses a spacecraft as "target" and searches for the optimal time-free maneuver to place the spacecraft into the final orbit maximizing its final mass within a maximum number of revolutions. As this problem is solved, position, velocity and date at the apogee of the final orbit are known for the target satellite and given as final conditions for the other spacecraft (the "chaser") which performs an optimal time-fixed maneuver, in order to reach the same final state as the target, with a fixed time delay that allows one to satisfy the phase constraint. In this way, the chaser satellite alone takes the entire cost of the phasing

(see the following section). In the parallel approach there are no "target" or "chaser" satellites but both spacecraft operate together to reach the target formation; hence the "cooperative" attribute. The motion of both satellites is analyzed simultaneously and the objective function (to maximize) becomes the sum of the final masses. Optimality conditions for the two strategies will now be derived and the associated Hamiltonian boundary value problem will be stated.

5.3.2 Chaser/Target Approach

In case of a sequential approach, the target spacecraft performs an optimal time-free mission, whereas the chaser spacecraft performs an optimal time-fixed transfer in order to reach exactly the final state of the target, but with an assigned delay. Sat 2 has been chosen as the target satellite, because it has a lower T/m ratio than Sat 1 has (thus, it is more maneuverable). Obviously, by splitting the optimization procedure into two distinct parts, one gains in computational speed and efficiency, but clearly one losses something in performance, that is, in overall final mass.

Two optimal control problems arise: the one concerning the target spacecraft is self-consistent, while the other one needs the solution of the former to be completely defined. In each problem the goal is to minimize the propellant consumption of the maneuvering spacecraft; therefore the merit index simply corresponds to the final mass of the S/C under optimization, that is alternatively $J = m_I|_f$ or $J = m_{II}|_f$.

The spacecraft state variables and dynamics were previously presented in section [5.2.1]: spacecraft position is given in polar coordinates, velocity is expressed in a local frame whose axes point to the radial, eastward, and northward directions. The spacecraft motion is described by a set of differential equations given by eq. (5.1), or in a synthetic form:

$$\dot{\bar{x}} = \bar{f}\left(\bar{x}, \bar{u}, t\right) = \begin{cases} \dot{\vec{r}} = \vec{V} \\ \dot{\vec{V}} = \bar{G}\left(\vec{r}\right) + \dfrac{\vec{T}}{m} + \vec{a}_p\left(\vec{r}, t\right) \\ \dot{m} = -T/c \end{cases} \tag{5.22}$$

The optimal control problem is solved by an indirect method, that is by applying the procedure described in Chapter 2. The first order necessary conditions are derived and the Hamiltonian boundary value problem which arises is solved by means of a simple shooting technique. The adjoint variables and the Hamiltonian are introduced.

Euler-Lagrange equations, which provide the time-derivatives of the adjoint variables, are calculated according to eq. (2.16). The system dynamics is affine in the control and its magnitude is bounded; therefore the problem which arises is a bang-bang optimal control problem like those dealt with in chapter 3. Recalling section [3.2.1], the optimal thrust direction is provided by eq. (3.10) or equivalently by Lawden primer vector theory. It follows that:

$$\vec{T} = T_{\max}\,\beta\,\vec{\lambda}_V \tag{5.23}$$

where $\vec{\lambda}_V = \begin{pmatrix}\lambda_u & \lambda_v & \lambda_w\end{pmatrix}^T$, is the vector which collects the adjoint variables corresponding to the velocity components, or "Primer Vector". By introducing the adjoint velocity vector $\vec{\lambda}_V$ and the the adjoint position vector $\vec{\lambda}_r = \begin{pmatrix}\lambda_r & \lambda_\vartheta \frac{1}{r} & \lambda_\phi \frac{1}{r\cos\phi}\end{pmatrix}^T$, the Hamiltonian can be rewritten concisely in order to highlight explicitly the switching function:

$$H = \vec{\lambda}_r^T\,\vec{V} + \vec{\lambda}_V^T\,\vec{G} + \vec{\lambda}_V^T\,\vec{T} - \lambda_m \frac{T}{c} \tag{5.24}$$

$$H = \vec{\lambda}_r^T\,\vec{V} + \vec{\lambda}_V^T\,\vec{G} + T\,S_F \qquad S_F = \left|\vec{\lambda}_V\right|/m - \lambda_m/c \tag{5.25}$$

Pontryagin Maximum Principle indicates whether the S/C has to maneuver or not. The Hamiltonian is linear in the thrust value, hence maximum thrust is exploited when the Switch Function S_F is positive, otherwise the engine is turned off. Both the Multi-Bound approach and the Continuation-Smoothing technique discussed in Chapter 3 can be employed to avoid the troubles linked to the control discontinuity.

The formulation of the boundary conditions is very similar between target and chaser trajectory optimization: starting conditions are formally identical while the difference is made by those at end of the transfer. At the departure point, the state variables of each spacecraft are completely defined. The departure date is assumed to be fixed[1]. Position, velocity and mass of the maneuvering spacecraft are set according to Table 5.3. As a result, all the adjoint variables are free at departure. The following conditions hold:

$$\begin{array}{ccccc} r = \tilde{r}_0 & & \vartheta = \tilde{\vartheta}_0 & & \varphi = \tilde{\varphi}_0 \\ u = \tilde{u}_0 & v = \tilde{v}_0 & & w = \tilde{w}_0 & m = \tilde{m}_0 \end{array} \tag{5.26}$$

[1]The departure date t_0 could be considered free and left as an unknown variable, but in that case, it is almost sure that the algorithm would converge just to a local optimum, as the allowed range of departure dates is too wide.

At the end point, the boundary conditions are pretty different between the two spacecraft. The target spacecraft (Sat 2) has to perform an optimal time-free mission to arrive at the apogee of the final orbit, whose semi-major axis $\tilde{a}_f$ and eccentricity $\tilde{e}_f$ are prescribed. These constraints are rewritten in terms of energy and momentum magnitude, to attain a simpler formulation:

$$u = 0 \tag{5.27}$$

$$r^2\left(v^2 + w^2\right) = \tilde{a}_f\left(1 - \tilde{e}_f^2\right) \tag{5.28}$$

$$v^2 + w^2 - \frac{2}{r} = -\frac{1}{\tilde{a}_f} \tag{5.29}$$

By applying the transversality conditions one obtains the algebraic equations that close the Hamiltonian boundary value problem:

$$H = 0 \tag{5.30}$$

$$\lambda_\vartheta = 0 \tag{5.31}$$

$$\lambda_\varphi = 0 \tag{5.32}$$

$$\lambda_v w - \lambda_w v = 0 \tag{5.33}$$

$$\lambda_m = 1 \tag{5.34}$$

On the other side, the chaser spacecraft (Sat 1) performs an optimal time-fixed mission. In this case the final state of the spacecraft is assigned, as it must be equal to the target state $\bar{x}^*_{f2}$ (except for the mass). The arrival time is fixed and delayed by a constant quantity with respect to the optimal arrival time t^*_{f2} of Sat 2. These conditions ensure that the two spacecraft share the same orbital parameters (except for the mean anomaly). The time delay $\Delta t_{\tilde{D}}$ is given by eq. (5.21) and here reported for the sake of completeness. Thus:

$$r = r^*_{f2} \tag{5.35}$$

$$\vartheta = \vartheta^*_{f2} \tag{5.36}$$

$$\varphi = \varphi^*_{f2} \tag{5.37}$$

$$u = 0 \tag{5.38}$$

$$v = v^*_{f2} \tag{5.39}$$

$$w = w^*_{f2} \tag{5.40}$$

$$t_f = t^*_{f2} + \Delta t_{\tilde{D}}; \qquad \Delta t_{\tilde{D}} = \tilde{D}/V_a \tag{5.41}$$

The transversality equations provide only one additional condition, which is related to the final mass via the merit index and involves the mass adjoint:

$$\lambda_m = 1 \tag{5.42}$$

5.3.3 Cooperative Approach

In case of a cooperative approach, there are no "target" or "chaser" satellites but both spacecraft operate to reach the desired formation. In this case the motion of the two satellites is analyzed simultaneously, and the goal (that is, the objective function) is to maximize the sum of their final masses. The equations of motion of each spacecraft, as well as the adjoint equations, remain unchanged with respect to the single spacecraft problem, but, obviously, the overall number doubles (28 equations, that is, 14 per each spacecraft).

Many considerations made in Chapter 4 (c.f. section [4.3.1]) still hold in this case. For example, in both cases the Hamiltonian can be written as the sum of the two Hamiltonians corresponding to each spacecraft. The presence of two distinct switching functions is again highlighted:

$$\begin{aligned} H = &\vec{\lambda}_{r_I}^T \vec{V}_I + \vec{\lambda}_{V_I}^T \vec{G}\left(\vec{r}_I\right) + \vec{\lambda}_{V_I}^T \vec{a}_p\left(\bar{x}_I, t\right) + \\ &\vec{\lambda}_{r_{II}}^T \vec{V}_{II} + \vec{\lambda}_{V_{II}}^T \vec{G}\left(\vec{r}_{II}\right) + \vec{\lambda}_{V_{II}}^T \vec{a}_p\left(\bar{x}_{II}, t\right) + \\ &T_{max} S_{F_I} \beta_I + T_{max} S_{F_{II}} \beta_{II} \end{aligned} \tag{5.43}$$

Each spacecraft has its own control law and different burn structures between the two spacecraft are possible. The thrust direction of each spacecraft is parallel to the Primer Vector corresponding to that spacecraft, whereas the search for the optimal thrust magnitude can be handled by imposing switching conditions (in the Multi-Bound approach) or by regularizing the control (Continuation-Smoothing technique). For both cases the methodology is the same as in Chapter 4. With respect to the Chaser/Target formulation, the optimal conditions for each satellite at departure are formally unchanged. The major difference arises at the final point. The capability of having two different time scales (one for each spacecraft) allows one to define this final boundary as the apogee of each spacecraft, regardless of the arrival time. The satellites have the same state (i.e., position and velocity) in order to assure that they are on the same orbit. The phase constraint is once again written as a time constraint between the two spacecraft arrival times.

$$u_1 = 0 \tag{5.44}$$

$$r_1^2 \left(v_1^2 + w_1^2\right) = \tilde{a}_f \left(1 - \tilde{e}_f^2\right) \tag{5.45}$$

$$v_1^2 + w_1^2 - \frac{2}{r_1} = -\frac{1}{\tilde{a}_f} \tag{5.46}$$

$$t_{f1} - t_{f2} = \Delta t_{\tilde{D}}; \qquad \Delta t_{\tilde{D}} = \tilde{D}/V_a \tag{5.47}$$

$$r_2 - r_1 = 0 \qquad \vartheta_2 - \vartheta_1 = 0 \qquad \varphi_2 - \varphi_1 = 0 \tag{5.48}$$

$$u_2 - u_1 = 0 \qquad v_2 - v_1 = 0 \qquad w_2 - w_1 = 0 \tag{5.49}$$

By applying the transversality conditions one obtains the remaining boundary conditions:

$$H_{TOT} = 0 \tag{5.50}$$

$$\lambda_{\vartheta_1} + \lambda_{\vartheta_2} = 0 \tag{5.51}$$

$$\lambda_{\varphi_1} + \lambda_{\varphi_2} = 0 \tag{5.52}$$

$$\left(\lambda_{v_1} + \lambda_{v_2}\right) w_1 - \left(\lambda_{w_1} + \lambda_{w_2}\right) v_1 = 0 \tag{5.53}$$

$$\lambda_{m_1} = 1 \tag{5.54}$$

$$\lambda_{m_2} = 1 \tag{5.55}$$

This set of optimal conditions presents a sort of symmetry between the two satellites at the arrival point. Being these conditions less tight than those of the sequential approach, they permit a more efficient split of the additional cost due to the phase constraint. However the computational efficiency decreases, as the number of differential equations to be integrated at each iteration of Newton's method doubles, and also the number of unknown initial values doubles. As the difficulty of the problem grows with the "square" of the unknowns' number, solving this cooperative problem is more difficult and computationally much more expensive than solving separately the two problems arising from the sequential approach.

5.4 Results in a Simplified Environment

5.4.1 Keplerian Mission

Keplerian Mission refers to an "idealized" deployment which is performed assuming a two-body, unperturbed, dynamical model. As the dynamics is autonomous (i.e., time-independent), the optimal solution of the problem does not depend on the initial date.

A physical analysis of the problem is required for choosing a reasonable starting guess. In particular, if the Multi-Bound approach is used, it is important to understand the mission structure in order to attain an good estimate of the engine switching instants. The right values of the other unknowns (i.e., the initial adjoint variables) are more difficult to guess. However, the physical meaning of the primer vector suggests that the adjoint vector to velocity should be parallel to the thrust direction, which is essentially horizontal and in the orbital plane for the initial burn; latitude has a minimal influence and longitude has no influence at all; the corresponding adjoint variables are therefore (roughly) zero. The magnitude of the primer vector $\vec{\lambda}_V$ and the adjoint variable to radius λ_r remain difficult to estimate; but using the previous estimate for the other unknown, one easily manages to get the convergence. The single spacecraft deployment should be studied first, as it is simpler. Once the convergence is obtained, the solution of this problem can be used as initial guess for formation deployment.

The deployment of a single satellite into the operational orbit is first analyzed, in order to understand the basic aspects of the mission. According to the Keplerian model, the initial conditions of Sat 2 permit an (almost) perfect ballistic attainment of the desired final apogee and the deployment require only the perigee raising. For Sat 1, the initial apogee is greater than the operative one of about 527 km (due to the injection ΔV) and a slight perigee maneuver is necessary to reduce the initial apogee (191643 km) to the final desired value (191118 km).

A simple impulsive analysis [77] shows that the optimal burn strategy is characterized by an apogee impulse (to accelerate) followed by a perigee one (to decelerate) for Sat 1 (the AP abbreviation is used to describe this burn sequence). Numerical results confirm this statement in the finite-thrust case; however, if multiple revolutions are allowed, the apogee impulse should be split into several apogee burns to reduce the velocity losses. In addition, a tiny perigee burn arises also for Sat 2: if the thrust is

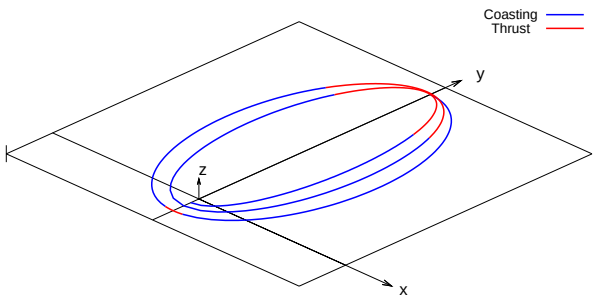

Figure 5.10: Trajectory for the Sat 2 single deployment, 2.5 revolutions AAP mission (Keplerian environment, $T = 1N$).

(partially) used during apogee burns to raise a bit the apogee itself, the perigee-raise cost becomes smaller due to the greater "force arm"; but, in that case, a perigee maneuver is needed to restore the initial apogee altitude. Therefore the optimal strategy for an assigned maximum number of revolutions has as many apogee burns as possible and a single perigee burn at the end of the transfer.

Table 5.6: Unconstrained deployment - Final mass of Sat 1 & Sat 2 for different transfer time-lengths (Keplerian environment, $T = 8N$).

Unconstrained solution		
Strategy	Sat 1	Sat 2
AP (1.5 revs)	846.339	1101.858
AAP (2.5 revs)	846.507	1102.235
AAAP (3.5 revs)	846.537	1102.304

The final masses corresponding to the independent deployment of either Sat 1 or Sat 2 are presented in Table 5.6 for different thrust strategies and number of revolutions; only optimal solution are here reported.

The previous analysis holds even in the case of the formation deployment. The low separation ΔV causes the two spacecraft to have similar orbital periods. Thus, the optimal mission profile (i.e., burn structure) for both satellite will be the same as the single deployment: a sequence as long as possible of apogee thrust arcs followed by a final perigee arc. Results for the Chaser/Target strategy are presented in Table 5.7.

Table 5.7: Chaser/Target deployment - Final mass of Sat 1 & Sat 2 for different transfer time-lengths (Keplerian environment, $T = 8N$).

Chaser/Target solution			
Strategy	Sat 1	Sat 2	Overall
AP (1.5 revs)	846.192	1101.858	1948.050
AAP (2.5 revs)	846.503	1102.235	1948.738
AAAP (3.5 revs)	846.536	1102.304	1948.840

Table 5.8: Cooperative deployment - Final mass of Sat 1 & Sat 2 for different transfer time-lengths (Keplerian environment, $T = 8N$).

Cooperative solution			
Strategy	Sat 1	Sat 2	Overall
AP (1.5 revs)	846.287791	1101.822479	1948.110
AAP (2.5 revs)	846.504983	1102.234185	1948.739
AAAP (3.5 revs)	846.536814	1102.303874	1948.841

Very close results are obtained by the cooperative strategies. As it was pointed out in the cooperative rendezvous (c.f. Chapter 4), if the initial conditions are close, the difference between the Chaser/Target and the Cooperative strategy is small. This sentence still holds for the Simbol-X deployment, at least for the mission features here considered. The difference would be more evident if bigger separation ΔV or lower thrust magnitude were considered [78].

5.4.2 J2 Mission

The deployment problem will be solved again in this section, but including into the dynamical model the gravitational perturbation related to Earth oblateness, that is, the second zonal harmonic (hence the name J2 mission). Even in this case, the deployment is independent of the departure date, as the dynamical model is autonomous.

As far as the "J2 mission" is concerned, the mission profile changes remarkably with respect to the Keplerian case. The effect of Earth oblateness on semi-major axis and eccentricity is null after a complete orbit, hence the perigee is unchanged, while the actual apogee of the initial orbit is lowered[1]. Therefore, when J2 is considered, the

[1] As far as a ballistic orbit is concerned, the apogee takes the same value again at any revolution.

actual difference between initial and final apogee radii is about -2281 km and -9172 km, respectively, for Sat 1 and Sat 2. The deployment mission now requires to raise both perigee and apogee, even though the apogee maneuver is far more expensive, from a propulsive point of view, than the (very small) perigee burn. An impulsive strategy would again prescribe two burns, but their order is the opposite with respect to the Keplerian case, because here the apogee has to be raised, while in the former case, lowered. Again, in the finite-thrust case it is convenient to split the apogee maneuvers into multiple burn arcs centered at the apsides, in order to reduce the propulsive losses. The perigee burn, which should precede all the apogee burns, is very short and, if the number of revolutions is limited (not too high), the split of the longer apogee burn is preferable in terms of propellant consumption. We can easily state that the optimal burn structure consists of a single perigee burn (to raise the apogee) followed by burns at every apogee passage. As an example, when 4.5 revolutions are permitted, only three apogee burns can be performed (engine cannot be used in the proximity of departure and arrival apsides): the optimal burn sequence is therefore PAAA.

Table 5.9: Chaser/Target deployment - Final mass of Sat 1 & Sat 2 for different transfer time-lengths (Mission J2, $T = 8N$).

Chaser/Target solution			
Strategy	Sat 1	Sat 2	Overall
PA - PA	845.3969	1100.5751	1945.9720
PAA - PAA	845.7344	1100.9129	1946.6474
PAAA - PAAA	845.7630	1100.9748	1946.7378

Table 5.10: Cooperative deployment - Final mass of Sat 1 & Sat 2 for different transfer time-lengths (Mission J2, $T = 8N$).

Cooperative solution			
Strategy	Sat 1	Sat 2	Overall
PA - PA	845.5300	1100.5289	1946.0589
PAA - PAA	845.7349	1100.9128	1946.6476
PAAA - PAAA	845.7632	1100.9747	1946.7379

The previous remarks on the solution of Keplerian Missions still hold in this case: the payload increases for longer missions as the apogee maneuver is split into a greater

number of burns. The thrust can be exploited in positions that are closer to the apogee (i.e. the optimal position in the impulsive case) and misalignment losses are reduced. This fact is more evident as the thrust level is lower or the number of revolutions is lower, and the propelled arcs longer.

5.4.3 Collision Avoidance

Previous results were obtained without caring about the collision risk, and the related constraint. That inequality constraint is difficult to enforce in its most general form, because it is not known in advance if it will be active only in a small arc or all along the mission. Rather than trying to enforce it directly, a different approach is used: first, the unconstrained solution is found and the respect of the security distance is checked; if the distance constraint is not fulfilled, the optimal unconstrained solution is purposely modified by adding a suitable, equivalent constraint to the problem. Numerical results

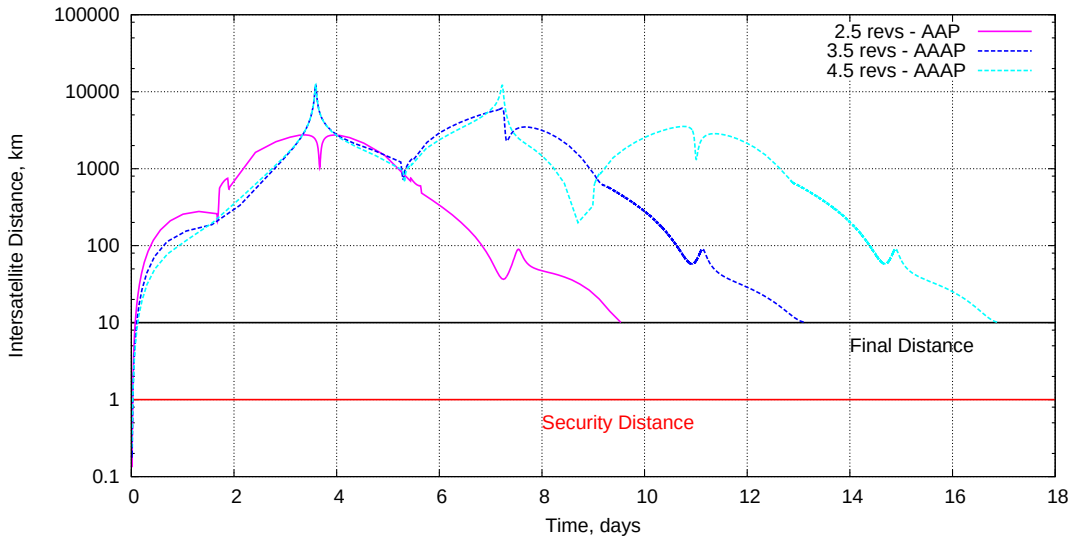

Figure 5.11: Intersatellite distance for optimal Keplerian 2.5-, 3.5-, 4.5- revolution missions.

show that the safety distance constraint is always fulfilled by the optimal Keplerian missions with strategy A..AP; instead, a collision is more likely to happen for the J2 missions, where the optimal burn structure is "PA..A" (the inequality constraint is not respected here).

In the latter case, the minimum distance is always reached near the second-last apogee. The two spacecraft recover gradually the initial phase angle (caused by having the spacecraft flying on two different orbits during the first ballistic revolution) during each maneuver. The recovering process is completed at the end of the last propelled arc; henceforward the two spacecraft have the right phase, but their distance varies along the orbit due to velocity changes along HEO. The critical maneuver is therefore the last one, where the two spacecraft approach each other.

In case of a A..AP burn structure, the last maneuver is performed at the maximum-velocity point, that is, where the spacecraft displacement is maximum. Actually, one finds out that the intersatellite distance is always greater that the final one (except soon after the separation, obviously). In case of a PA..A burn structure, the situation is more risky, as the last maneuver is performed at the minimum-velocity point, that is where the spacecraft displacement is minimum. The intersatellite distance for the

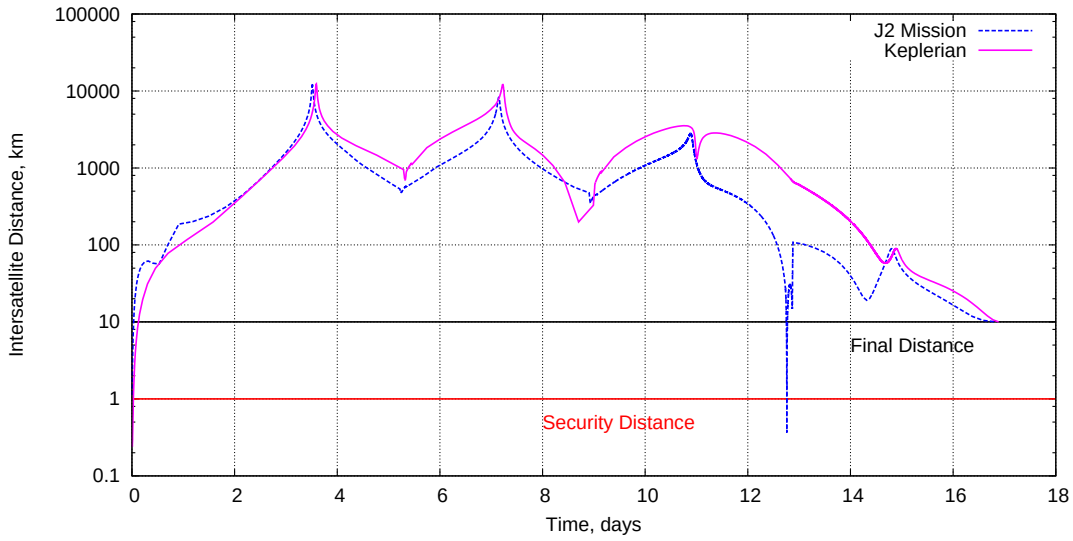

Figure 5.12: Intersatellite distance for optimal 4.5 revolution mission: Keplerian mission (AAAP) and J2 Mission (PAAA).

Keplerian and J2 cooperative 4.5 revolutions missions are presented in Figure 5.12. The optimal solution of J2 mission (structure PAAA for both satellites) violates the security distance constraint.

An efficient way to attain the respect of the safety distance constraint (without explicitly imposing it), consists in constraining the difference between the second last

apogee radii of the two spacecrafts. The precise value to enforce in order to attain an exact minimum distance can be found by an iterative procedure. The respect of an assigned minimum distance is attained in a few iterations if a bisection or secant method is used.

The Multi-Bound formulation allows an easy identification of the apogee passage for any spacecraft, because the radial velocity is null there ($u_1 = 0$, $u_2 = 0$). At the penultimate apogee, the further constraint $r_1 - r_2 = \tilde{d}_{apo}$ must hold. Since a state variable is constrained at an internal boundary, the corresponding adjoint has a discontinuity, which is usually free (c.f. section [2.3.1]); in this case, by applying the transversality conditions, one obtains that the adjoints λ_r of the two spacecrafts have a jump, which has the same free magnitude but different sign:

$$\lambda_{r1+} = \lambda_{r1-} + \mu \qquad \lambda_{r2+} = \lambda_{r2-} - \mu \tag{5.56}$$

where the plus and minus sign in the subscripts refers to the value just after and before the boundary, respectively.

Table 5.11 presents the minimum distance during the last apogee burn as a function of the enforced difference between the apogee radii for the 4.5 revolutions J2 mission; by setting this difference at 1.6055 km the distance between the satellites during the whole deployment, which is shown in Figure 5.13, is never below 1 km. The mass budget to fulfill the distance constraint is extremely low (less than one gram).

According to Table 5.11, for this thrust level the minimum separation distance before the arrival cannot be increased at will; in fact, for an apogee difference larger than 2.5 km, the minimum distance point is located at the end of the last propelled arc. As remarked previously, the two spacecrafts cannot maneuver near the arrival point; the proper phasing is already achieved at the end of the last apogee burn. Here the velocity is lower than at the apogee but very close, because the maneuver arc is quite short. Thus the inter-satellite distance will be slightly greater than the one that has to be acquired at the end of the deployment.

5.5 Results in a Realistic Environment

This section is focused on feasible strategies for the deployment of the two-spacecraft formation in a more realistic environment, which involves a more complete dynamical

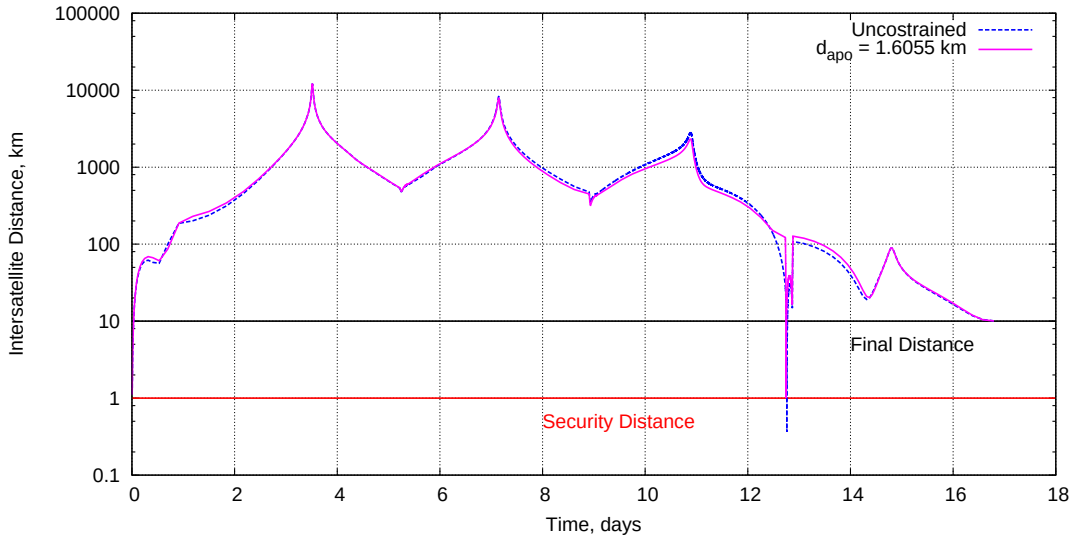

Figure 5.13: Intersatellite distance for constrained and unconstrained suboptimal (A-P-A) three-burn strategies ($T = 8N$, $\Delta V = 0.5m/s$).

Table 5.11: Results for the recovery strategy, Mission J2 PAAA 4.5 revolutions.

Cooperative strategy			
d_{apo} km	Minimum Distance km	Final mass kg	Mass Loss g
0.478884	0.36635	1946.738	\
1.50	0.742812	1946.738	-0.205
1.60	0.9301	1946.738	-0.247
1.6055	1.0000	1946.738	-0.249
1.75	2.959958	1946.738	-0.316
2.00	6.39068	1946.737	-0.448
2.50	10.08852	1946.737	-0.776
3.00	10.08852	1946.737	-1.181
5.00	10.08846	1946.734	-3.429
10.00	10.08844	1946.726	-11.797

model. Perturbation due to Earth asphericity, lunar and solar gravitational attraction are here considered. It will be shown, through a preliminary analysis, that the perturbations can significantly alter the spacecraft trajectories and that the burn structure may change as different departure date and/or different spacecraft features are taken into account.

The use of a Multi-Bound approach becomes troublesome because the number of candidate PMP burn structures arises quickly as the allowed number of revolutions increases. The Continuation-Smoothing approach will be adopted, to overcame the impossibility of discerning with simple physical reasoning the optimal burn structure for any departure date. Use is made of the fully automatic initialization procedure described in the following. The single spacecraft deployment is used as benchmark to verify the effectiveness of the proposed method. This is a good test case because the number of PMP-candidate burn structures is low and a complete picture can be drawn by manually governing the Multi-Bound approach. Eventually, results for the Formation Deployment mission using both Chaser/Target and Cooperative strategies are presented.

The Simbol-X deployment problem presented in the previous chapter relies on the position-velocity variable set to describe the state of each spacecraft. This formulation of problem is straightforward but induces significant numerical instabilities in the evaluation of the shooting function, due to the perturbed spacecraft dynamics and the high eccentricity of the orbits involved in this specific mission. As far as the Multi-Bound approach is concerned, these numerical instabilities are not worrisome; the loss of accuracy along the integration can be reduced by tightening the integration tolerance. Instead, when the Continuation-Smoothing technique is employed, these instabilities sum up to those related to the control discontinuities and usually prevent convergence. In order to reduce the numerical issues due to the spacecraft dynamics, the problem has been reformulated using the modified equinoctial elements as state variables. This set of variables features a more stable set of dynamical equations, but it is less intuitive and the derivation of the first order optimality condition is harder. For the sake of clearness, the complete position of the Simbol-X deployment problem with this alternate set of variables, considering both the Chaser/Target and the Cooperative strategy, is provided in Appendix B.

5.5.1 Perturbative effects on the Switching Structure

In section [5.3.1] the deployment problem was solved assuming a simplified, two-body dynamical model. For missions longer than 1.5 revolutions, a payload increment was attained by splitting the single apogee firing of the fastest mission into many shorter burns. Indeed, an almost uniform splitting occurred in case of single spacecraft deployment, because misalignment losses are reduced by an equal distribution of the duty among all the apogee burns.

The situation becomes more complex if a full perturbation dynamic environment is considered. The main propulsion effort is spent to raise the perigee radius to the operative value, but the actual effort depends on the third-body gravitational perturbations of Moon (mostly) and Sun, which can act in both ways (i.e., by decreasing or increasing the perigee) depending on the relative position of the bodies. Therefore the overall mission consumption depends on the initial phasing of the relevant bodies, hence on the mission departure date.

Moon has a complex influence on the spacecraft trajectories. Its perturbative effects depend on the relative phasing of the spacecraft at the apogee, where it spends most of its time (c.f. section [5.2.2]). The spacecraft phase at subsequent apogee passages changes due to the (relatively fast) motion of the moon during one orbital period. Favorable and unfavorable phasing (more or less strong) alternate along the same mission.

The thrust can be used to change the phasing with the Moon of all the spacecraft apogee passages (except the first). A longer thrust arc at the first apogee increases the total time of flight. On the contrary, when the first apogee burn vanishes, the following orbital periods are shorter and the whole mission is faster. A proper use of this mechanism (i.e., adjusting the burn lengths to vary the intermediate orbital periods) permits to put forward or push back the apogee passages in order to enhance/reduce the effects of favorable/unfavorable geometrical configurations.

The trip time for a 4.5 revolutions mission may differ more than 12 hours (about 6 degree in angular position of the Moon). The trip time range is lower for shorter missions, and almost null for the 2.5 revolutions missions. Although the relative position of the bodies throughout the deployment is decided mainly by the departure date, it also depends on the spacecraft maneuvers: perigee raising/lowering effects change rapidly

with the Moon phase, and even few degrees make a difference between high and low performance missions.

As a result, the optimal splitting of the apogee burn becomes less straightforward, since now there are two conflicting ways to increase the payload: by reducing the misalignment losses through an equal repartition of the propulsive effort over each apogee, or by taking advantage of the lunar perturbation by means of a "fine tuning" of the intermediate orbital periods. For this reason, the optimal switching structure, that is, the structure that respects Pontryagin's Maximum Principle, may change according to departure date, thrust level and characteristics of the relevant spacecraft. For some departure dates the optimal solution may be "incomplete", that is, one or more apogee burns vanish completely in order to attain the maximum benefit from the Moon-Spacecraft phasing. The presence of incomplete burn structures can be envisaged by looking at the relative importance of lunar perturbation gain and misalignment losses, expressed in terms of payload increment.

Lunar Perturbation Gain The lunar attraction is the most important (time dependent) perturbation in this specific problem and can be exploited to reduce the propellant consumption. A proper evaluation of the gain related to the lunar perturbation (LPG) is quite difficult to perform. A reasoning on the order of magnitude is useful. As an estimate of saved propellant, we considered the amount needed to perform an impulsive maneuver equivalent to the maximum perigee raise that can be achieved by the Moon pull after one complete revolution of the spacecraft. Assuming a maximum variation of the apogee phase of 6°, a free perigee raise up to 108 km can be attained, which equals an impulsive maneuver with $\Delta V = 2.907$ m/s corresponding to 1.29 kg of propellant. This is the order of magnitude of LPG (for a fixed departure date).

Misalignment Losses Reduction The Misalignment Losses Reduction (MLR), which is provided by the split of the apogee maneuver, can be evaluated as at the differences on the final masses between missions in the Keplerian environment with different switching structures. In fact, the difference in terms of payload is almost completely linked to MLR.

Table 5.12: Misalignment Losses Reduction due to apogee splitting.

Keplerian environment: Sat 0 - Final Mass [kg]				
Strategy	T = 8 N	T = 4 N	T = 2 N	T = 1 N
A	846.374	845.639	842.345	816.527
A-A	A +0.179	A + 0.735	A + 3.294	A + 25.813
A-A-A	A +0.212	A + 0.868	A + 3.841	A + 28.315

Values in Table 5.12 refer to the optimal deployment in the Keplerian environment of a fictitious "Sat 0" which is halfway between Sat 1 and Sat 2: it has the same propulsive features of Sat 1 but its initial orbit is the same as Sat 2. This table shows that the importance of MLR with respect to LPG decreases as the thrust level increases. Incomplete solutions are more likely to arise if a high thrust level is considered, whereas they probably would not occur in case of lower thrust levels. Sun is not considered in this simplified analysis because its position varies more slowly than the Moon does. Thus, the same changes in spacecraft period modify Sun effects less than Moon ones. Indeed, the sun-spacecraft phasing can be hardly modified by using the spacecraft thrust.

The optimal burn structure might have one apogee burn less or even two. In theory, for a mission of n_{rev} number of revolutions (i.e., $n_{rev} = 2.5,\ 3.5,\ 4.5$), considering only maneuvers at the perigee and at the apogee, except the first and the last, the number of possible burn combinations is $2^{2(n_{rev}-0.5)}$. In practice, the number of useful, PMP-candidate solutions can be reduced considerably by assuming that the first burn is at perigee, and is the only perigee maneuver. Under theses assumption, for the longer single satellite mission (4.5 revs.) we have one complete structure (PAAA), three 1-incomplete structures (P0AA, PA0A, PAA0), etc.

5.5.2 Automation of the Solution Process

The Multi-Bound approach can be used to find the optimal solution for a deployment in a perturbed environment. If the solution for one specific departure date is sought, the convergence process can be carried out manually (with some efforts). If many solutions, corresponding to many different departure dates, are needed, one can try to extend a known solution by performing a continuation on the departure date (to reduce the

amount of manual work). This extension process works by exploiting the continuous dependence of the differential equation system on the initial conditions and the fact that the Multi-Bound method has a convergence radius sufficiently wide to allow reasonably long steps (in the present case, variation on the departure date from few hours to few days are possible, depending on the time scale of the dynamical model).

Unfortunately, the optimal burn structure changes with the departure date. A simple approach to face this issue is to find for the same date the solutions corresponding to a set of burn structures (those that are reputed to be best candidates) and extend all of them by continuation. The optimal solution, by definition, will be the one with the highest merit index. The switching function is then inspected to ensure that PMP is respected. If even the solution with the highest merit index does not satisfy PMP, none of the considered burn structures is optimal. Thus, a different burn sequence has to be found and added to the set of candidate burn structures.

This way of handling the shortcoming is pretty effective if the number of potentially optimal burn structures is low, that is, when the number of revolutions is small. As the revolution number increases, the possibilities increase, and this solution process becomes longer, but in principle still valid. The main limit of this strategy is that solutions corresponding to a given burn structure may not exist for some dates; thus the continuation process ends abruptly.

The fact that an augmented problem might not have solution, if the burn structure does not correspond to the optimal one, was highlighted in section [3.3.1]. Here, in particular, a physical solution is not attained whenever the imposed burn structure has more burns than the optimal one. The explanation is quite simple: if more switching conditions (i.e., zeros of the switching function) are enforced than the actual number of roots of the switching function, all the switching conditions at the interior boundaries cannot be fulfilled and the convergence cannot be obtained: the Newton method may diverge or, more often, a non physical solution is attained, because new roots of the switching function are created by means of a time inversion. Whether case arises is, however, not predictable.

If the extension process is halted, it can be restarted by skipping to a successive date. The problem is that a new "starting" solution is now needed and it should be found manually; in fact if the restart is attempted in an automatic way and the convergence is still not attained, the reason may be either a poor choice of the initial guess or the fact

that the solution does not exists for that specific date. Being impossible to distinguish the two cases without manual intervention, some interesting solutions might be lost.

The Continuation-Smoothing approach does not require the optimal burn structure to be known (or guessed) in advance; thus it seems naturally apt for solving the deployment in this complex environment. Once again, the fully automatic initialization procedure described in section [3.4.3] can be exploited. A further continuation phase needs to be interposed between the solution of the starting problem and the orbit-shape continuation. This phase aims to introduce progressively the perturbing accelerations, which are present in the actual dynamic model, but are neglected in the starting problem dynamics (in order to keep its solution as simple as possible). This continuation is attained by scaling each perturbation by a coefficient α_p which is initially zero and progressively increased to one.

5.5.3 Single Satellite Deployment

This section presents results for the single deployment problem, obtained by using either the Multi-Bound and the Auto-CS algorithms. Missions up to 4.5 revolutions are investigated over a whole month. Since the mission structure changes (mostly) according to the Moon phase, this range is wide enough that all the possible burn structures arise.

As anticipated in section [5.5.1], the optimal solution (hence the related payload and burn structure) changes according to mission length, departure date and features of the relevant spacecraft. Figures 5.14, 5.15, and 5.16 consider short (2.5 revs.), medium (3.5 revs.), and long length (4.5 revs.) missions, respectively, for the deployment of Sat 2. Solid lines refer to solutions obtained by the original Multi-Bound approach, via the extension procedure on the departure date explained in section [5.5.2]. Instead, dots refer to solutions obtained by using the Auto-CS algorithm. As far as the 2.5 revs. mission is concerned, the transfer is so short that the spacecraft capability of maneuvering in order to exploit (or avoid) the Moon pull is very limited. Indeed, the optimal burn structure is PA for any departure date. The picture becomes more tangled as far as longer missions are taken into account: for the 3.5 revolution missions two burn structures are alternatively optimal (for different departure dates), whereas for the 4.5 revolution missions the optimal burn structure is one of the four proposed in Figure 5.16. In any case, the optimal solution varies remarkably according to the

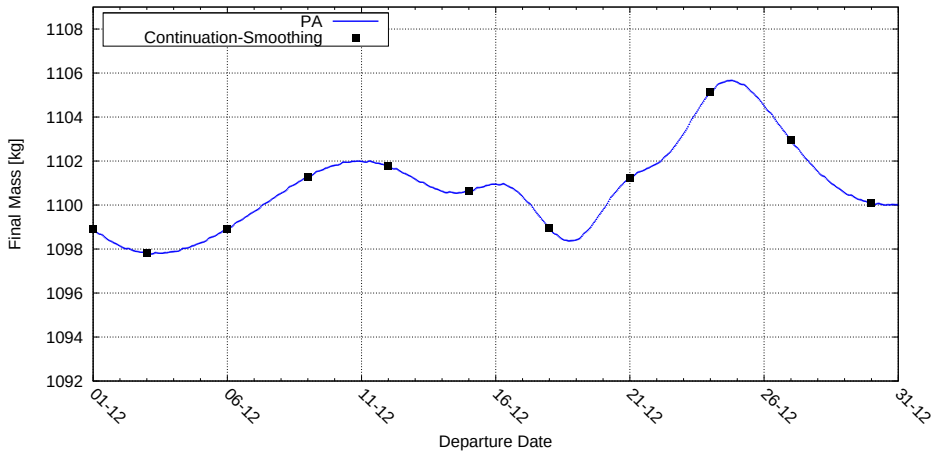

Figure 5.14: Final mass for the 2.5 revolution deployment of Sat 2.

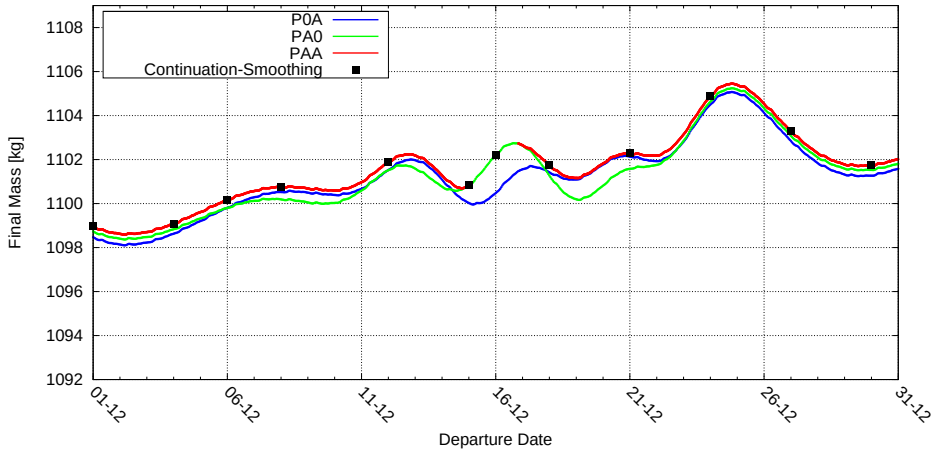

Figure 5.15: Final mass for the 3.5 revolution deployment of Sat 2.

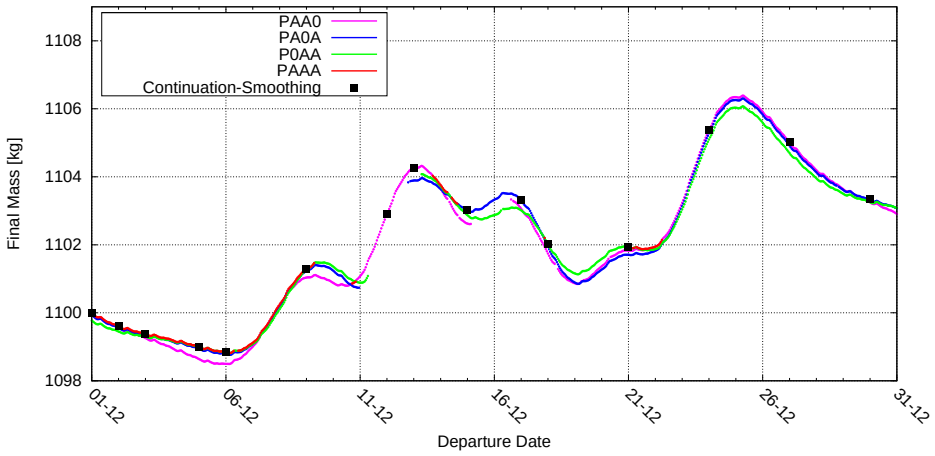

Figure 5.16: Final mass for the 4.5 revolution deployment of Sat 2.

departure date, and up to 8 kg of propellant (over an average consumption of roughly 150 kg) can be saved/lost by varying the departure date.

The single spacecraft deployment is also a good benchmark to evaluate the effectiveness of the Auto-CS algorithm, as many different situations arise. The proposed algorithm performs very well in a wide range of situations, as testified by Figures 5.14-5.16. Minor differences (a few grams) in the propellant consumption are due to numerical errors that cannot be avoided without forcing a very high precision to the integrator. The computation time required for a single solution varies from a pair of minutes to almost ten minutes, depending on the mission length, the choice of the integration tolerance, and the maximum allowed step of the continuation process (for either orbit-shape and smoothing parameters).

As far as short and medium length missions are concerned, the Continuation-Smoothing approach always captures the optimal solution. Some issues arose in rare cases of long-length (4.5 revs.) missions when the first apogee burn vanishes and the perigee one is delayed by one revolution. In those cases the continuation on the smoothing parameter stopped prematurely (i.e., before the stopping condition on the smoothing parameter is met). Even though the exact origin of this shortcoming cannot be proved, it is possible to relate the shortcoming to two unlucky circumstances:

1. the thrust level does not increase simultaneously in both the perigee burns;

2. the trajectory is very sensitive to perigee maneuvers, where velocity is high, and even a very small burn can alter drastically both the state and adjoint variables in the following part of the mission.

During the continuation on the smoothing parameter, the burn located at the first perigee passage has an early "grow". As the continuation progresses, the first apogee burn tends to vanish and simultaneously a second perigee burn raises. However, this happens when the smoothing parameter is already very low ($\varepsilon = 10^{-4} \div 10^{-5}$) and the solution is already too "rigid" (or "stiff") to accept the required change. This effect does not appear in the fixed-structure approach because the thrust magnitude at each perigee is assumed to be zero or maximum, since the beginning of the convergence process. A specific patch can be designed for this problem by modifying the optimization algorithm. It consists in denying the spacecraft the possibility of maneuver at the second perigee passage. In this way, the convergence process is made more stable, all the previous optimal solutions are still attained, but (obviously) the attained solution is not PMP in those rare cases when the standard algorithm did not work. Some numerical issue remains, and in few cases the integrator tolerance has been tightened to satisfy the boundary conditions with the standard precision.

An example of a troublesome mission is given by the single deployment of Sat 0 in date 5/12/2015 @ 00:00. Here, the first apogee burn vanishes, and the perigee burn is delayed to better exploit the Lunar pull, thus the optimal solution has the odd (or delayed) 0PAA burn structure and the final mass is 844.141 kg. The "non-patched" Continuation-Smoothing approach does not converge for this date, whereas the "patched" Continuation-Smoothing approach converge to a P0AA solution (final mass equals to 844.079 kg), which is sub-optimal, but the overall propellant consumption is almost the same (the difference is below 70 grams). These peculiar aspects of the Simbol X mission deployment has been extensively analyzed in [79, 80].

5.5.4 Formation Deployment

In this section the Continuation-Smoothing technique is applied to the Formation Deployment problem. Numerical results are presented for both Chaser/Target and Cooperative strategies.

Chaser/Target Strategy

Very good results are obtained when the Auto-CS algorithm is applied to the formation deployment problem, according to the Chaser/Target approach. The optimization process is carried out successfully for almost every tested mission (for both short and long transfers). Convergence problems rarely occur. Results concerning missions with different lengths are summarized in Table 5.13. The overall final mass obtained for departure dates during a whole month are shown in Figure 5.17.

Table 5.13: Chaser/Target deployment - Final mass and computational time for different-length missions (J2 + Lunisolar perturbation).

Mission	Final Mass, kg			CPU TIME, min	
	Sat 1	Sat 2	Overall	Sat 1	Sat 2
JLS - 2.5 @ 1/12/2015	844.129	1098.920	1943.049	10:11	05:34
JLS - 3.5 @ 1/12/2015	844.233	1098.956	1943.189	13:12	07:22
JLS - 4.5 @ 1/12/2015	845.026	1099.993	1945.019	16:29	10:04

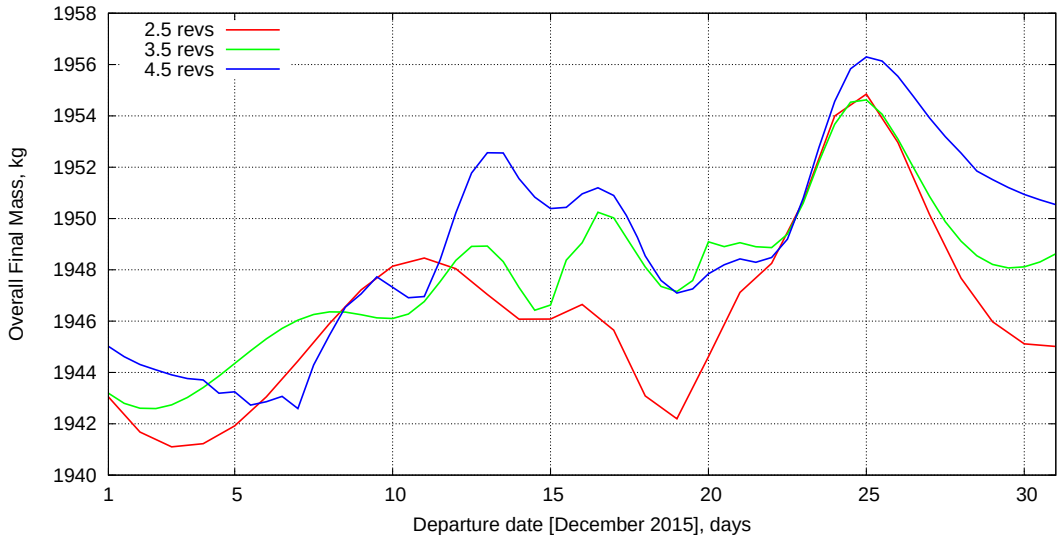

Figure 5.17: Final mass for the JLS 2.5, 3.5, and 4.5 revolution Chaser/Target formation deployment.

The crucial role that the departure date plays in the transfer is evident: improvement up to 13 kg with respect to the minimum overall final mass value can be obtained

by varying the departure date. Differently from the Keplerian and J2 missions, a longer mission duration does not always corresponds to a payload increment. This fact can be explained by considering that the perturbation effects (of the Moon, in particular) tend to average over a long time horizon; instead if a short time period is considered, and a proper choice of the departure date is made, the spacecraft experience only the most favorable pulls. Thus, for some departure dates, shorter missions are more performing than longer. On the other hand, the mean payload value over a long interval (e.g. a month) increases with the mission length (1946.447 kg, 1947.887 kg, and 1948.957 kg for the 2.5-, 3.5-, and 4.5-revolutions mission, respectively).

Cooperative Strategy

As far as the cooperative strategy is concerned, the number of vehicles increases, the problem becomes numerically more difficult and the Continuation-Smoothing algorithm is severely stressed. The optimization process often ends "prematurely" during the continuation on the smoothing parameter (that is, before a very law smoothing parameter value is reached). For this reason, the attained control law remains smoother then the optimal (bang-bang), causing a loss of performance (i.e., a loss of payload, or an extra propellant consumption) which depends on how far the obtained control law is from reaching the bang-bang law. Figure 5.18 presents an example of variation of the merit

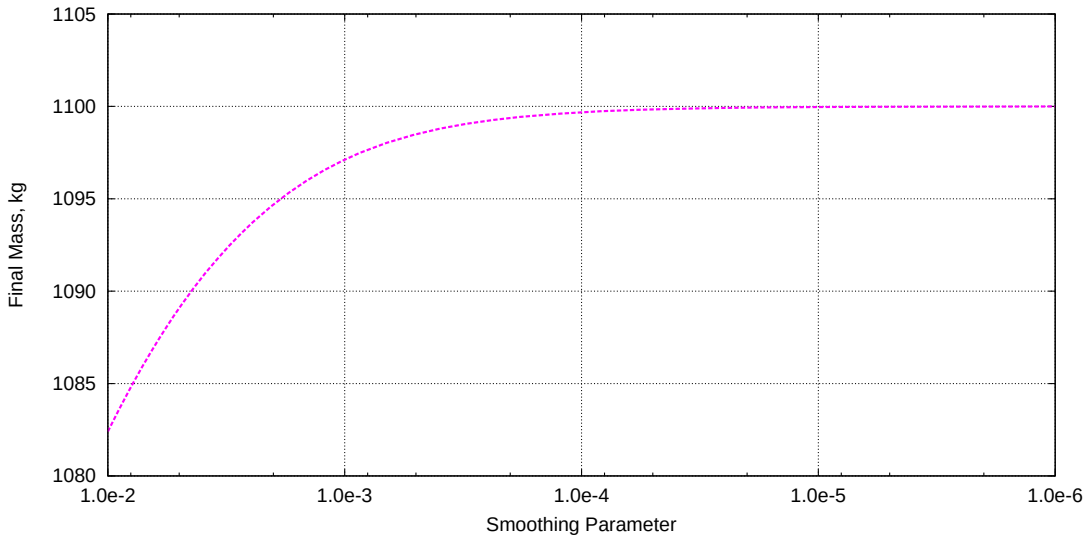

Figure 5.18: Final mass behavior during the continuation process for a single spacecraft.

index (the final mass) during the continuation procedure: the increment of the final mass continues until a critical value of the continuation parameter ($\varepsilon = 10^{-6}$) is reached; for lower values the mass remains almost constant. In the case of the Chaser/Target approach this critical value is almost always reached, while usually the continuation ends with $\varepsilon = 10^{-4}$ or $\varepsilon = 10^{-5}$ in the cooperative case.

The cooperative approach is also computationally more expensive than solving the same problem with the Chaser/Target (i.e., by solving the chaser and the target problem separately). For example, in the case of a Chaser/Target strategy, the time required to optimize a 4.5 revs. mission accounting for the effects of Earth oblateness and the Lunisolar gravitational perturbations is about 22 minutes (8 for Sat 2 and 14 for Sat 1); instead, in case of the cooperative strategy, about 45 minutes are required the to reach $\varepsilon_{\text{limit}} = 10^{-4}$, and 52 minutes for $\varepsilon_{\text{limit}} = 10^{-5}$. The time needed for any optimization can be reduced if the maximum allowed continuation step is increased (i.e., it passes from 5% to 10% of the smoothing parameter value), but in some cases convergence might not be obtained.

For an assigned smoothing parameter value (e.g. 10^{-4}), the difference in the final mass using either the smooth or the bang-bang control does not depend noticeably on the departure date. Therefore, as far as the same value of the smooth parameter is attained for all the departure dates, it is always possible to make peer comparison between the attained results. From a practical point of view, this is quite important as it allows the detection of best departure date.

Results concerning missions with different lengths , for departure dates ranging in a whole month, are shown in Figure 5.19. For any departure date, the optimal solution (which is the solution of interest from a theoretical viewpoint) can be found by post-processing the smooth solution with Multi-Bound approach. The proper burn structure can be envisaged by inspecting the attained control law, which also provides tentative values for the corresponding switch-on/off times. The presence of a burn is revealed by "peaks" in the control magnitude graph, as in Figure 5.20. Initial guesses at the other unknowns are provided by the smooth solution. A threshold β_{thld} on the nondimensional value of the thrust ($\beta = T/T_{\max}$) is assumed; burn and coast arcs are detected accordingly. This threshold value must be high enough to avoid "false burns", because the multi-boundary program would not converge. "Missed burns" are better tolerated: the multi-boundary program is conducted towards a suboptimal solution but

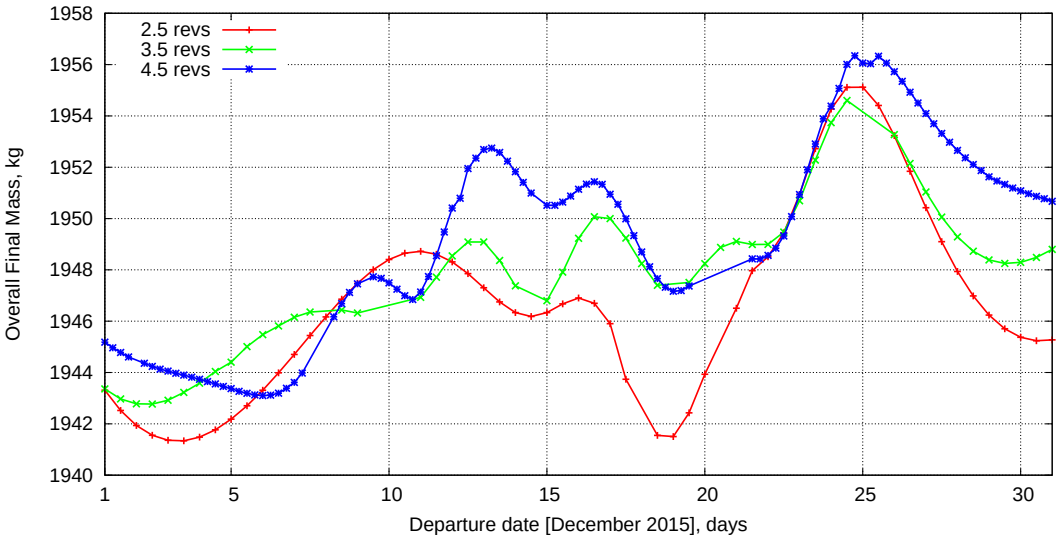

Figure 5.19: Final mass for the JLS 2.5, 3.5, and 4.5 revolution Cooperative formation deployment, Smooth control: Logarithmic barrier, $\varepsilon = 10^{-4}$.

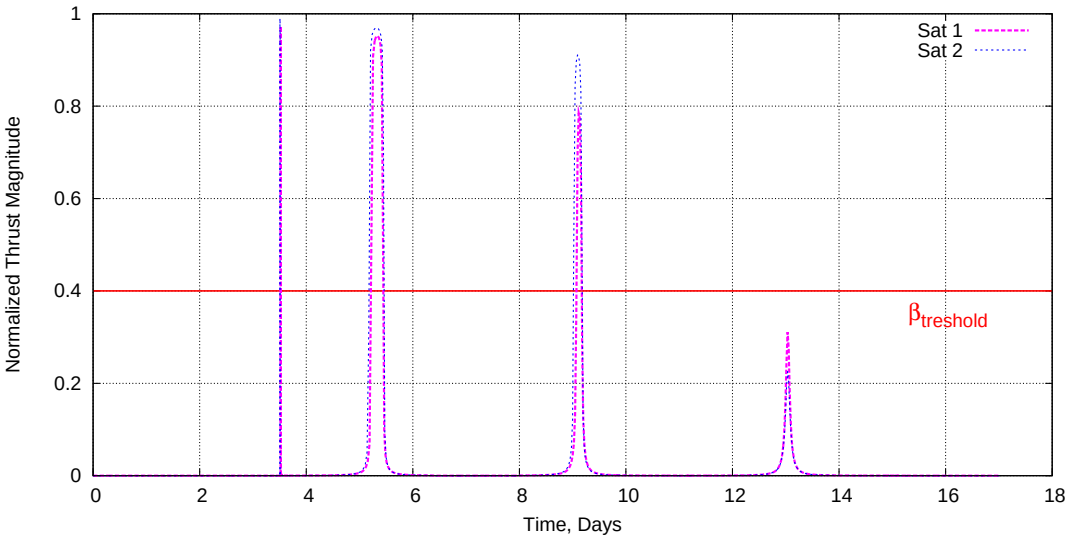

Figure 5.20: Example of thrust history during a cooperative mission (continuation stopped at $\epsilon = 10^{-4}$).

it will converge; one will discover that the attained solution is not optimal according to PMP, only by inspecting its switching function.

The structure becomes clearer as the continuation on the smoothing parameter progresses. For the current problem, the choice of $\beta_{thld} = 0.4$ permitted to detect the a burn structure corresponding to the PMP one for most of the departure date already for $\varepsilon \approx 10^{-4}$. In case the optimal (PMP) solution presents a very tiny apogee burn (e.g., 20 minutes) it might not be detected using a threshold so high, hence at the end of the process the solution is bang-bang, but it does not satisfy PMP. However, in these cases the difference in terms of final mass between the PMP and the obtained solution is very small. This situation arises, as an example, for the cooperative JLS - 4.5 revolution mission departing on 1/12/2015. The PMP optimal solution is PAAA - PAA0 and the last apogee burn of Sat 1 lasts only 0.004 rad. Using the threshold $\beta_{thld} = 0.4$, if the continuation process is stopped at $\varepsilon = 10^{-4}$ the PAA0 - PAA0 structure is detected and the bang-bang solution will remain suboptimal. Instead, the guessed structure will be PAAA-PAA0 on the basis of the smoothed solution corresponding to $\varepsilon = 10^{-5}$, and in that case the PMP optimal solution will be eventually obtained. The difference in terms of overall final mass is however minimal (a few grams).

Table 5.14: Final mass for a cooperative mission (JLS 4.5 revs 1/12/2015 - Multi-Bound method).

Strategy	Final Mass, kg		
	Sat 1	Sat 2	Overall
PA00 - PA00	845.110	1099.733	1944.842
PAA0 - PA00	845.181	1099.787	1944.969
PAA0 - PAA0	845.227	1099.993	1945.220
PAAA - PAA0	845.228	1099.994	1945.222

One should also notice that the solution of the less performing Chaser/Target strategy with the critical value of the continuation parameter $\varepsilon = 10^{-6}$, which corresponds to an almost bang-bang control, exhibits a higher final mass than the Cooperative approach with a "higher" value of the continuation parameter ($\varepsilon = 10^{-4}$). This apparent contradiction disappears when solutions with the same value of the continuation parameter are considered. However, the maximum performance needs to be calculated by using the Multi-Bound procedure.

Table 5.15: Final mass for different strategies and smoothing parameters - 3.5 revs mission.

JLS 3.5 @ 2015/12/02			
Strategy	Sat 1	Sat 2	Overall
C/T(1e-4):	843.738	1098.386	1942.125
C/T(1e-5):	843.954	1098.603	1942.557
C/T(1e-6):	843.978	1098.627	1942.606
COOP(1e-4):	843.932	1098.386	1942.318
COOP(1e-5):	844.150	1098.604	1942.754
COOP(_MB_):	844.175	1098.628	1942.803

Table 5.16: Final mass for different strategies and smoothing parameters - 4.5 revs mission.

JLS 4.5 @ 2015/12/02			
Strategy	Sat 1	Sat 2	Overall
C/T(1e-4):	843.955	1098.603	1942.558
C/T(1e-5):	844.455	1099.326	1943.781
C/T(1e-6):	844.708	1099.602	1944.31
COOP(1e-4):	844.529	1099.243	1943.772
COOP(1e-5):	844.867	1099.568	1944.435
COOP(_MB_):	844.902	1099.604	1944.506

Chapter 6

Conclusions

This thesis was focused on indirect optimization methods for the design of space missions, and, in particular, to a specific class of optimal control problems whose solution exhibits a discontinuous control law: the so called bang-bang optimal control problems.

Any attempt to solving such problems by using an indirect method without any specific treatment of the bang-bang control resulted inevitably into a failure, except for trivial problems (rocket sled - Chapter 3). In order to work properly, the shooting method requires the shooting function to be smooth. Unfortunately, the presence of discontinuous control terms causes the shooting function to be discontinuous, or not defined, and its Jacobian may be singular at some points in its domain. This limits by far the convergence basin of the root-finding method and the user capability of attaining a correct solution. Moreover, the loss of accuracy along the integration (due to the numerical noise related to the discontinuous control law and to the problem dynamics) may be so pronounced to cause imprecise evaluation of the Jacobian matrix. Therefore, even though the resulting HBVP is numerically well conditioned and the initial guess is very close to the solution, the shooting algorithm may be unable to converge.

The Continuation-Smoothing technique mitigates these issues by finding at first the solution of a regularized problem and then by attaining the solution of the original problem by progressively reducing the magnitude of the regularization (or perturbative) term. In practice this technique gives brilliant results for problems with a simple

dynamics (cooperative rendezvous problem - Chapter 4), and fair results as far as a more complex dynamics (Simbol-X deployment problem - Chapter 5) is considered. The reasons of the not complete success in the latter case is that the Continuation-Smoothing technique does not remove entirely the source of the numerical issues previously described. At the beginning of the continuation, the control is quite smooth and numerical issues are negligible; thus the regularized problem is solved easily. However, as the continuation progresses, the control resumes its original behavior and the associate numerical noise grows forcefully. Eventually, this may lead to such an imprecise evaluation of the Jacobian matrix that convergence cannot be attained anymore and the continuation process cannot progress any further. If this happens before the control law has become almost bang-bang (e.g. in the case of the longest Simbol-X deployment), the optimization usually cannot be considered as a complete success.

The Multibound approach is almost completely unaffected by these numerical issues, as the discontinuous terms are fully removed from each integration domain (they are present only at arc extremities). This enhancement allows to obtain a numerical solution with a very strict tolerance (nondimensional residual lower than 10^{-7}) in any tried case, even the most complex one. Moreover, the convergence radius is enlarged by this technique (with respect to the straightforward application of optimal control theory): the subdivision of the trajectory into many arcs, each one with an assigned thrust level, greatly reduces the sensitivity of the trajectory to the values of initial adjoint variables. Besides, the additional unknown parameters, which correspond to the engine switch on/off times, permit to enforce easily a physical initial guess.

Indeed, the multibound approach requires a lot of work from the user, which has to find out and to set up the proper burn structure for each mission of interest. This task may become really burdensome, or even impossible, when huge parametric analyses have to be performed, especially when there is no clue on the optimal burn structure (as in the Simbol-X deployment problem). On this side, the Continuation-Smoothing method is more appealing than the multibound one. An almost automatic procedure has been described and adopted. Albeit no proof of convergence to the optimum can be stated, in practice this initialization process demonstrated to be capable of achieving the optimal solution in most cases, while sub-optimal solutions were found just in a few cases. It permitted, as an example, to solve the Simbol-X deployment problem for any departure date and any mission length, without necessity of any user action, obtaining

always results in good agreement with those found out using the multibound approach and manually attaining the convergence.

Despite the Multi-Bound and the Continuation-Smoothing technique were presented here one against the other, nothing precludes their synergistical use. In particular, results obtained in case of cooperative strategy for the Simbol-X formation deployment suggest the use the Continuation-Smoothing as an initialization step for the multibound approach. The Continuation-Smoothing is capable of capturing the right burn structure, whereas the Multi-Bound approach is good to refine it. The passage from one formulation to the other is quite straightforward, as the system of ODE and the (external) boundary conditions are the same. Once a suitable burn structure has been individuated, one has only to enforce as many conditions as the number of switching points.

6.1 Future Work

Future research may be directed towards finding even smoother control laws than those considered in this thesis, in order to further improve the effectiveness of the Continuation-Smoothing approach. Efforts should be directed towards a better integration of the two methods, which may reduce computational time and also improve the accuracy of the solution. The development of an "efficient" initialization procedure is also an interesting research field. Advances could be attained by considering continuation paths different from the one used in this thesis. Finding a proper automatic initialization for the most common space missions, such as multi-revolution orbit transfer, would allow to create reliable, automatic tools which could be employed in the design of more complex missions. As an example, a debris-removal mission would greatly benefit of such automated solver. Here the goal is to remove as many debris as possible (or to reduce the propellant for a given list of target debris), within a given time. As the best sequence of targets is unknown, a great number of target-to-target transfers has to be analyzed. A huge number of possibilities exists because the optimal transfer from a debris to another depends on the time (through the debris relative phase). Clearly, a tool for optimize autonomously each single leg would be really useful, as it would leave the user only the task of deciding the removal sequence.

Formation flying missions (here used as a benchmark for the numerical solution method) provide another interesting topic of future research: the reconfiguration problem, that is, how moving efficiently a spacecraft formation from one configuration to another. Time-constrained, minimum-fuel reconfigurations are desired as they allow to extend the lifetime of a formation, but it is a very challenging problem due great number of locally optimal solutions and the presence of a collision avoidance inequality constraint which may be activated many times in a maneuver which has spacecraft often flying in close proximity.

Appendix A

Perturbation Acceleration due to Earth Asphericity and Lunisolar Attraction

In order to take into account the effects of Earth Asphericity, Moon and Sun gravitational attraction, a perturbing acceleration has to be added into the spacecraft equations of motion.

The satellite position with respect to an inertial frame is given by a set of polar coordinate r, ϑ, and φ. The reference frame $\left\{\hat{i};\hat{j};\hat{k}\right\}$, chosen to describe the S/C velocity, is topocentric and rotating, which follows the spacecraft during its motion, keeping the axes pointed in the radial $\hat{i}$, eastward $\hat{j}$, and northward $\hat{j}$ directions.

The three unit vectors $\hat{i}$, $\hat{j}$, $\hat{k}$ are defined with respect to the inertial reference frame $\{\hat{g}_1;\hat{g}_2\}$ by the following equations:

$$\begin{Bmatrix}\hat{i}\\ \hat{j}\\ \hat{k}\end{Bmatrix} = \begin{bmatrix}\cos\vartheta\cos\varphi & \sin\vartheta\cos\varphi & \sin\varphi\\ -\sin\vartheta & \cos\vartheta & 0\\ -\cos\vartheta\sin\varphi & -\sin\vartheta\sin\varphi & \cos\varphi\end{bmatrix}\begin{Bmatrix}\hat{g}_1\\ \hat{g}_2\\ \hat{g}_3\end{Bmatrix} \tag{A.1}$$

The velocity is expressed by means of the radial u, estward v, and northward w components, respectively. The motion of a spacecraft in a general-perturbed environment can be described by the following set of differential equations:

$$\dot{\bar{x}} = \bar{f}\left(\bar{x}, \bar{u}, t\right) = \begin{cases} \dot{r} = u \\ \dot{\vartheta} = v/\left(r\cos\varphi\right) \\ \dot{\varphi} = w/r \\ \dot{u} = -\mu/r^2 + \left(v^2 + w^2\right)/r + T_u/m + \left(a_p\left(\bar{x}, t\right)\right)_u \\ \dot{v} = \left(-uv + vw\tan\vartheta\right)/r + T_v/m + \left(a_p\left(\bar{x}, t\right)\right)_v \\ \dot{w} = -\left(uw + v^2\tan\vartheta\right)/r + T_w/m + \left(a_p\left(\bar{x}, t\right)\right)_w \\ \dot{m} = -T/c \end{cases} \tag{A.2}$$

where:

- $\bar{u} = \vec{T} = \begin{pmatrix} T_u & T_v & T_{\mathrm{w}} \end{pmatrix}$ is the control vector;
- $\vec{a}_p\left(\bar{x}, t\right)$ is the overall perturbing acceleration acting on the spacecraft.

In the following sections, analytical expressions are given fore the perturbing acceleration due to Earth asphericity or the third body gravitational attraction. Obviously, the overall perturbing acceleration is just the sum of the acceleration due to each perturbing source.

A.1 Earth Asphericity

Perturbations due to Earth asphericity account for the effects related to a non newtonian gravitational potential and will be indicated as $\bar{a}_J$. A more realistic Earth's potential description is based on the Earth Gravitational Model EGM2008, which provides normalized spherical harmonic coefficients for Earth's gravitational potential; the "Tide Free" system is used [81]. The developed code can be quickly modified to consider higher degree terms or the "Zero Tide" system. The Earth's rotation is assumed to be uniform, neglecting precession and nutation. The EME2000 reference frame is adopted. The gravity model is described in details in [82]. According to EGM2008, the potential corresponding to the Earth asphericity is expressed as

$$\Phi = -\mu/r \sum_{n=2}^{N} \left(\frac{r_E}{r}\right)^n \sum_{m=0}^{n} \left(C_{nm}\cos m\lambda + S_{nm}\sin m\lambda\right) P_{nm}(\sin\varphi) \tag{A.3}$$

where μ is the Earth gravitational parameter and r_E is the semimajor axis of the Earth ellipsoid. In this article N is chosen equal to 8. The associated Legendre functions $P_{nm}(\sin\varphi)$ and the spherical harmonic coefficients C_{nm} and S_{nm} are used in the unnormalized form that permits faster computations. Normalized quantities would allow for a greater accuracy, which is not necessary for the present application.

The terrestrial latitude coincides with declination φ, as nutation is neglected. The terrestrial longitude λ is obtained as $\lambda = \vartheta - \vartheta_{G\mathrm{ref}} - \omega_E(t - t_{\mathrm{ref}})$, where $\vartheta_{G\mathrm{ref}}$ is the Greenwich right ascension at the reference time t_{ref} (51544.5 MJD); ω_E is evaluated on the basis of the sidereal day, neglecting precession.

The perturbing acceleration due to Earth's asphericity is the gradient of $-\Phi$, and its components in the topocentric frame are thus evaluated as

$$(a_J)_u = -\partial\Phi/\partial r \tag{A.4}$$

$$(a_J)_v = -(\partial\Phi/\partial\vartheta)/(r\cos\varphi) \tag{A.5}$$

$$(a_J)_w = -(\partial\Phi/\partial\varphi)/r \tag{A.6}$$

Differentiation with respect to r and ϑ is straightforward; derivatives with respect to φ require the derivatives of the associated Legendre functions, which are obtained recursively, exploiting the properties of Legendre polynomials. Derivatives are evaluated directly with respect to φ (some authors use the colatitude $\pi/2-\varphi$, the only difference being a sign change of the derivatives); one has, posing $P_{nm} = 0$ for $m > n$,

$$\frac{\mathrm{d}P_{nm}}{\mathrm{d}\varphi} = \begin{cases} P_{n1} & \text{for} \quad m = 0 \\ [P_{n(m+1)} - (n+m)(n-m+1)P_{n(m-1)}]/2 & \text{for} \quad m > 0 \end{cases} \tag{A.7}$$

Further details can be found in [83] and [84].

A.2 Third body Perturbation

Third body perturbations account for the presence of attracting bodies other than the primary (here the Earth) and the spacecraft. In particular the perturbing acceleration $\bar{a}_{bg}$ on the spacecraft, which is caused by a body with gravitational parameter μ_b and position vector with respect to the Earth $\bar{r}_b = x_b\hat{g}_1 + y_b\hat{g}_2 + z_b\hat{g}_3$, is given by the difference of the gravitational accelerations that the perturbing body causes on spacecraft and Earth, that is:

$$\bar{a}_{bg} = -(\mu_b/R^3)\bar{R} - (\mu_b/r_b^3)(\bar{r}_b) \tag{A.8}$$

where $\bar{R} = \bar{r} - \bar{r}_b$ is the spacecraft relative position vector with respect to the perturbing body, as shown in Figure 5.3.

The third body position (either Moon or Sun) can be evaluated using DE405 JPL ephemerids [85], which directly provide the body position in rectangular coordinates x_b, y_b, z_b with respect to the Earth in the International Celestial Reference Frame, and therefore in the EME2000 frame (differences between these frame are very small and can be neglected in the present problem).

The perturbing acceleration $\bar{a}_{bg}$ is projected onto the topocentric frame (based on the spacecraft position) to attain its components in that reference frame:

$$(a_{bg})_u = (\mu_b/R^3)[(r_b)_u - r] - (\mu_b/r_b^3)(r_b)_u \tag{A.9}$$

$$(a_{bg})_v = (\mu_b/R^3)(r_b)_v - (\mu_b/r_b^3)(r_b)_v \tag{A.10}$$

$$(a_{bg})_w = (\mu_b/R^3)(r_b)_w - (\mu_b/r_b^3)(r_b)_w \tag{A.11}$$

with $R = \sqrt{[r - (r_b)_u]^2 + (r_b)_v^2 + (r_b)_w^2}$. The position components of the perturbing body in the spacecraft topocentric frame are

$$(r_b)_u = x_b \cos\vartheta \cos\varphi + y_b \sin\vartheta \cos\varphi + z_b \sin\varphi \tag{A.12}$$

$$(r_b)_v = -x_b \sin\vartheta + y_b \cos\vartheta \tag{A.13}$$

$$(r_b)_w = -x_b \cos\vartheta \sin\varphi - y_b \sin\vartheta \sin\varphi + z_b \cos\varphi \tag{A.14}$$

The perturbing acceleration $\bar{a}_{bg}$ is thus a function of time and state variables (namely, only r, ϑ, and φ, as gravity forces only depend on position). Eventually, the luni-solar perturbation is calculated as the sum of the gravitational perturbations due to Moon ($b = l$) and Sun ($b = l$).

Appendix B

Simbol-X Deployment Problem using Modified Equinoctial Elements

In this appendix, the deployment problem of the Symbol-X formation is reformulated using the Modified Equinoctial Elements (MEEs) as state parameters. This set of variables is soon presented and the relationships with classical orbital parameters and position and velocity vectors are stated. Then, the dynamics equations are derived. Eventually, optimality conditions for both Chaser/Target and Cooperative approaches are provided.

B.1 The set of modified equinoctial orbital elements

The modified equinoctial orbital elements are a set of orbital elements useful for trajectory analysis and optimization, which is valid for circular, elliptic, and hyperbolic orbits. Differently from the classical orbital elements, this set of variables exhibits no singularity for zero eccentricity and orbital inclinations equal to 0 and 90 degrees. However, two of the components are singular for an orbital inclination of 180 degrees. Modified equinoctial elements are defined in terms of classical orbital elements by the

following equations:

$$p = a\left(1 - e^2\right) \tag{B.1}$$

$$e_x = e\cos\left(\omega + \Omega\right) \tag{B.2}$$

$$e_y = e\sin\left(\omega + \Omega\right) \tag{B.3}$$

$$h_x = \tan\left(i/2\right)\cos\left(\Omega\right) \tag{B.4}$$

$$h_y = \tan\left(i/2\right)\sin\left(\Omega\right) \tag{B.5}$$

$$L = \Omega + \omega + \nu \tag{B.6}$$

This modified set of orbital parameters is related to the classical one by the following equations:

$$e = \sqrt{e_x^2 + e_y^2} \tag{B.7}$$

$$a = p/1 - e^2 \tag{B.8}$$

$$i = 2\arctan\left(h_x^2 + h_y^2\right) \tag{B.9}$$

$$\Omega = \mathrm{atan2}\left(h_y, h_x\right) \tag{B.10}$$

$$\omega = \mathrm{atan2}\left(e_y, e_x\right) - \Omega \tag{B.11}$$

$$\nu = L - \Omega - \omega \tag{B.12}$$

Modified equinoctial elements are also appealing as state variables because the dynamics equations associated to this set of parameters are more stable and easier to integrate than those associated to the position-velocity variable set (which, on the other hand, are more intuitive). The dynamics equations for MEEs can be derived following the classical Variation of Parameter approach, that allows the inclusion of both the conservative (e.g., third body and geopotential perturbation) and nonconservative (e.g., drag and thrust) forces acting on the spacecraft. The component resolution of these external forces can be made in various rotating orbital frames, such as the Euler-Hill or polar orbital frame, the equinoctial frame, or even the tangential frame. In this work the radial-tangential-normal frame has been chosen: the radial direction is along the geocentric radius vector of the spacecraft measured positive in direction away from the geocenter, the normal direction is positive along the angular momentum vector, and the tangential direction is chosen to complete the right-handed coordinate system.

$$\hat{i}_r = \frac{\vec{r}}{\|\vec{r}\|} \qquad \hat{i}_n = \frac{\vec{r}\times\vec{V}}{\left\|\vec{r}\times\vec{V}\right\|} \qquad \hat{i}_t = \hat{i}_n \times \hat{i}_r \tag{B.13}$$

The set of differential equations which completely describes the evolution of a spacecraft state is given by the dynamics equations for MEEs plus the mass equation:

$$\dot{\bar{x}} = \begin{cases} \dot{\bar{x}}_c = \bar{f}_0\left(\bar{x}_c, t\right) + \bar{\bar{g}}(\bar{x}_c, t)^T \left(\dfrac{\vec{T}}{m} + \vec{a}_p\right) \\ \dot{m} = -\dfrac{T}{c} \end{cases} \tag{B.14}$$

where $\bar{x}_c = \begin{pmatrix} p & e_x & e_y & h_x & h_y & L \end{pmatrix}^T$ is the vector which collects all the MEEs for one spacecraft and

$$\bar{f}_0 = \sqrt{\frac{\mu}{p}}\frac{W^2}{p}\begin{bmatrix} 0 \\ 0 \\ 0 \\ 0 \\ 0 \\ 1 \end{bmatrix} \tag{B.15}$$

$$\bar{\bar{g}} = \sqrt{\frac{p}{\mu}}\frac{1}{W}\begin{bmatrix} 0 & 2p & 0 \\ W\sin L & W\cos L + \eta_x & -Ze_y \\ -W\cos L & W\sin L + \eta_x & +Ze_x \\ 0 & 0 & \frac{C}{2}\cos L \\ 0 & 0 & \frac{C}{2}\sin L \\ 0 & 0 & Z \end{bmatrix} \tag{B.16}$$

$$C = 1 + h_x^2 + h_y^2 \qquad W = 1 + e_x\cos L + e_y \sin L \qquad Z = h_x \sin L - h_y \cos L \tag{B.17}$$

$$\eta_x = e_x + \cos L \qquad \eta_y = e_y + \sin L \tag{B.18}$$

Further details on modified equinocitial elements, such as the relationship between the cartesian components of the position and veloctity vectors and MEEs, can be found in [86].

Notice that here, $\vec{a}_p$ is the perturbing acceleration expresses in the RTN reference frame; equations provided in Appendix A are still valid, but need to be calculated in this reference frame in order to be properly used.

B.2 Optimization using a Chaser/Target Approach

Using the Chaser/Target strategy, two optimal control problems arise: the one concerning the target spacecraft is self-consistent, while the other one needs the solution of the former to be completely defined.

In both problems, the goal is to maximize the final mass of the relevant spacecraft, that is alternatively $J = m_I|_f$ or $J = m_{II}|_f$. For either spacecraft, the state vector is defined by Modified Equinoctial Elements plus the spacecraft mass; its evolution in time is given by eq. (B.14)

Both problems are solved by the same indirect method used through all the thesis. First order necessary conditions need to be derived and the Hamiltonian boundary value problem which arises is solved by means of a simple shooting technique. The adjoint variables $\bar{\lambda}_{x_c} = \begin{pmatrix} \lambda_p & \lambda_{e_x} & \lambda_{e_y} & \lambda_{h_x} & \lambda_{h_y} & \lambda_L \end{pmatrix}^T$ and λ_m and the Hamiltonian are introduced. Euler-Lagrange equations, which provide the time-derivatives of the adjoint variables, are calculated according to eq. (2.16).

Notice that a analytical derivation of Euler-Lagrange equations is much more difficult when MEEs variables are adopted, with respect to the position-velocity set. The reader can refers to [87] for the analytical expression of Euler-Lagrange equations in absence of external perturbative terms. In this thesis, the analytical (hand-by) derivation of the adjoint equations is avoided, as the need to take into account many perturbative forces would made that task too long, complex and error-prone. Instead, the numerical values of the adjoint derivatives are computed by using an automatic differentiation procedure [88]. This choice relieves the user from any concern about the analytical expression of the Euler-Lagrange equations; the only drawback is a much slower computation with respect to the analytic one (speed factor is usually about $\frac{1}{2} \div \frac{1}{4}$).

The optimal control law for either spacecraft can be computed formally in the same fashion. As far as the modified equinoctial elements are concerned, Lawden primer vector theory cannot be exploit anymore to determinate the control law, as no velocity vector $\vec{\lambda}_V$ exists if MEEs are chosen as state variables. However, the quite general formulation provided in Chapter 3, section [3.2.1], apply to this problem, as the system dynamics is affine in the control vector and the magnitude of the control is bounded.

Optimal thrust vector is decomposed in magnitude and direction: $\vec{T} = T_{\max}\, \beta\, \hat{v}$.

The optimal direction $\hat{v}$ is calculated according to eq. (3.10):

$$\hat{v}\left(t\right)=\frac{\bar{\bar{g}}(\bar{x}_c\left(t\right))^T\,\bar{\lambda}_{x_c}\left(t\right)}{\left\|\bar{\bar{g}}(\bar{x}_c\left(t\right))^T\,\bar{\lambda}_{x_c}\left(t\right)\right\|} \tag{B.19}$$

while, the optimal thrust magnitude β is decided on the basis of the switching function value, which can be highlighted easily by explicating the optimal thrust direction in the Hamiltonian:

$$\begin{aligned} H &= \bar{\lambda}_{x_c}^T\bar{f}_0\left(\bar{x}_c\right)+\bar{\lambda}_{x_c}^T\,\bar{\bar{g}}(\bar{x}_c)^T\left(\frac{\vec{T}}{m}+\vec{a}_p\right)-\lambda_m\frac{T}{c}= \\ &= \bar{\lambda}_{x_c}^T\left(\bar{f}_0\left(\bar{x}_c\right)+\bar{\bar{g}}(\bar{x}_c)^T\vec{a}_p\right)+T_{max}S_F \end{aligned} \tag{B.20}$$

where

$$S_F=\left\|\bar{\bar{g}}\left(\bar{x}_c\right)^T\,\bar{\lambda}_{x_c}\right\|/m-\lambda_m/c \tag{B.21}$$

Pontryagin Maximum Principle indicates whether the spacecraft has to maneuver or not. The Hamiltonian is linear in the thrust value, hence maximum thrust is exploited when the switching function is positive, otherwise the engine is turned off. Assuming that the Continuation-Smoothing technique discussed in Chapter 3 is employed to avoid the troubles linked to the control discontinuity, the thrust magnitude β can be directly calculated by using equation eq. (3.77) or (3.86), depending on the choice of a quadratic or logarithmic term for the regularization, respectively.

In the following paragraphes, constraints and optimality conditions for the Chaser/Target approach will be presented. A clear distinction is made between the deployment of Target and Chaser spacecraft, as explained in Chapter 5.

B.2.1 Deployment Problem of Target Spacecraft

At the departure point, the state of spacecraft is fully assigned. The initial constraints (eq.s 5.26) can be expressed as:

$$p=\tilde{p}_0 \qquad e_x=\tilde{e}_{x_0} \qquad e_y=\tilde{e}_{y_0} \tag{B.22}$$

$$h_x=\tilde{h}_x \qquad h_y=\tilde{h}_y \qquad t_f=\widetilde{t_f} \qquad m=\tilde{m}_0 \tag{B.23}$$

Terminal constraints for the Target spacecraft (eq. 5.29) become:

$$p = \tilde{a}_f \left(1 - \tilde{e}_f^2\right) \tag{B.24}$$

$$e_x^2 + e_y^2 = \tilde{e}_f^2 \tag{B.25}$$

$$\nu = \pi \rightarrow \cos L \sqrt{e_x^2 + e_y^2} + e_x = 0 \tag{B.26}$$

By applying the transversality conditions one obtains the algebraic equations that close the Hamiltonian boundary value problem for the Target spacecraft:

$$H = 0 \tag{B.27}$$

$$\lambda_{h_x} = 0 \tag{B.28}$$

$$\lambda_{h_y} = 0 \tag{B.29}$$

$$-\lambda_{e_x} + \lambda_{e_y} e_x / e_y - \lambda_L / \left(\sin L \sqrt{e_x^2 + e_y^2}\right) = 0 \tag{B.30}$$

$$\lambda_m = 1 \tag{B.31}$$

B.2.2 Deployment Problem of Chaser Spacecraft

The deployment of the chaser spacecraft features a set of initial conditions which is formally the same as the Leader problem, as the state of the chaser is fully assigned at the departure point:

$$p = \tilde{p}_0 \qquad e_x = \tilde{e}_{x_0} \qquad e_y = \tilde{e}_{y_0} \tag{B.32}$$

$$h_x = \tilde{h}_x \qquad h_y = \tilde{h}_y \qquad t_f = \widetilde{t_f} \qquad m = \tilde{m}_0 \tag{B.33}$$

Difference is made by those at final point. Here the final state of the chaser spacecraft is assigned, as it must be equal to the optimal final state $\bar{x}_{f2}^*$ of the target spacecraft (Sat 2), except for the mass. The arrival time is fixed and delayed by a constant quantity with respect to the optimal arrival time t_{f2}^* of Sat 2. These conditions ensure that the two spacecraft share the same orbital parameters (except for the mean anomaly). The time delay $\Delta t_{\tilde{D}}$ is given by eq. (5.21) and here reported for the sake of completeness.

Thus, terminal constraints for the chaser spacecraft become:

$$p = p^*_{f2} \tag{B.34}$$

$$e_x = e_{x^*_{f2}} \tag{B.35}$$

$$e_y = e_{y^*_{f2}} \tag{B.36}$$

$$h_x = h_{x^*_{f2}} \tag{B.37}$$

$$h_y = h_{y^*_{f2}} \tag{B.38}$$

$$L = L^*_{f2} \tag{B.39}$$

$$t_f = t^*_{f2} + \Delta t_{\tilde{D}}; \qquad \Delta t_{\tilde{D}} = \tilde{D}/V_a \tag{B.40}$$

The transversality equations provide only one additional condition, which is related to the final mass via the merit index and involves the mass adjoint:

$$\lambda_m = 1 \tag{B.41}$$

Optimal control equations for the chaser spacecraft are formally the same as the target one. The reader can refers to previous section or Chapter 3 for the details.

B.3 Optimization using a Cooperative Approach

In the Cooperative approach, a unique Hamiltonian boundary value problem is setup, by considering simultaneously the motion of the two satellites. The objective of the optimization is one again maximizing the sum of the spacecraft final masses. The equations of motion of each spacecraft, as well as the adjoint equations, remain unchanged with respect to the single spacecraft problem, but, obviously, the overall number doubles (28 equations, that is, 14 per each spacecraft).

Many considerations made in Chapter 5 (c.f. section 5.3.3) still hold in this case. Most important, in both cases the Hamiltonian can be written as the sum of the two Hamiltonians corresponding to each spacecraft. The presence of two distinct switching functions is again highlighted:

$$\begin{aligned} H =& \bar{\lambda}^T_{x_{c_I}} \left(\bar{f}_0 \left(\bar{x}_{c_I} \right) + \bar{\bar{g}}(\bar{x}_{c_I})^T \left(\vec{a}_p \left(\bar{x}_{c_I}, t \right) \right) \right) + \\ & \bar{\lambda}^T_{x_{c_{II}}} \left(\bar{f}_0 \left(\bar{x}_{c_{II}} \right) + \bar{\bar{g}}(\bar{x}_{c_{II}})^T \left(\vec{a}_p \left(\bar{x}_{c_{II}}, t \right) \right) \right) + \\ & T_{max} S_{F_I} \beta_I + T_{max} S_{F_{II}} \beta_{II} \end{aligned} \tag{B.42}$$

B. SIMBOL-X DEPLOYMENT PROBLEM USING MODIFIED EQUINOCTIAL ELEMENTS

For each spacecraft, the optimal control law is evaluated in the same fashion of section B.2. The thrust direction of each spacecraft is given by eq. (3.10), whereas the optimal (regularized) thrust magnitude is given by eq. (3.77) or (3.86), depending on the choice of a quadratic or logarithmic term for the regularization, respectively.

With respect to the Chaser/Target formulation, the optimal conditions for each satellite at departure are formally unchanged: all the MEEs and initial mass of the two spacecraft are assigned. Arrival boundary constraints presented in Chapter 5 (eq.s 5.44-5.49) can be rewritten in terms of modified equinoctial elements as:

$$p_I = \tilde{p} \tag{B.43}$$

$$e_{x_I}^2 + e_{y_I}^2 = \tilde{e}^2 \tag{B.44}$$

$$e_{x_I} \sin L_I - e_{y_I} \cos L_I = 0 \tag{B.45}$$

$$t_I - t_{II} = \Delta t_{\tilde{D}}; \qquad \Delta t_{\tilde{D}} = \tilde{D}/V_a \tag{B.46}$$

$$p_I - p_{II} = 0 \qquad e_{x_I} - e_{x_I I} = 0 \qquad e_{y_I} - e_{y_I I} = 0 \tag{B.47}$$

$$h_{x_I} - h_{x_I I} = 0 \qquad h_{y_I} - h_{y_I I} = 0 \qquad L_I - L_{II} = 0 \tag{B.48}$$

By applying the transversality conditions one obtains the remaining boundary conditions:

$$H = 0 \tag{B.49}$$

$$-\left(\lambda_{e_{x_I}} + \lambda_{e_{x_{II}}}\right) e_{y_I} + \left(\lambda_{e_{y_I}} + \lambda_{e_{y_{II}}}\right) e_{x_I} + \left(\lambda_{L_I} + \lambda_{L_{II}}\right) = 0 \tag{B.50}$$

$$\lambda_{h_{x_I}} + \lambda_{h_{x_{II}}} = 0 \tag{B.51}$$

$$\lambda_{h_{y_I}} + \lambda_{h_{y_{II}}} = 0 \tag{B.52}$$

$$\lambda_{m_I} = 1 \tag{B.53}$$

$$\lambda_{m_{II}} = 1 \tag{B.54}$$

Notice that once again two different time scales (one for each spacecraft) are used in order to define this final boundary as the apogee of both spacecraft, regardless of the arrival time.

Bibliography

[1] D.F. Lawden. *Optimal trajectories for space navigation*. Butterworths mathematical texts. Butterworths, 1963. URL http://books.google.it/books?id=jLFxAAAAMAAJ. 2

[2] D.F. Lawden. *Analytical Methods of Optimization*. Dover Books on Mathematics. Dover Publications, 1976. ISBN 9780486450346. 2

[3] L. Euler. Elementa calculi variationum. *Originally published in Novi Commentarii academiae scientiarum Petropolitanae*, 10:51–93, 1766. 2

[4] D.E. Kirk. *Optimal control theory: an introduction*. Prentice-Hall networks series. Prentice-Hall, 1970. URL http://books.google.it/books?id=cPBQAAAAMAAJ. 2

[5] L.S. Pontryagin. *The mathematical theory of optimal processes*. International series of monographs in pure and applied mathematics. Pergamon Press; [distributed in the Western Hemisphere by Macmillan, New York], 1964. URL http://books.google.it/books?id=aakrAAAAYAAJ. 2

[6] R.R. Bate, D.D. Mueller, and J.E. White. *Fundamentals of Astrodynamics*. Dover Books on Aeronautical Engineering Series. Dover Publications, 1971. ISBN 9780486600611. URL http://books.google.it/books?id=UtJK8cetqGkC. 2

[7] B. Conway. *Spacecraft Trajectory Optimization*. Cambridge Aerospace Series. Cambridge University Press, 2010. ISBN 9780521518505. URL http://books.google.it/books?id=gde1Vb104coC.

[8] P. Gurfil. *Modern Astrodynamics*. Elsevier Astrodynamics Series. Academic, 2006. ISBN 9780123735621. URL http://books.google.it/books?id=vwir24X66sQC. 2

[9] Lorenzo Casalino, Guido Colasurdo, and Matteo Rosa Sentinella. 1st act global trajectory optimisation competition: Results found at the politecnico of turin. *Acta Astronautica*, 61(9):769 – 774, 2007. ISSN 0094-5765. doi: 10.1016/j.actaastro.2007.03.005. URL http://www.sciencedirect.com/science/article/pii/S0094576507001713. ¡ce:title¿Global Trajectory Optimization. Results of the First Competition Organised by the Advanced Concept Team (ACT) of the European Space Agency (ESA). 3

[10] Lorenzo Casalino, Dario Pastrone, Francesco Simeoni, Guido Colasurdo, and Alessandro Zavoli. 5th ACT Global Trajectory Optimisation Competition: Results Found at Sapienza-Università di Roma and Politecnico di Torino. *Acta Futura*, 2013. Preprint submitted to Acta Futura January 22, 2013. 3, 47

[11] J. Borde, F. Teston, S. Santandrea, and S. Boulade. Feasibility of the Proba 3 formation flying demonstration mission as a pair of microsats in GTO. In B. Warmbein, editor, *Small Satellites, Systems and Services*, volume 571 of *ESA Special Publication*, November 2004. 4

[12] P. Ferrando, M. Arnaud, U. Briel, O. Citterio, R. Clédassou, P. Duchon, F. Fiore, P. Giommi, A. Goldwurm, G. Hasinger, E. Kendziorra, P. Laurent, F. Lebrun, O. Limousin, G. Malaguti, S. Mereghetti, G. Micela, G. Pareschi, Y. Rio, J. P. Roques, L. Strüder, and G. Tagliaferri. Simbol-x: mission overview. volume 6266, page 62660F. SPIE, 2006. doi: 10.1117/12.673266. URL http://link.aip.org/link/?PSI/6266/62660F/1. 4, 105

[13] G. Colasurdo and D. Pastrone. Indirect optimization method for impulsive transfer. In AIAA, editor, *AIAA/AAS Astrodynamics Conference, Scottsdale, AZ*, number 94-3762, pages 558–563. AIAA, August 1994. 7, 42, 78

[14] R. Bertrand and R. Epenoy. New smoothing techniques for solving bangbang optimal control problemsnumerical results and statistical interpretation. *Optimal Control Applications and Methods*, 23(4):171–197, 2002. ISSN 1099-1514. doi: 10.1002/oca.709. URL http://dx.doi.org/10.1002/oca.709. 7, 33

[15] Betts, John T. Survey of numerical methods for trajectory optimization. *Journal of Guidance Control and Dynamics*, 21(2):193–207, 1998. 11, 15, 18

[16] H.B. Keller. *Numerical methods for two-point boundary-value problems*. Dover Publications, 1992. 12, 26

[17] Uri M. Ascher and Linda R. Petzold. *Computer Methods for Ordinary Differential Equations and Differential-Algebraic Equations*. Society for Industrial and Applied Mathematics, Philadelphia, PA, USA, 1st edition, 1998. ISBN 0898714125. 12, 26

[18] MATLAB. *version 7.10.0 (R2010a)*. The MathWorks Inc., Natick, Massachusetts, 2010. 16

[19] Wolfram Alpha. Wolfram mathematica. *Mathematica*, 2007. URL http://www.wolfram.com/mathematica/. 16

[20] David G Hull. Conversion of optimal control problems into parameter optimization problems. *Journal of Guidance Control and Dynamics*, 20(1):57–60, 1997. 17

[21] H G Bock and K J Plitt. A multiple shooting algorithm for direct solution of optimal control problems. *Proceedings 9th IFAC World Congress Budapest*, XLII(2): 243–247, 1984. 17

[22] W. E. Williamson. Use of polynomial approximations to calculate suboptimal controls. *AIAA Journal*, 9:2271–2273, November 1971. doi: 10.2514/3.6499. 17

[23] John T Betts. *Practical Methods for Optimal Control using Nonlinear Programming*, volume 55. SIAM, 2001. 17

[24] C R Hargraves and S W Paris. Direct trajectory optimization using nonlinear programming and collocation. *Journal of Guidance Control and Dynamics*, 10(4):338–342, 1987.

[25] Paul J Enright and Bruce A Conway. Discrete approximations to optimal trajectories using direct transcription and nonlinear programming. *Journal of Guidance Control and Dynamics*, 15(4):994–1002, 1990. 17

BIBLIOGRAPHY

[26] J T Betts and P D Frank. A sparse nonlinear optimization algorithm. *J Optim Theory Appl*, 82:519–541, 1994. 17

[27] Philip E Gill, Walter Murray, and Michael A Saunders. Snopt: An sqp algorithm for large-scale constrained optimization. *SIAM Journal on Optimization*, 12(4):979–1006, 2002. 17

[28] S. Kirkpatrick, C. D. Gelatt, and M. P. Vecchi. Optimization by simulated annealing. *Science*, 220:671–680, 1983. 18

[29] C.R. Reeves and J.E. Rowe. *Genetic Algorithms: Principles and Perspectives : a Guide to GA Theory*. Operations Research/Computer Science Interfaces Series. Kluwer Academic Publishers, 2002. ISBN 9781402072406. 18

[30] Carlos A. Coello Coello. Theoretical and numerical constraint-handling techniques used with evolutionary algorithms: A survey of the state of the art, 2002. 18

[31] J. Kennedy and R. Eberhart. Particle swarm optimization. In *Neural Networks, 1995. Proceedings., IEEE International Conference on*, volume 4, pages 1942 –1948 vol.4, nov/dec 1995. doi: 10.1109/ICNN.1995.488968. 18

[32] Vlases, W. G., Paris, S. W., Lajoie, R. M., Martens, M. J., and Hargraves, C. R. Optimal trajectories by implicit simulation. Technical Report WRDC-TR-90-3056, Boeing Aerospace and Electronics, Wright-Patterson Air Force Base, 1990. 19

[33] Betts, J. T. and Huffman, W. P. Sparse Optimal Control Software - SOCS. Technical Report MEA-LR-085, Boeing Information and Support Services, the Boeing Company, P. O. Box 3797, Seattle, WA, 98124-2297, July 1997. 19

[34] Gath, P.F. and Well, K.H. Trajectory Optimization Using a Combination of Direct Multiple Shooting and Collocation. AIAA 2001-4047. AIAA Guidance, Navigation, and Control Conference, Montréal, Québec, Canada, 69 August 2001. 19

[35] von Stryk, O. *User's Guide for DIRCOL (version 2.1): A Direct Collocation Method for the Numerical Solution of Optimal Control Problems*. Fachgebiet Simulation und Systemoptimierung (SIM), Technische Universitt Darmstadt, 2000. 19

[36] M. B. Milam. *Real-time optimal trajectory generation for constrained dynamical systems*. PhD thesis, California Institute of Technology, 2003. 19

[37] Ross, I. M. and Fahroo, F. User's Manual for DIDO: A MATLAB Package for Dynamic Optimization. Technical Report 04-01.0, Dept. of Aeronautics and Astronautics, Naval Postgraduate School, February 2004. 19

[38] H. J. Oberle and W. Grimm. BNDSCO - a program for the numerical solution of the optimal control problems. Technical Report 515-89/22, Institute for Flight Systems Dynamics, DLR, Oberpfaffenhofen, Germany, 1989. 19

[39] A E Bryson and Y C Ho. *Applied Optimal Control*. Blaisdell, 1975. 22, 36

[40] J N Damoulakis, A Miele, and R E Pritchard. Sequential gradient-restoration algorithm for optimal control problems. *Journal of Optimization Theory and Applications*, 16(3/4):277–301, 1970. 25, 28

[41] A. Miele, T. Wang, and V.K. Basapur. Primal and dual formulations of sequential gradient-restoration algorithms for trajectory optimization problems. *Acta Astronautica*, 13(8):491 – 505, 1986. ISSN 0094-5765. doi: 10.1016/0094-5765(86)90028-7. 25

[42] U.M. Ascher, R.M.M. Mattheij, and R.D. Russell. *Numerical Solution of Boundary Value Problems for Ordinary Differential Equations*. Classics in Applied Mathematics. Society for Industrial and Applied Mathematics, 1988. ISBN 9780898713541. 26

[43] M. Powell. A hybrid method for nonlinear equations. *Numerical Methods for Nonlinear Algebraic Equations*, pages 87–144, 1970. 26, 36

[44] E. Hairer, S.P. Nørsett, and G. Wanner. *Solving Ordinary Differential Equations: Nonstiff problems*. Springer Series in Computational Mathematics. Springer, 1993. ISBN 9783540566700. 26

[45] J. J. Moré, B. S. Garbow, and K. E. Hillstrom. User Guide for MINPACK-1. *ANL-80-74, Argonne National Laboratory*, 1980. 27

[46] B.S. Garbow. *Implementation Guide for Minpack-1*. ANL (Series). Argonne National Laboratory, 1980. 27

[47] Numerical Algorithms Group. *NAG Fortran Library Manual, Mark 16: F03-F06*. NAG Fortran Library Manual, Mark 16. NAG, 1993. ISBN 9781852060916. URL http://books.google.it/books?id=of4YAQAAIAAJ. 27, 36

[48] Guido COLASURDO and Lorenzo CASALINO. Optimal DV-Earth-Gravity-Assist Trajectories in the Restricted Three-Body Problem. In *Advances in the Astronautical Sciences*, volume 103, pages 1681–1694. Univelt Inc., 1999. 27

[49] Alessandro Zavoli. Ottimizzazione Indiretta di una Missione DV-EGA a Spinta Finita nel Problema Ristretto dei Tre Corpi. Master's thesis, Sapienza - Università di Roma, October 2009. 27

[50] E.L. Allgower and K. Georg. *Numerical continuation methods: an introduction*. Springer series in computational mathematics. Springer-Verlag, 1990. ISBN 9783540127604. URL http://books.google.it/books?id=BzPvAAAAMAAJ. 32

[51] Layne T. Watson. Probability-one homotopies in computational science. *J. Comput. Appl. Math.*, 140(1-2): 785–807, March 2002. ISSN 0377-0427. doi: 10.1016/S0377-0427(01)00473-3. URL http://dx.doi.org/10.1016/S0377-0427(01)00473-3. 32

[52] S. A. Dadebo, K. B. McAuley, and P. J. McLellan. On the computation of optimal singular and bangbang controls. *Optimal Control Applications and Methods*, 19(4):287–297, 1998. ISSN 1099-1514. doi: 10.1002/(SICI)1099-1514(199807/08)19:4⟨287::AID-OCA628⟩3.0.CO;2-S. URL http://dx.doi.org/10.1002/(SICI)1099-1514(199807/08)19:4<287::AID-OCA628>3.0.CO;2-S. 33, 56

[53] T. F. Edgar and L. Lapidus. The computation of optimal singular bang-bang control i: Linear systems. *AIChE Journal*, 18(4):774–779, 1972. ISSN 1547-5905. doi: 10.1002/aic.690180419. URL http://dx.doi.org/10.1002/aic.690180419. 33

[54] T. F. Edgar and L. Lapidus. The computation of optimal singular bang-bang control ii. nonlinear systems. *AIChE Journal*, 18(4):780–785, 1972. ISSN 1547-5905. doi: 10.1002/aic.690180420. URL http://dx.doi.org/10.1002/aic.690180420. 33

[55] D H Jacobson, S B Gershwin, and M M Lele. Computation of optimal singular controls. *IEEE Transactions on Automatic Control*, 15(1):6773, 1970. URL http://ieeexplore.ieee.org/xpls/abs_all.jsp?arnumber=1099360. 33

[56] L.F. Shampine. *Numerical Solution of Ordinary Differential Equations*. Number v. 4 in Chapman & Hall mathematics. Chapman & Hall, 1994. ISBN 9780412051517. URL http://books.google.it/books?id=bHAarJTsapQC. 36

[57] C. W. Gear and O. Osterby. Solving ordinary differential equations with discontinuities. *ACM Trans. Math. Softw.*, 10(1):23–44, January 1984. ISSN 0098-3500. doi: 10.1145/356068.356071. URL http://doi.acm.org/10.1145/356068.356071. 36

[58] David Stewart. A high accuracy method for solving odes with discontinuous right-hand side. *Numerische Mathematik*, 58:299–328, 1990. ISSN 0029-599X. URL http://dx.doi.org/10.1007/BF01385627. 10.1007/BF01385627. 36

[59] Lorenzo Casalino, Guido Colasurdo, and Dario Pastrone. Optimization Procedure for Preliminary Design of Opposition-Class Mars Missions. *Journal of Guidance, Control, and Dynamics*, 21(1), January 1998. 42

[60] A. C. Hindmarsh. ODEPACK, A Systematized Collection of ODE Solvers , R. S. Stepleman et al. (eds.), North-Holland, Amsterdam, (vol. 1 of), pp. 55-64. *IMACS Transactions on Scientific Computation*, 1:55–64, 1983. 51

[61] Gergaud, J. *Résolution numérique de problémes de commande optimale à solution Bang-Bang par des methodes homotopiques simpliciales*. PhD thesis, Institut National Polytechnique de Toulouse, 1989. 53

[62] D.J. Bell and D.H. Jacobson. *Singular optimal control problems*. Mathematics in science and engineering. Academic Press, 1975. ISBN 9780120850600. URL http://books.google.it/books?id=Ov9QAAAAMAAJ. 53

[63] Joseph Gergaud and Joseph Noailles. Application of simplicial algorithms to a spacecraft trajectory optimization problem. June 1989. 56

[64] Yaobin Chen and Jian Huang. A continuation method for singular optimal control synthesis. In *American Control Conference, 1993*, pages 1256 –1260, june 1993. 56

[65] D.G. Luenberger and Y. Ye. *Linear and Nonlinear Programming*. International Series in Operations Research & Management Science. Springer, 2008. ISBN 9780387745022. URL http://books.google.it/books?id=-pD62uvi9lgC. 57

[66] K. Mirfakhraie and B. A. Conway. Optimal cooperative time-fixed impulsive rendezvous. *Journal of Guidance Control Dynamics*, 17:607–613, May 1994. 71

[67] J. Wang, H. Baoyin, J. Li, and F. Sun. Optimal four-impulse rendezvous between coplanar elliptical orbits. *Science in China G: Physics and Astronomy*, 54:792–802, April 2011. doi: 10.1007/s11433-011-4289-x.

[68] ChangQing Chen and YongChun Xie. Optimal impulsive ellipse-to-circle coplanar rendezvous. *Science in China Series E: Technological Sciences*, 52:1435–1445, 2009. ISSN 1006-9321. URL http://dx.doi.org/10.1007/s11431-009-0141-1. 10.1007/s11431-009-0141-1.

[69] J E Prussing. Optimal two- and three-impulse fixed-time rendezvous in the vicinity of a circular orbit. *Journal of Spacecraft and Rockets*, 40(6), 1970.

[70] J E Prussing. Optimal four-impulse fixed-time rendezvous in the vicinity of a circular orbit. *AIAA Journal*, 7(5):928–935, 1969. URL http://doi.aiaa.org/10.2514/3.5246.

[71] Conway, Bruce A. Prussing, John E.,. Optimal terminal maneuver for a cooperative impulsive rendezvous. *Journal of Guidance, Control, and Dynamics*, 12(3):433–435, 1989. doi: 10.2514/3.20427.

[72] D R Taur, J E Prussing, and V Coverstone-Carroll. Optimal impulsive time-fixed orbital rendezvous and interception with path constraints. *Journal of Guidance Control and Dynamics*, 18(1):54–60, 1990. URL http://doi.aiaa.org/10.2514/3.56656. 71

[73] Xincheng Yue, Ying Yang, and Zhiyong Geng. Continuous low-thrust time-optimal orbital maneuver. In *Decision and Control, 2009 held jointly with the 2009 28th Chinese Control Conference. CDC/CCC 2009. Proceedings of the 48th IEEE Conference on*, pages 1457 –1462, dec. 2009. doi: 10.1109/CDC.2009.5399622. 71

[74] J E Prussing and J H. Chiu. Optimal multiple-impulse time-fixed rendezvous between circular orbits. *Journal of Guidance Control and Dynamics*, 9(1):17–22, 1986. URL http://doi.aiaa.org/10.2514/3.20060. 71

[75] Philippe Ferrando, Monique Arnaud, Bertrand Cordier, Andrea Goldwurm, Olivier Limousin, Jaques Paul, Jean L. Sauvageot, Pierre-Olivier Petrucci, Martine Mouchet, Giovanni F. Bignami, Oberto Citterio, Sergio Campana, Giovanni Pareschi, Gianpiero Tagliaferri, Ulrich G. Briel, Guenther Hasinger, Lothar Strueder, Peter Lechner, Eckhard Kendziorra, and Martin J. L. Turner. Simbol-x: a new-generation hard x-ray telescope. volume 5168, pages 65–76. SPIE, 2004. doi: 10.1117/12.521998. 105

[76] G. Pareschi and HEXIT-SAT and SIMBOL-X Collaborations. The HEXIT-SAT and SIMBOL-X Hard X-ray missions. *Memorie della Societa Astronomica Italiana Supplementi*, 5:362, 2004. 105

[77] G. A. Hazelrigg, Jr. Globally optimal impulsive transfers via Green's theorem. *Journal of Guidance Control Dynamics*, 7:462–470, August 1984. 131

BIBLIOGRAPHY

[78] Alessandro Zavoli, Francesco Simeoni, Lorenzo Casalino, and Guido Colasurdo. Optimal cooperative deployment of a two-satellite formation into a highly elliptic orbit. In *Proceedings of the 2011 AAS/AIAA Astrodynamics Specialist Conference*, number 11-641. AAS, August 2011. 133

[79] Simeoni, Francesco, Casalino, Lorenzo, Zavoli, Alessandro, and Guido Colasurdo. Indirect optimization of satellite deployment into a highly elliptic orbit. *International Journal of Aerospace Engineering*, 2012:14 pages, 2012. doi: 10.1155/2012/152683. 147

[80] Simeoni, Francesco, Casalino, Lorenzo, Zavoli, Alessandro, and Colasurdo, Guido. Deployment of a Two-Spacecraft Formation into a Highly Elliptic Orbit with Collision Avoidance. In *Proceedings of the 2012 AIAA/AAS Astrodynamics Specialist Conference*, number 2012-4740 in AIAA. AIAA, August 2012. 147

[81] Nikolaos K Pavlis, S A Holms, Steve C Kenyon, and John K Factor. An earth gravitational model to degree 2160: Egm2008. *Assembly*, 2008. 160

[82] National Imagery and Mapping Agency NIMA. World geodetic system 1984 - its definition and relationships with local geodetic systems. (TR 8350.2, 3rd edition, Amendment 2), 2004. 160

[83] M. Abramowitz and I.A. Stegun. *Handbook of Mathematical Functions: With Formulas, Graphs, and Mathematical Tables*. Applied mathematics series. Dover Publications, 1964. ISBN 9780486612720. URL http://books.google.it/books?id=MtU8uP7XMvoC. 161

[84] W Bosch. On the computation of derivatives of legendre functions. *Physics and Chemistry of the Earth, Part A: Solid Earth and Geodesy*, 25(911):655 – 659, 2000. ISSN 1464-1895. doi: 10.1016/S1464-1895(00)00101-0. URL http://www.sciencedirect.com/science/article/pii/S1464189500001010. 161

[85] E M Standish. Jpl planetary and lunar ephemerides, de405/le405. *JPL IOM 312F 98 048*, 1998. 162

[86] J. Betts and S. Erb. Optimal low thrust trajectories to the moon. *SIAM Journal on Applied Dynamical Systems*, 2(2):144–170, 2003. doi: 10.1137/S1111111102409080. URL http://epubs.siam.org/doi/abs/10.1137/S1111111102409080. 165

[87] Jean Albert Kechichian. Optimal low-thrust rendezvous using equinoctial orbit elements. *Acta Astronautica*, 38(1):1 – 14, 1996. ISSN 0094-5765. doi: 10.1016/0094-5765(95)00121-2. URL http://www.sciencedirect.com/science/article/pii/0094576595001212. 166

[88] Stamatiadis, S., Prosmiti, R., and Farantos, S.C. auto_deriv: Tool for automatic differentiation of a fortran code. *Computer Physics Communications*, 127(2?3):343 – 355, 2000. ISSN 0010-4655. doi: 10.1016/S0010-4655(99)00513-5. URL http://www.sciencedirect.com/science/article/pii/S0010465599005135. 166